Development of Organic and Organic/Inorganic Hybrid Thin Film Transistors for Sensing Applications

Thesis submitted in partial fulfillment for the award of degree

Doctor of Philosophy

By

Shipra Gupta

SCHOOL OF MATERIALS SCIENCE AND TECHNOLOGY
INDIAN INSTITUTE OF TECHNOLOGY
(BANARAS HINDU UNIVERSITY)
VARANASI-221005,
INDIA

Roll No.: 18111010

2024

CERTIFICATE

It is certified that the work contained in the thesis titled ***"Development of Organic and Organic/Inorganic Hybrid Thin Film Transistors for Sensing Applications"*** by ***'Shipra Gupta'*** has been carried out under my supervision and that this work has not been submitted elsewhere for a degree.

It is further certified that the student has fulfilled all the requirements of comprehensive examination, candidacy and SOTA for the award of Ph.D. Degree.

Prof. Rajiv Prakash

(Supervisor)
School of Materials Science & Technology,
Indian Institute of Technology,
Banaras Hindu University,
Varanasi–221005, India

Professor/आचार्य
School of Materials Science & Technology/पदार्थ विज्ञान एवं प्रौद्योगिकी स्कूल
Indian Institute of Technology/भारतीय प्रौद्योगिकी संस्थान
(Banaras Hindu University), Varanasi/काशी हिन्दू विश्वविद्यालय, वाराणसी

Dr. Bhola Nath Pal

(Co-Supervisor)
School of Materials Science & Technology,
Indian Institute of Technology,
Banaras Hindu University,
Varanasi–221005, India

Associate Professor/सह-आचार्य
School of Materials Science & Technology/पदार्थ विज्ञान एवं प्रौद्योगिकी स्कूल
Indian Institute of Technology/भारतीय प्रौद्योगिकी संस्थान
(Banaras Hindu University), Varanasi/काशी हिन्दू विश्वविद्यालय, वाराणसी

DECLARATION BY THE CANDIDATE

I, "**Shipra Gupta**", certify that the work embodied in this thesis is my own bonafide work and carried out by me under the supervision of "**Prof. Rajiv Prakash**" from "**July 2018**" to "**December 2024**", at the "**School of Materials Science and Technology**", Indian Institute of Technology (BHU), Varanasi. The matter embodied in this thesis has not been submitted for the award of any other degree/diploma elsewhere. I declare that I have faithfully acknowledged and given credits to the research workers wherever their works have been cited in my work in this thesis. I further declare that I have not willfully copied any other's work, paragraphs, text, data, results, etc., reported in journals, books, magazines, reports dissertations, theses, etc., or available at websites and have not included them in this thesis and have not cited as my own work.

Date.....

Place: Varanasi

Shipra Gupta

(Shipra Gupta)

Certificate by the Supervisor/Co-Supervisor

This is to certify that the above statement made by the candidate is correct to the best of my knowledge.

Rajiv Prakash

(Prof. Rajiv Prakash)
Supervisor

Professor/आचार्य
School of Materials Science & Technology/पदार्थ विज्ञान एवं प्रौद्योगिकी स्कूल
Indian Institute of Technology/भारतीय प्रौद्योगिकी संस्थान
(Banaras Hindu University), Varanasi/काशी हिन्दू विश्वविद्यालय, वाराणसी

Bpal

(Dr. Bhola Nath Pal)
Co-Supervisor

Associate Professor/सह-आचार्य
School of Materials Science & Technology/पदार्थ विज्ञान एवं प्रौद्योगिकी स्कूल
Indian Institute of Technology/भारतीय प्रौद्योगिकी संस्थान
(Banaras Hindu University), Varanasi/काशी हिन्दू विश्वविद्यालय, वाराणसी

(Prof. Akhilesh Kumar Singh)
Coordinator

Coordinator/समन्वयक
School of Materials Science & Technology/पदार्थ विज्ञान एवं प्रौद्योगिकी स्कूल
Indian Institute of Technology/भारतीय प्रौद्योगिकी संस्थान
(Banaras Hindu University), Varanasi/काशी हिन्दू विश्वविद्यालय, वाराणसी

COPYRIGHT TRANSFER CERTIFICATE

Title of the Thesis: Development of Organic and Organic/Inorganic Hybrid Thin Film Transistors for Sensing Applications

Candidate's Name: Shipra Gupta

Copyright Transfer

The undersigned hereby assigns to the Indian **Institute of Technology (Banaras Hindu University) Varanasi, India** all rights under copyright that may exist in and for the above thesis submitted for the award of the **Doctor of Philosophy**.

Date:

Place: Varanasi

Shipra Gupta.

(Shipra Gupta)

Note: However, the author may reproduce or authorize others to reproduce material extracted verbatim from the thesis or derivative of the thesis for the author's personal use provided that the source and the Institute's copyright notice are indicated.

Acknowledgement

It's my great pleasure to acknowledge the help, support, encouragement and guidance that I have received from number of peoples in the course of completion of the thesis. I feel privileged to recognize their invaluable contributions, which have made this journey both meaningful and memorable.

At this moment of accomplishment, first and foremost, I pay homage to the founder of Banaras Hindu University, ***Pandit Madan Mohan Malviya Ji****, whose vision established this glorious institution dedicated to spiritual, technical, and scientific knowledge about this vast existing universe.*

I embrace this opportunity to express my profound respect and heartfelt gratitude to my thesis supervisor, ***Prof. Rajiv Prakash****, School of Materials Science and Technology, IIT (BHU), Varanasi, for his valuable suggestions, exceptional guidance, kind encouragement, and constant support that made this research possible. His unwavering belief in my abilities inspired me to persevere through the challenges I faced during this journey. His patience, wisdom, and nurturing mentorship, created an environment where I could flourish both as a researcher and as an individual. His constant motivation and scholarly perspective have been pivotal in shaping my work, and his kindness, generosity and affectionate personality have left a lasting impression on me. It has been an honor and privilege to work under his guidance, and I carry forward his teachings with gratitude and respect in my heart.*

I would like to express my sincere gratitude to my co-supervisor, ***Dr. Bhola Nath Pal****, Associate Professor, School of Materials Science and Technology, IIT (BHU), Varanasi, for his invaluable support and guidance throughout my research journey. His knowledge and constructive feedback have significantly shaped my work and helped me navigate the challenges I faced during this journey. His expertise, advice, and patience have been invaluable to me, and I truly appreciate the time and effort he invested in my work.*

Acknowledgement

I consider myself fortunate to have had you both as exceptional mentors, and I look forward to applying the knowledge and skills I have gained under your guidance in my future endeavors. Thank you for playing a pivotal role in my academic development.

I am also grateful to ***Prof. V.N. Mishra****, Professor, Department of Electronics Engineering, IIT (BHU), Varanasi, for providing experimental facilities during the course of research work. I want to express my sincere thanks to RPEC members* ***Dr. S. K. Mishra*** *and* ***Prof. I. Sinha*** *for research advice and valuable suggestions from the beginning to the successful completion of my research.*

I am sincerely grateful to ***Prof. D. Pandey, Prof. P. Maiti, Prof. C. Rath, Prof. Akhilesh K. Singh, Dr. C. Upadhyay, Dr. A. K. Mishra, Dr. Sanjay Singh, Dr. Nikhil Kumar, Dr. R. Panwar*** *and* ***Dr. U. Shankar*** *from the School of Materials Science and Technology, IIT-BHU, Varanasi, for their insightful discussions and suggestions during seminars.*

Many of the results presented in this thesis would not have been attainable without the constructive feedback from anonymous reviewers that allowed me to refine my work. Their critiques have not only enhanced my writing but have also instilled in me a greater level of patience and perseverance in my scientific endeavors.

My acknowledgment would be incomplete without recognizing my lab seniors, who taught me the intricacies of lab culture and modeled the resilient spirit necessary for navigating the challenges of research. I extend my thanks to ***Dr. Monika Srivastava, Dr. Narsingh Raw Nirala, Dr. Ashish Kumar, Dr. Neeraj Giri, Dr. Rajiv Kumar Pandey, Dr. Uday Pratap Azad, Dr. Chandan Kumar, Dr. Vinita, Dr. Vineet Kumar Mall, Dr. Ravi Prakash Ojha, Dr. Nikhil Verma and Dr. Aniruddha Jaiswal, Dr. Shweta Pal and Dr. Priya Singh*** *whose support particularly during research discussions, proved to be both beneficial and instrumental in the successful completion of this work.*

Acknowledgement

Additionally, I would like to acknowledge my fellows and juniors ***Ankit Verma, Prashant Kumar, Shivam, Nupur, Rajpal, and Preetam*** *for their supportive behavior. I would also like thank my friends* ***Sameeksha, Pooja, my roommates Akansha Di and Saloni*** *for their support and encouragement have been a source of strength during difficult times. Furthermore, I appreciate all those whose names I could not mention but who have assisted me directly or indirectly throughout this journey.*

My heartfelt thanks also extend to all non-teaching staff of the School of Materials Science and Technology, IIT (BHU), and the Central Instrument Facility Center (CIFC) for their cooperation at all levels.

I owe a profound gratitude to my grandparents, ***Shri Mool Chandra Gupta****,* ***Smt. Ram-murti Gupta****, and parents* ***Shri Rajesh Chandra Gupta****,* ***Smt. Sadhna Gupta*** *for their unwavering love and support throughout this journey. I cannot express enough my appreciation for my sisters,* ***Shikha Gupta*** *and* ***Shiksha Gupta*** *for their continuous support, love, and encouragement.*

Lastly, I gratefully acknowledge the Ministry of Human Resource Development (MHRD) and our institute for providing the necessary funding and fellowship to pursue my research work.

This journey would not have been possible without the blessings of "Lord Shiva".

DEDICATION

TO THE GOD

For the shower of blessings throughout the journey and successful completion

TO MY BELOVED PARENTS AND FAMILY

For their love, support and encouragement

TO MY RESPECTED SUPERVISORS

For their sincere guidance, motivation and encouragement

TABLE OF CONTENTS

TABLE OF CONTENTS

TABLE OF CONTENTS

TABLE OF CONTENTS

TABLE OF CONTENTS

LIST OF FIGURES

LIST OF FIGURES

LIST OF FIGURES

LIST OF FIGURES

LIST OF FIGURES

LIST OF FIGURES

LIST OF TABLES

LIST OF EQUATIONS

LIST OF ABBREVIATIONS

Abbreviation	Details
AFM	Atomic Force Microscopy
FTM	Floating Film Transfer Method
FETs	Field-Effect Transistors
HOMO	Highest Occupied Molecular Orbital
LUMO	Lowest Unoccupied Molecular Orbital
LOD	Limit of detection
MOS	Metal-Oxide-Semiconductor
MW	Molecular Weight
MOSFET	Metal Oxide Semiconductor Field-Effect Transistor
OTFT	Organic Thin Film Transistor
OFETs	Organic Field-Effect Transistors
P3HT	Poly(3-hexylthiophene)
PANI	Polyanilines
PBTTT-C14	Poly[2,5-bis(3-tetradecylthiophen-2-yl)thieno[3,2-b]thiophene]
ppm	Part per million
PQT-12	Poly(3,3”’-dialkylquaterthiophene)
QDs	Quantum Dots
SAED	Selected Electron Diffraction Pattern
SEM	Scanning Electron Microscopy
SMU	Source and Measuring Unit
TEM	Transmission Electron Microscopy
TFT	Thin Film Transistor
UV-Vis	Ultraviolet-Visible
XRD	X-ray Diffraction

LIST OF SYMBOLS

Symbol	Abbreviation
Au	Gold
Cu	Copper
α	Absorption Coefficient
C_{ox}	Capacitance per unit area of insulator
CV	Capacitance-Voltage
L	Channel Length of Transistor
W	Channel Width of Transistor
R^2	Correlation Coefficient
I_{DS}	Drain to Source Current
V_{DS}	Drain to Source Voltage
E_F	Fermi Energy Level
m	slope
σ_{rms}	root-mean-square deviation
R	Gas Response
V_{GS}	Gate to Source Voltage
μ	Mobility
t_{ox}	Oxide Gate Thickness
SS	Subthreshold Swing
SiO_2	Silicon dioxide
V_{th}	Threshold Voltage

Preface

The emergence of the Internet of Things (IoT) will significantly increase demand for sensors and actuators, which are essential physical components that are used in many different applications. Devices that respond to different gases in the environment are recognized as gas sensors. Since industrial processes, safety, and environmental monitoring are becoming increasingly crucial, there has been a steady increase in demand for gas detecting sensors across a range of fields.

π-conjugated materials are typically used as the active gas sensitive layer in organic semiconductor gas sensors, serving as both a transducer and a receptor. A three-terminal field effect transistor (FET) or a two-terminal resistor could be the device configuration. Among them, the main advantage of using organic thin film transistor (OTFT) as a gas sensor is its exceptional properties like smaller size, signal amplification, accumulation and depletion mode investigations, including the variation in threshold voltage and field effect mobility, allowed it to be employed as a multi-parametric gas sensor. However, it was necessary to optimize the active layer material which is due to the thickness, microstructure and processing dependent response of the conducting channel of OTFT that determines the gas detection performance.

This thesis presents the development and characterization of ammonia gas sensors designed to detect ammonia (NH_3) at low concentrations. The prime objective of this study is to investigate the performance of the gas sensor in terms of sensitivity, selectivity, stability, and response/recovery times, under varying environmental conditions. The outcomes of this study contribute to advancing the field of gas sensing technology, particularly in the context of ammonia detection, where there is an emergent need for cost-effective, instantaneous, and portable solutions.

Preface

This thesis work is briefly discussed in 7 chapters in which ***Chapter 1*** includes the introduction of different classes of chemical gas sensors, NH_3 gas sensors and their application in different areas. Besides, it is also discussed about different classes of materials and devices that are used for electronics based chemical gas sensors. Particularly organic materials that have been used as the sensitive layers of OTFT device architectures are discussed in detail. In addition, it also discussed the fabrication technique of OTFT channels, charge transport in OTFT channels etc.

Chapter 2 summarizes the material synthesis that has been used in this thesis work. This discussion includes stepwise experimental techniques for the fabrication of OTFT sensor devices like facile thin film deposition procedure called floating film transfer method (FTM) and electrode deposition via thermal evaporator. Besides, this chapter also discussed the characterization of the materials and OTFT sensor devices including optical, structural and electronic characterizations.

Chapter 3 has been discussed about an Organic/inorganic heterojunction (PBTTT–C14/MoS_2-QDs) thin film deposition via an inexpensive and simplistic FTM thin film fabrication technique that has been used as conductive channel of an OTFT and ammonia sensitive layer of the sensor. The synthesis section of this chapter has explored the hydrothermal synthesis of MoS_2-QDs along with characterization, and the device fabrication followed by the formation of nano-composite based ammonia sensitive layers. In which heterojunction depleted zones cover a very significant part of the surface of the OTFT channel. This depleted zone of the film is more reactive to NH_3 gas that can effectively enhance the sensitivity of the device. Therefore, the sensitivity of the designed OTFT sensor in accumulation and depletion modes is examined with the important parameters. Additionally, the sensing mechanisms have also been discussed.

Conclusively, this heterojunction based OTFT sensor designed in a very easy and economical way, which can meet all the requirements needed for its practical utilization as an NH_3 sensor.

The motivation of ***Chapter 4*** is the adoption of a related quantum dot as WS_2-QDs that has higher band off-set compared to the MoS_2-QDs to form a wider depletion region in the organic/inorganic heterojunction thin film. Since WS_2 has higher energy CB w.r.t the CB of MoS_2, therefore WS_2 has a higher band off-set with PBTTT-C14 that is supposed to form a wider depleted region. That may provide better sensitivity compared to PBTTT-C14/MoS_2-QDs based sensors. Initially material synthesis, device fabrication with characterization is discussed in this chapter. Enhanced ammonia sensitivity, different important parameters in accumulation/depletion modes and device physics has been explored along with the sensing mechanism. In this chapter broadband photosensitivity of the device is also tested due to the photo-electrical conversion capability of the WS_2-QDs. Conclusively, this OTFT sensor is fulfilling the majority of the basic requirements for its use as a NH_3 sensor and broadband photo-detector in real-world applications.

Chapter 5 presented an Organic homo-junction based thin film transistor fabrication for improved NH_3 detection. A good-poor mixed solvent has been used to dissolve the PBTTT-C14 polymer that produces a fractional part of the film by crystalline fibrillar polymer on air-liquid interface. Polymeric fibrillar morphology for its higher specific surface area may provide additional sites for the ammonia molecule interactions. Ammonia detection is determined from the drain current variation with NH_3 concentration in both accumulation and depletion modes. Additionally, the variations in currents are quite linear with the ammonia concentration. The change in key parameters of the OTFT sensors and other sensing results are also explored.

Chapter 6 includes a synthesis method of Li-based high k-dielectric film for low-operating voltage OTFT fabrication. This work utilizes the fibrillar polymer layer as NH_3 sensitive film of the sensor as described in the previous chapter. The introduction of high-k dielectric with homo-junction of the polymer tuned the ammonia sensitivity of the sensor, which is compared with the previous study. In addition, the broadband photosensitivity of this device is also examined. The aim of this study is to design an affordable, low-voltage operating, solution-processed OTFT device based NH_3 sensor and photo sensor which can meet basic requirements for practical use.

Chapter 7 presents a summary of the research findings conducted during the course of the investigations. The primary objective was to explore the sensitivity, selectivity, and stability of the sensor in response to ammonia (NH_3) gas and the outcomes verified that the ammonia-sensing capabilities of organic/hetero-junction and homo-junction based OTFTs appeared promising. The future scope of this huge study is further outlined in this chapter.

Chapter 1

Introduction and Literature Review

1.1. Introduction

In recent decades there has been a significant amount of research on organic electronics due to their affordable, lightweight, easily processed nature and mechanical flexibility [1-3]. There has been demonstration of a variety of devices, such as organic field-effect transistors (OFETs) [4, 5], organic light-emitting diodes (OLEDs) [6], photo-voltaics (OPVs) [7] and bio (chemical) sensors [8, 9]. OLEDs, which were designed for solid-state lighting and flat panel display applications currently, exist in consumer electronics, such as mobile phones, automotive audio systems, and other devices. The evolution of organic thin-film transistors (OTFTs) is aimed at utilizing them in disposable electronics and display backplanes, including RFID tags, smart cards, and sensor arrays. Photo-voltaics (OPVs), which includes solar cells and photo-detectors have also drawn significant research efforts and advanced to a great extent during the last decade [10, 11].

In the expanding electronic industries, organic semiconductors have become crucial for producing inexpensive, flexible, and portable electronic components. The efficiency of organic semiconductors is intimately correlated with their purity, crystallinity, and molecular packing much like that of typical inorganic semiconductors. The formation of organic semiconductor crystals is ascribed to weak van der Waals interactions among molecules, unlike inorganic semiconductor crystals that rely on covalent bonds between atoms [12, 13].

Organic semiconducting films possess flexible intermolecular forces, enabling the development of innovative electronic devices that are impractical with traditional, brittle inorganic semiconductors [14]. Over the past several decades, significant progress has been made in the synthesis of both n-type and p-type organic semiconductor channels. These materials can be processed through vapor deposition or solution-based methods and have demonstrated higher

on/off ratios and charge carrier mobilities compared to those of amorphous silicon (on/off ratio ~ 10^5 and charge carrier mobility ~1 cm^2/v.sec.) [15, 16].

1.2. Conducting polymers

Conducting polymers, a unique group of materials in which the creation of lightweight electronic devices with relatively easy processing compared to their inorganic equivalents attained enormous attention. They have recently gained attention in the wearable electronics industry due to their flexibility and minimal stiffness when conducting electricity. In 1977, the work "Synthesis of Electrically Conducting Organic Polymers: Halogen Derivatives of Polyacetylene, (CH)x" in "Chemical Communications" established a novel discipline of chemistry, "Electrically Conducting Polymers". Alan J. Heeger, Alan G. MacDiarmid, and Hideki Shirakawa's discovery of polyacetylene, a conductive material similar to metal, changed the way people think of polymers. In recognition of their transformative contribution, **the Nobel Prize in Chemistry 2000** was awarded jointly to **Heeger, MacDiarmid, and Shirakawa** for "the discovery and development of electrically conducting polymers [17]. The discovery that plastics and polymers may carry electricity has led to important advancements in research. Later, several additional conjugated polymeric materials and their derivatives were discovered to be electrically conductive [18-22]. Polyaniline (PANI), polypyrrole (PPy), and polythiophene (PTh) are the most studied polymers due to their diverse electrical conductivity, ease of synthesis, exceptional redox characteristics, inexpensiveness, stability, and potential relevance in energy storage, super-capacitors, gas sensors and as corrosion resistant materials [23-27]. Some of the examples of commonly used organic semiconductors are given in Fig. 1.1.

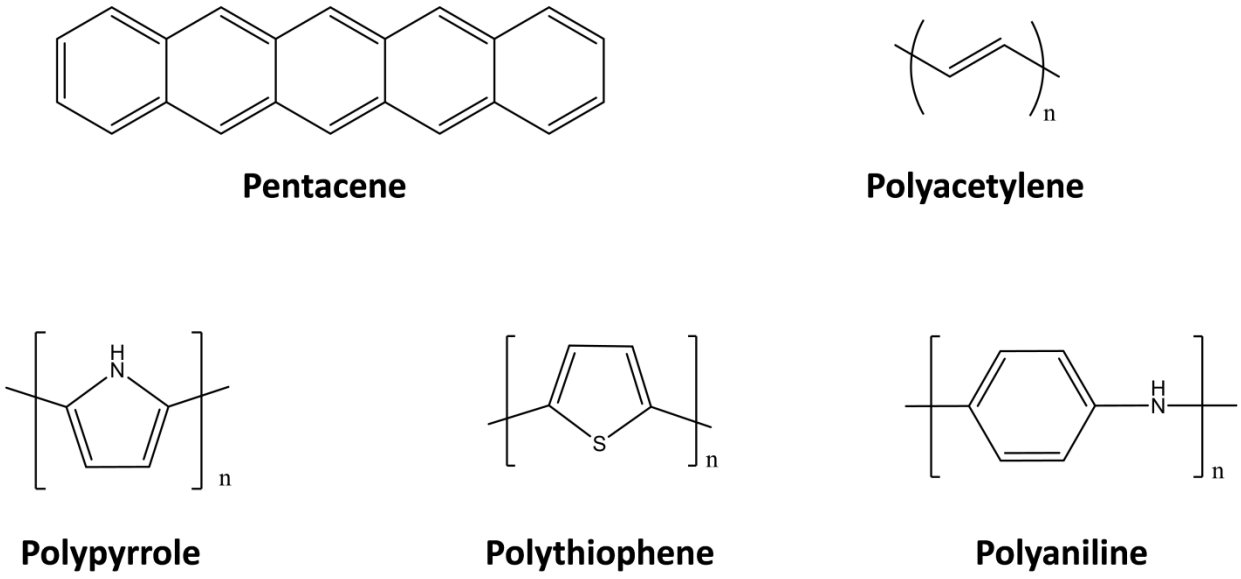

Fig. 1.1. Examples of the some commonly used organic semiconductors.

Using conducting polymers to create nano-composites has gained popularity in recent times. Such nano-composites are two-phase systems with at least one phase having nanometer-sized dimensions. Hybrids of organic polymers (like PANI, PPy, PTh etc.) with metal oxides and carbonaceous materials are extremely interesting nanocomposite systems [28-31]. Combining conducting polymers with nano-structured particles can create polymer nano-composites with unique properties, making them ideal for new and innovative applications. These nano-composites can take several forms, including nano-fibers, nano-rods, and thin films etc. [32-34]. The potential to tune the electrical conductivity of conducting polymers over several orders of magnitude by varying the synthetic parameters (dopant, solvent, oxidation states and synthetic processes etc.) is one of the most fascinating characteristics. Conducting polymers can be easily oxidized or reduced due to their extensive π-systems. Controlling the oxidation and reduction processes allow for exact changes to the optical and electrical characteristics of these polymers.

1.2.1. Intrinsic π-Conjugated polymeric materials

Conjugated polymers are organic polymer molecules consisting of alternating single and multiple bonds (double bonds). The π-electrons in double bonds are distributed throughout the polymer chain, not just over a single C atom. Such organic polymers can conduct current in their intrinsic form and are commonly used as solution processable organic semiconductor for various electronics device applications including OTFT, OLED etc. It is known that the electronic interactions between the unit cells of a polymer lead to the creation of electronic bands. The lowest unoccupied levels are recognized as Lowest Unoccupied Molecular Orbital (LUMO), which is akin to the conduction band, while the highest occupied electronic levels make form a valence band referred as Highest Occupied Molecular Orbital (HOMO), which is akin to valence band. The intrinsic electrical properties of these materials are dependent upon the width of the band gap (Eg), which is the forbidden energy band between the HOMO and LUMO.

1.2.2. Thiophene-containing conjugated polymers

Among the most commonly employed building blocks for conjugated polymer production is the thiophene ring, which has garnered significant attention from researchers as potential active elements in organic electronic devices. Since thiophene chemistry has been well-established and explored for a long period of time, extensive and fascinating structural variants allow for the tuning of the electrical characteristics in a broad range.

Early studies on substituent-free polythiophenes were conducted in the 1980s for FET applications, and the results showed only 10^{-5} cm^2/Vs of mobilities [35]. Several PT derivatives have already found usage throughout the field of electronics, and many are being investigated for

potential application in electronic devices. The basic chemical structure of some polythiophene derivatives are displayed in Fig. 1.2.

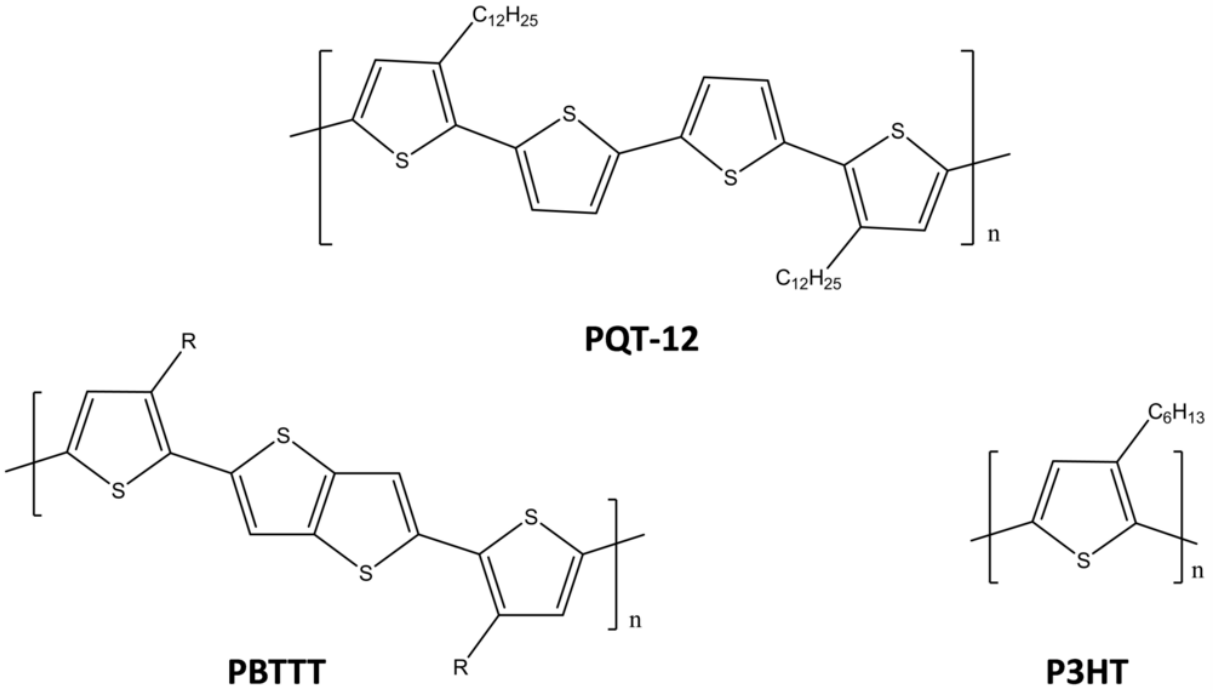

Fig. 1.2. Basic chemical structures of polythiophene derivatives.

1.2.3. Charge transport in organic semiconductors

Organic semiconducting materials are generally classified into small molecules and conductive polymers. Since polymers have higher molecular weights than their counterparts, their mobility is observed to be lower. The semiconductor grains need to be larger in order to get greater mobility. The potential to create conducting characteristics is maintained by conjugated polymers, which are sp^2-hybridized linear carbon chains. The carbon atom is in a double bond with the sp^2-$2p_z$ structure. The creation of a σ bond is caused by the intramolecular contact of two carbon atoms overlapping their sp^2-orbitals [36]. On the other hand, two p_z-orbitals result in π and π* (bonding and anti-bonding) orbitals.

The localization of states brought on by non-crystalline structure and the presence of imperfections have an impact on organic materials. The hopping of charges among these localized and discrete states of a molecule is the process that produces conduction. The standard models of charge transfer can be expanded and modified because they are amorphous in nature. Multiple trapping and release (MTR) and variable range hopping (VRH) models are commonly used to describe charge transfer in organic materials.

Charge hopping between localized states overcomes energy differences by phonon emission or absorption. Miller et al. studied the rate of single phonon jumps to mimic hopping in inorganic semiconductors [37]. Vissenberg et al. [38] studied how energy distribution and hopping distance affect carrier mobility in amorphous transistors. The multiple trapping and release model assumes that extended states are accessible to charge transfer. However, most injected carriers entrap on multiple occasions in confined states within the forbidden gap. The release of carriers thermally through theses states results in effective mobility, as defined

$$\mu_{Ef} = \mu_0 a exp\left(-\frac{E_{tr}}{K_b T}\right) \quad (1.1)$$

Where, μ_0 is the material's intrinsic mobility, K_B denotes the Boltzmann constant, Etr represents the energy level of a single trap, and T is the temperature.

1.3. Evolution of thin film transistor (TFT)

The technology of thin film transistor has advanced rapidly during the last few years, particularly in large-area, large-scale, low-temperature production. Recent technological developments in thin film transistors (TFT) suggest the availability of new information appliances in the future that will complement modern information infrastructures and lifestyles. Approximately thirty

years ago, thin-film transistors were first made available for the use in liquid crystal display applications. The main benefits of thin-film transistor technologies over conventional silicon complementary metal-oxide-semiconductor (CMOS) transistors are their direct integration onto a range of flexible substrates due to their capacity to be produced on large substrates at lower processing temperatures and at low-priced per unit area [39].

Despite being patented in 1925 by Julius Edger Lilienfeld and in 1934 by Osker Heil, the field effect transistor concept only received significant attention in the late 1970s. Examining numerous device architectures and semiconductor materials, the thin film transistor (TFT) was forced to take second place due to competition from silicon-based metal oxide semiconductor field effect transistors (MOSFETs). The early 1970s observed scientists considering alternatives to crystalline silicon due to the need for economical electronics for large-area applications. TFT technology is therefore a leader in this situation. The three scientists Spear, Ghaith, and LeComber first described TFT in 1979 using hydrated amorphous silicon as a semiconductor material. The use of active channel layer material is then modified in a number of ways by technology in order to obtain notable switching ratios and carrier mobility. Since the mid-1980s, silicon-based TFTs have effectively impacted large area liquid crystal display (LCD) technology and have grown to be the key component of organic light emitting diode and active matrix LCD applications. Meanwhile, organic semiconductor channel layer-based TFTs with electron mobility comparable to hydrated amorphous silicon are launched in the 1990s [40]. It appears that this kind of TFTs could be an appropriate match for integration on flexible substrates. However, they also have lower carrier mobility, which restricts their use in circuits that need to operate at high current and fast speed.

1.3.1. Architecture of thin film transistor (TFT)

There are four OTFT configurations exist based on the manner in which source, drain and gate electrodes are arranged in relative to the semiconductor layer. Based on the electrode positions, TFT may be designed into four fundamental structures: bottom gate bottom contact (BGBC), top gate top contact (TGTC), bottom gate top contact (BGTC), and top gate bottom contact (TGBC).

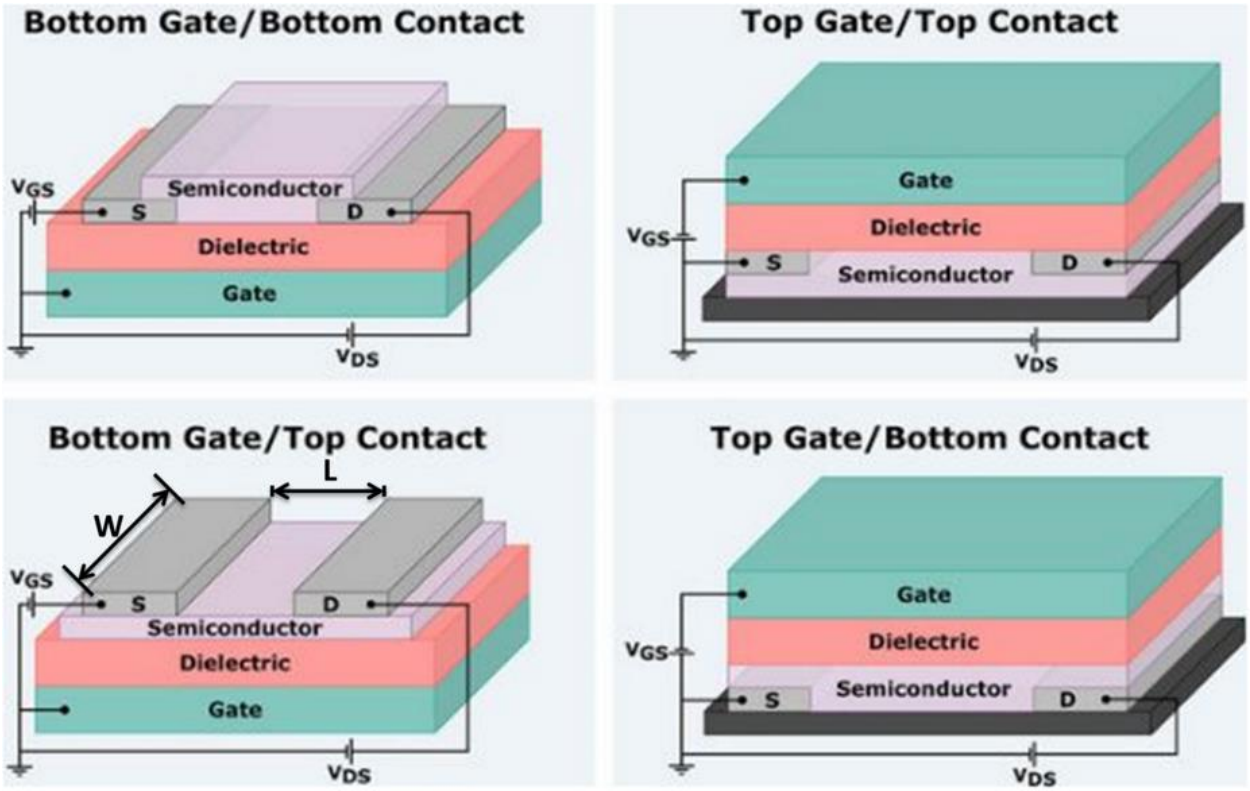

Fig. 1.3. TFT configurations: (a) Bottom-gate bottom-contact; (b) Top-gate top-contact; (c) Bottom-gate top-contact; and (d) Top-gate bottom-contact (image credit) [41].

It is fascinating that different TFT configurations (Fig.1.3.) can use the same materials and have remarkably distinct device characteristics. Thin film transistor is a unique category of field effect transistor that is manufactured by depositing thin films onto a supporting substrate that include the dielectric layer, active semiconductor channel, and metallic contacts.

A thin film transistor resembles a plate capacitor made up of an organic semiconducting layer and a gate electrode. In the operation, when a gate voltage is pulsed, a conductive channel is created when the carriers gather close to the interface between the organic and dielectric layers. Following the injection of carriers into the organic layer from the source electrode, transport occurs to the drain electrode via the conductive channel. Fig. 1.4 displays a more comprehensive illustration of the TFTs' operating concept.

1. **Linear regime:** The concentration of charge carriers in the transistor channel is constant when source-drain bias is not applied. Applying a small source-drain voltage ($V_D \ll V_G - V_T$) causes the charge concentration to be distributed.
2. **Pinched off:** The channel is "pinched off" when the source-drain voltage is raised to a point where $V_D = V_G - V_T$. In the conductive channel close to the drain electrode, there is no longer any potential difference between the gate and the drain electrode; this is termed as the "pinched off" voltage. Additionally, a depletion area forms close to the drain electrode, where no charge carriers remain.
3. **Saturation regime:** Although increasing the source-drain voltage further causes the depletion region to expand and the channel to slightly shorten, it does not significantly enhance the current. The transistor functions in the saturation regime in this situation.

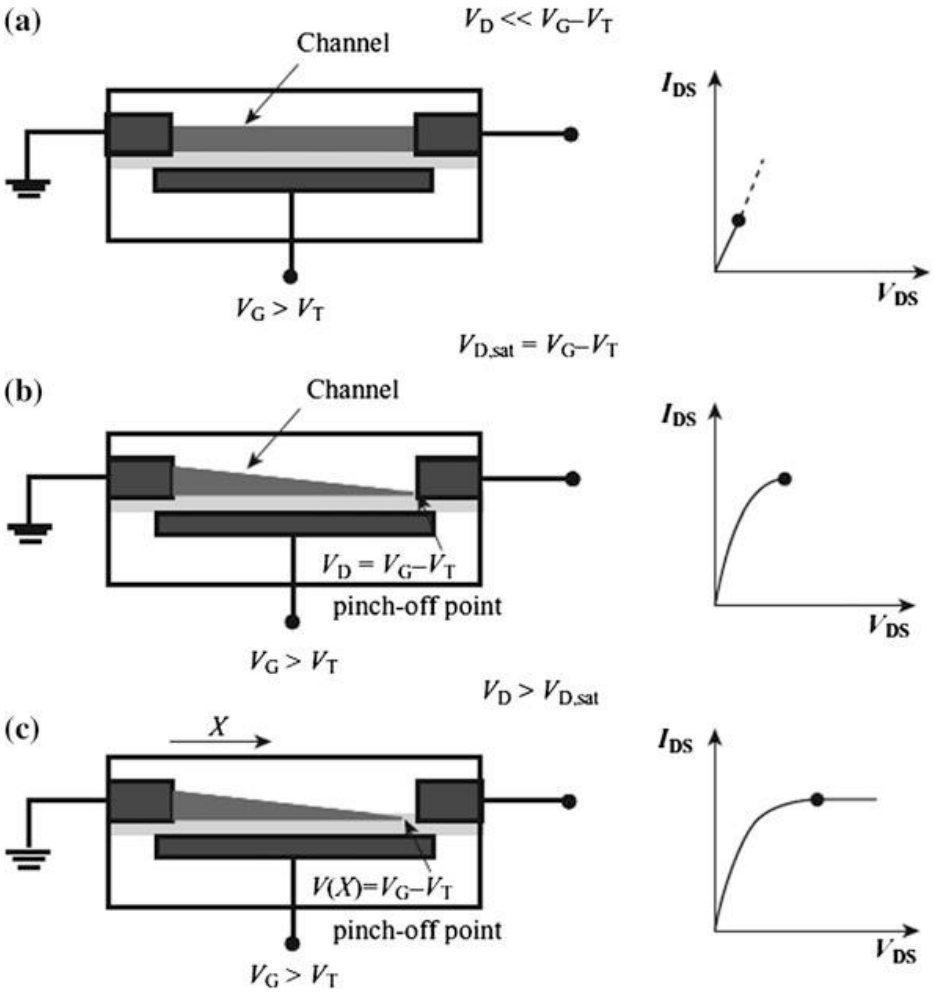

Fig. 1.4. Schematic work principles of thin film transistor: (a) linear regime; (b) start of saturation regime at pinch-off; (c) saturation regime and corresponding current–voltage characteristics (image credit) [42].

The electrical properties of TFT are typically measured using two characteristics and four device parameters.

These two electrical characteristics (Fig. 1.5) are:

1. Output characteristics (I_{DS}-V_{DS})
2. Transfer characteristics (I_{DS}-V_{GS})

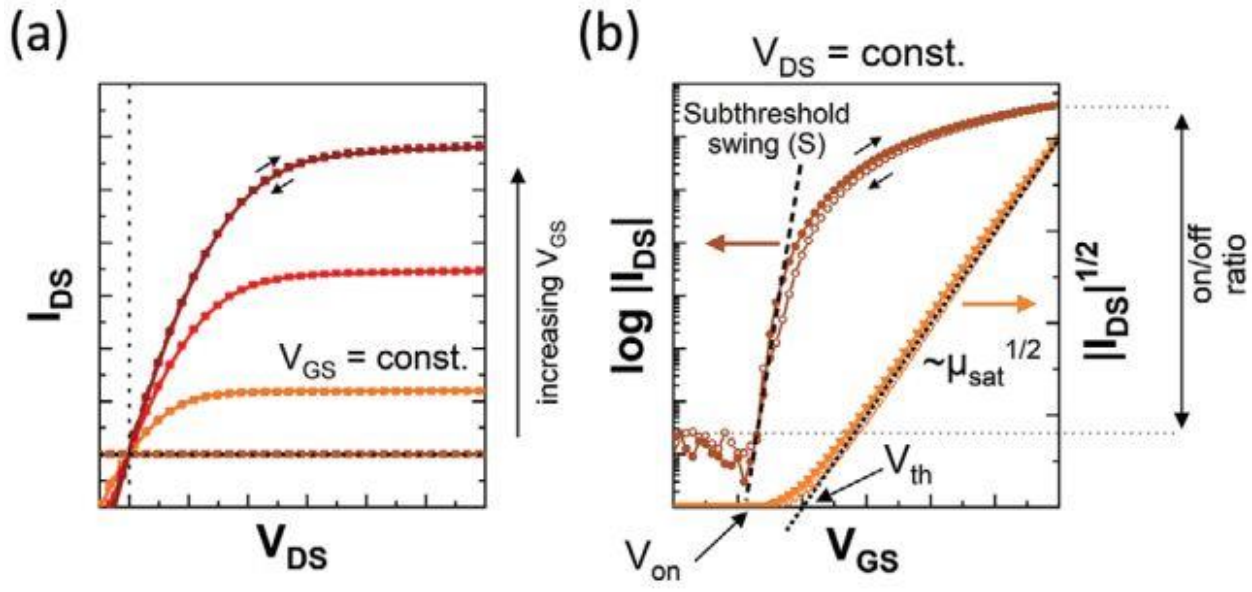

Fig. 1.5. Typical (a) Output characteristics and (b) transfer characteristics of a TFT to extract the device parameters (image credit) [43].

And four device parameters are:

1. **Charge carrier mobility (μ):** It represents the drift velocity of the carrier at the unit electric field. μ can be divided into two categories: the commonly utilized charge carrier mobility of the saturation regime and the charge carrier mobility of the linear regime. The two μ classifications are determined using the following equations:

For linear regime $$I_{DS} = \frac{W\mu C}{L}(V_G - V_{Th})V_D \quad (1.2)$$

For saturation regime: $$I_{DS} = \frac{W\mu C}{2L}(V_G - V_{Th})^2 \quad (1.3)$$

Where, μ is the field-effect mobility, W is the channel width, L is the channel length, and C is the insulator's capacitance, V_G is the gate voltage, V_{Th} is the threshold value, and V_D is the drain voltage.

2. **Current ratio (Ion/Ioff):** The ratio of the highest possible on-state current value to the lowest possible off-state current value. OTFTs typically exhibit on/off ratios ranging from 10^4 to 10^6.
3. **Threshold voltage (V_{Th}):** The minimum gate voltage essential to turn on the transistor is termed as the threshold voltage. Typically the value of V_{th} is 0 V to 0.4 V for OTFTs.
4. **Subthreshold slope (SS):** The subthreshold slope is a crucial factor in device performance. It is a measurement of the effectiveness with which a voltage differential applied to the gate can turn off the transistor. It is typically expressed as the reciprocal value of the subthreshold swing Ss-th.

$$S_{S-th} = \ln(10)\frac{kT}{q}\left(1 + \frac{C_{\text{dep}}}{C_{\text{ox}}}\right) \quad (1.4)$$

Where, kT/q is the thermal voltage, C_{ox} is the gate oxide capacitance and C_{dep} is the depletion layer capacitance.

TFTs can be operated in either enhancement or depletion mode, depending on whether a gate voltage is needed to initiate channel conduction. The channel conductance is low for an enhanced mode of operation, when there is no gate voltage applied. For this mode to be accomplished, the channel must have a low carrier density. In the case of an enhancement mode, a channel must be created. The channel is enhanced as the gate source voltage rises. Then, the drain current flows when voltage is applied between the drain and source terminals. In contrast, the drain current will flow for zero gate source voltage in the depletion mode if the drain source voltage is applied.

1.3.2. Organic TFT (OTFT)

Organic thin film transistors (OTFTs) are gaining interest due to their potential uses in smart cards, flexible screens, and ID tags. The first organic transistor, developed in 1984, uses an electrolyte as the gate media [44]. Tsumura et al. reported the first OTFT in 1986, and it demonstrated clear transistor behavior [35]. Because of its simpler fabrication method, OTFTs are gaining popularity in comparison to traditional silicon technology.

The OTFT has multiple functional layers of organic semiconductor (OSC), gate dielectric, and electrode that contribute considerably to its operation. The device's effectiveness depends on its layers; therefore selecting the right materials and ensuring compatibility are essential throughout assembly. The OSCs play an essential character to the OTFT's performance since charge transport happens there. Consequently, to enhance the performance of OTFT, high-quality OSCs are required. The two primary groups into which OSCs can be divided are small molecules and conducting polymers. There are two common methods for depositing the OSC layer including solution-based procedures and vapor deposition. When it comes to OSCs, p-types OSCs have higher mobility than n-types. This happens because of the small band gap and low work function of materials in p-type OSCs resulting in a lower hole injection barrier compared to electron injection [45]. Additionally, electron transport can lead to charge trapping in the OSC layer, thus impacting the OTFT's performance [46].

Significant progress has been achieved in the past decade to create new organic semiconductors that will enhance transistor performance [47-49]. Stability, effective charge injection at the contacts, ordered molecular arrangement of the semiconductor channel, and the interface of metal and dielectric with semiconductor are some significant performance influencing elements that are improving over the time to fill the gap for their commercial applications. Several

research investigations have been performed to use small molecules and polymers as the active layer of OTFTs.

1.4. Conjugated polymer thin film deposition methods

One of the fundamental procedure for easily and extensively preparing organic electrical devices is solution processing. Compared to Si-based electronics, organic electronics have an advantage since their processing feature makes the process both energy-efficient and inexpensive. However, arbitrary mixing and molecular alignment during solid phase condensation results in a range of film morphologies in organic-semiconductor films made using the solution technique. The most popular technique for creating CP thin films is spin coating, yet their use is still restricted on an industrial scale by issues including high material waste and surface roughness [50]. Meanwhile, a number of thin-film fabrication methods have been developed, including capillary action [51], flow coating [52], and slide coating [53] etc. For the large-scale manufacture of organic electronic devices, intriguing issues like an easy fabrication method with thickness homogeneity and the ability to fabricate multilayer thin films still need to be resolved.

As the film morphology changes the electronic characteristics also varies significantly. Therefore, the process of casting, which creates the film of organic semiconductors, is very essential in maximizing the potential of these materials. The inherent anisotropy of OSCs with respect to their geometric and electronic structures is linked to the origin of this diverse film morphology. So, in order to utilize the benefit of its anisotropy, the CP orientation methodology with an easy and rapid approach is highly demanded. In this thesis work, the Floating Film

Transfer Method (FTM) has been used for depositing CPs that has been used as a conducting channel of OTFT. A concise description of this method is specified in the following section.

1.4.1. Floating Film Transfer Method (FTM)

A unique thin film fabrication approach, to offer a cooperative solution to issues with the spin-coating and other methods is the Floating Film transfer method. Floating thin film deposition of CPs from low boiling point (BP) solvents, such as chloroform, onto an orthogonal liquid substrate, not only improves device performance, besides it also helps attain molecular orientation for several CPs with potential applications in anisotropic optoelectronics [54, 55]. The technique holds significance because it uses a liquid substrate to cast thin films. A homogenous film is formed by the mobile surface that liquid substrate gives the solidifying components to join with one another. Specifically, after spreading the solution on the liquid substrate, floating-film solidification occurs instantly if a volatile solvent like chloroform is utilize for the casing solution. In this instance, a floating film formed during spreading and solidification, which caused the film to compress due to the movement of the liquid substrate and result in an orientated floating film. Numerous variables, including the solvent's volatility, the solution's spreading speed, and the material's solidification speed, will impact the orientation properties in dynamic FTM. Earlier a great number of research shows the orientation of π-conjugated polymers has a direct relation with molecular packing that influences device performance[56].

It has been shown that the aligned conjugated polymers display superior charge transport capabilities in electronic devices w.r.t the amorphous phase of those polymeric films [57, 58]. Therefore, these FTM grown films are expected to improve device performance significantly w.r.t the conventional spin coating thin films.

1.5. Applications of OTFTs

Organic semiconductors offer new prospects for lightweight, flexible, and environmental friendly electronics. They provide greater flexibility for shaping, manufacturing, and customization than inorganic materials. Organic compounds with π-π bonding have higher conductivity for holes and electrons [59] [60]. OSCs have revolutionized our understanding of electronics by offering a substitute to traditional inorganic-based devices and enabling ultrathin, lightweight, and flexible devices due to their special characteristics of electrical, chemical, and mechanical capabilities. Organic materials have become competing substitutes for photovoltaic cells (OPV), organic light-emitting diodes (OLEDs), and organic thin-film transistors (OTFTs) [6, 61, 62]. Particularly, OTFT provide a straightforward platform in terms of construction and is suited well with flexible circuits, inexpensive radio-frequency identification (RFID) cards, and biological or chemical sensors in particular [9, 49, 63].

OTFT-based sensors are commonly utilized for a range of applications, such as drug delivery, food preservation, in-situ medical diagnostics, environmental monitoring, and the detection of chemical warfare agents. Aside from organic materials, electronic detection-based sensors are perfect for an extensive variety of detection applications, ranging from big biological molecules in complex settings to diluted compounds in vapor.

A chemical binding event can be easily measured, amplified, analyzed and it can be converted into an electric signal. These sensors offer an alternative to costly, heavy equipment with lengthy sampling and analysis times that limits current technologies. Instead, they can lead to low-cost, portable detection units that consume less power and should be easy to integrate with other devices. These different applications of OTFTs are summarized in Fig. 1.6.

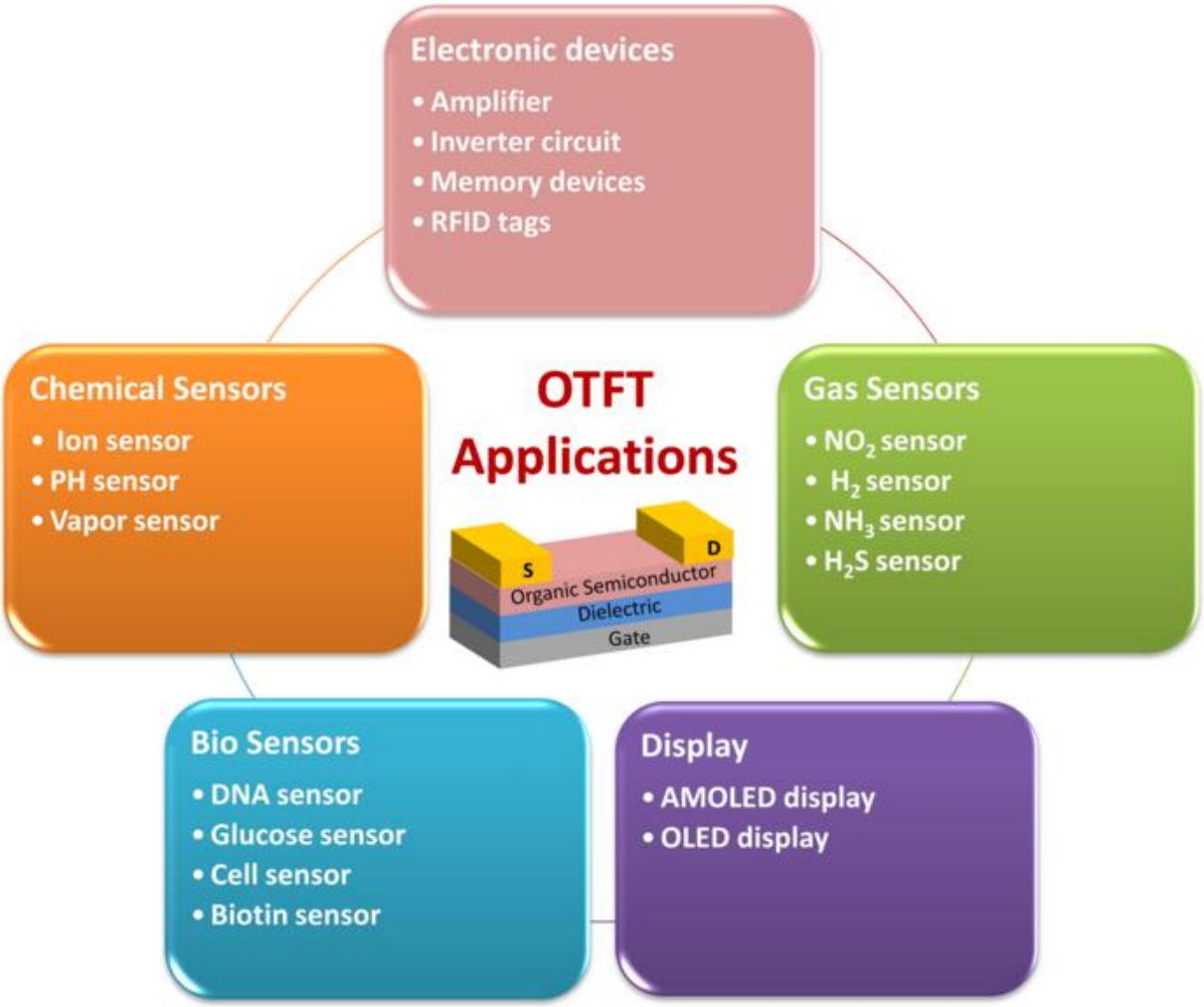

Fig.1.6. Summarizes the typical OSCs for OTFT applications.

The progress of novel and highly sensitive sensors has become imperative due to the growing worries about the protection of the environment and living things, as well as the widespread need for extremely accurate process monitoring. The unique redox chemistry of conducting polymers and their nano-composites has led them be considered as noble sensing materials. Hybrid materials incorporating CPs and a range of inorganic components including carbons (graphene and carbon nano-tubes), metal nano-particles, and metal oxide nanostructures also exhibit

enormous potential for highly developed sensors because of the modulation of redox features, improved surface adsorption, and electronic interactions. In terms of construction and design, organic thin-film transistors (OTFT) provide an easy-to-use platform for electronic sensors by which a chemical binding event can be easily measured, amplify, analyzed, and converted into an electric signal.

1.5.1. Gas sensors

Rapid industrialization and the world's population growth are major contributors to the rapidly rising levels of air pollution, which have harmful effects on both the human health and the environment. Notably, the World Health Organization's (WHO) 2018 air quality database reports that 7 million people die annually as a result of living in hazardous environments where 9 out of 10 people have exposure levels to toxic chemicals over the allowed limits [64]. The primary cause of the environmental changes leading to a raise in temperature of the Earth, is air pollutants such NO_2, COx, and CH_4 etc. In addition to polluting gases, the environment also contains a number of other dangerous gases, such as NH_3, H_2, and H_2S, which can explode when combined with air in specific amounts. In addition to these poisonous gases, another class of dangerous chemicals that poses a risk to human health is the vapors of several volatile organic compounds (VOCs), including ethanol, toluene, formaldehyde, acetone, and triethylamine (TEA). Thus, sensing of these gases is essential for environmental study, medical diagnosis, industrial emission monitoring, agriculture, public protection and safety. Gas sensors that are highly sensitive, portable, and cost-effective are therefore in high demand.

Traditional methods of gas leak detection, which generate devices that give off an auditory alert to aware people to harmful or toxic gas leaks, are essentially unreliable because of the need for precise real-time investigations of the gas concentration. However, from the past few decades,

centuries have been utilized numerous gas sensor technologies such as catalytic, optical, electrochemical, semiconductor and acoustic gas sensors to detect different gases. A number of factors determine the performance characteristic of each sensor, such as selectivity, sensitivity, detection limit, reaction time and recovery time.

Metal-oxide sensors (MOSs) have been commercially successful for a number of useful applications, such as hand-held ethanol sensors for cases of drunk driving, hydrogen and methane sensors for the protection of laborers in mines and industries, and gas sensors for acetone and toluene that are used to diagnose lung cancer and diabetes [65]. For these real-world sensing applications, SnO_2, TiO_2, WO_3, ZnO, CuO, CdO, and In_2O_3 have all received a lot of attention. These all kind of gas sensors has a high sensitivity; however their relatively high operating temperature requires more cost for maintenances and operations. Thus, in recent decades, new alternatives have been investigated as sensing materials to address the abovementioned problems, such as carbon nanomaterials (CNMs) [66-68]. CNMs can reach great sensitivity because of their large surface area for absorption. CNMs, or carbon nanotubes, graphene, and its variants, have excellent electron transport qualities and minimal electronic noise. Additionally, CNMs gas sensors allow for fast UV light recovery. Furthermore, their durability makes them perfect for creating flexible and portable devices that are highly sensitive [69-71]. Despite pristine CNMs having a lot of benefits, they also possess several noteworthy disadvantages, like poor repeatability, low selectivity, and non-uniformity of the functional groups on graphene derivatives or CNT walls [72, 73]. The 2D inorganic materials have a number of advantages, including ultra-high surface area, surface functionality, high stability and solution-based processibility [74, 75]. Nevertheless, these materials have drawbacks, like the fact that they are poisonous and non-biocompatible. Owing to these

constraints, there is a significant emphasis within the scientific community on investigating organic semiconductors [7, 76].

The novel conception that plastics or polymers can conduct electricity gave rise to a fascinating field of study, and substantial progress has been made in this area. Later, it was investigated that a wide variety of added conjugated polymeric materials and their derivatives exhibited electrical conductivity [18, 22, 77]. Among these polymers, researchers are most interested in polyaniline (PANI), polypyrrole (PPy), and polythiophene (PTh) because of their extensive array of electrical conductivity from insulating to metallic, their ease of synthesis, special redox properties, good stability, affordability, and potential uses in a range of industries, including supercapacitors, gas sensors, corrosion protection, and energy storage [78, 79].

Due to the redox characteristics, PANI, PPy, and PTh are commonly employed as sensing materials [80-82]. Electronic conduction can be controlled through doping or dedoping, resulting in conducting or non-conducting states. The electrical conductivity of these polymers is determined by the amount and type of dopant employed, which creates charge carriers for conduction. The conductivity of a doped polymer is affected by any analytic interactions that change the amount and charge carrier's movement along the chain, as well as hopping across chains. Chemical-vapor sensing materials rely on this fundamental chemical principle. CPs based sensors exhibit higher sensitivity and rapid response/recovery times, particularly at ambient temperatures [83-85].

1.5.2. Influencing factors of Conducting Polymers/Nano-composites in gas sensing response

Understanding the phenomena of doping and dedoping as well as the impact of adding nano-particles on the surface area and electronic features of the polymer or polymer/nano-composites is crucial for developing high performance gas sensors by conducting polymer nano-composites.

1. Electrical Conduction

A conjugated backbone of polymer facilitates the mobility of charge carriers, which is necessary for conductivity. Compared to regular polymers, conjugated polymers are more readily oxidized or reduced. Owing to the π-conjugated structure, "doping" is used to enhance electrical conductivity, which creates additional charge-carriers in the form of free electrons or holes. In this thesis work, carrier modulation of CPs thin film channel of OTFT via doping or dedoping method for detecting the analyte gas like NH_3 has been utilized.

2. Doping Process

The function of dopant is to either remove or supply electrons or works as charge transfer agents to the polymer. Doping (p-type oxidation or n-type reduction) can significantly enhance the electronic conductivity of the polymer. The doping reaction can be presented as follows:

Oxidation: $P + n\,X^+\,A^- \longrightarrow [P : n\,X^+]\,[nA^-]$ (p - type doping) (1.5)

Reduction: $P + n\,X^+\,A^- \longrightarrow [P : n\,A^-]\,[n\,X^+]$ (n - type doping) (1.6)

Where, P represents a polymer chain segment. The process begins with the formation of a soliton or polaron (cation or anion), followed by a second electron transfer to generate a dication or dianion, also known as a bipolaron.

3. Dedoping Process

Doping can also be reversed, a process known as dedoping, in which a doped polymer like p-type doped reacts with a reducing substance to return to its higher resistive state. Through a charge-transfer reaction, the dedoping agent diffuses into the polymer matrix and neutralizes the charge carriers partly of the system. The procedure could entail chemical processes that result in neutralization via charge transfer among the dedoping agent and the carbonium ion or/and dopant. Thermal treatments can also have an impact on dedoping as seen in the case of PTh. Numerous techniques, including optical spectroscopy, x-ray diffraction, electrical conductivity measurements, can be used to study the kinetics of dedoping.

4. Surface Area Aspects

The sensing signal is often caused by the functional groups on the polymer surface. Porous or meso-porous materials contain a larger amount of exposed functional groups and therefore show stronger reactions, however, inter-coiled or compressed polymeric structures will respond poorly because they have fewer unexposed functional sites. The entire surface area of the polymer nanocomposite is significantly impacted by the addition of nano-particles to the polymeric system. Conducting polymer solution-cast films usually show low porosity, while electrochemical deposition of polymers has the potential to create high porosity that can maximize the surface area [86, 87]. Under ideal circumstances, the in situ polymerization process for the creation of polymer nano-composites usually results in the polymer wrapping nano-

particles, and increasing the surface area of the sensing material that results in improved sensitivity of the sensor [88, 89].

5. Role of Environmental Conditions

The conductivity of polymers increases with rising temperature and humidity. Therefore, investigation of device performance with different temperature and humidity are very important studies. The interaction with the analyte molecules to the CPs and their adsorption on the detecting surface of the film are important processes to understand the sensing mechanism which are highly dependent on temperature. Since low temperatures are more favorable for adsorption, any increase in temperature will cause the equilibrium to shift and favor analyte desorption [90, 91]. Therefore, sensitivity decreases as temperature rises. On the other hand, because of the higher reaction rate caused by rising temperatures, the sensitivity of redox reaction-based sensors increases. In real terms, sensors are highly sensitive to humidity, and in that situation, water vapor acts as an analyte. Because the reaction of sensing material to the analyte gas and humidity is identical, the data from the sensor may be deceptive, when there is humidity present [91].

1.6. OTFT based gas sensors

π-Conjugated organic semiconductors have demonstrated a unique combination of charge-transport properties and low-temperature, solution-based processing capabilities. These characteristics have led to promising potential and play a critical role in enabling essential charge-transportation in the two-dimensional accumulation layer of a TFT. For the design and fabrication of electronic gas sensors, OTFT offers an inexpensive and accessible platform. The detection of gases with OTFTs involves a change in electronic performance when gas molecules react with the active transport layer of organic semiconductors (Fig. 1.7).

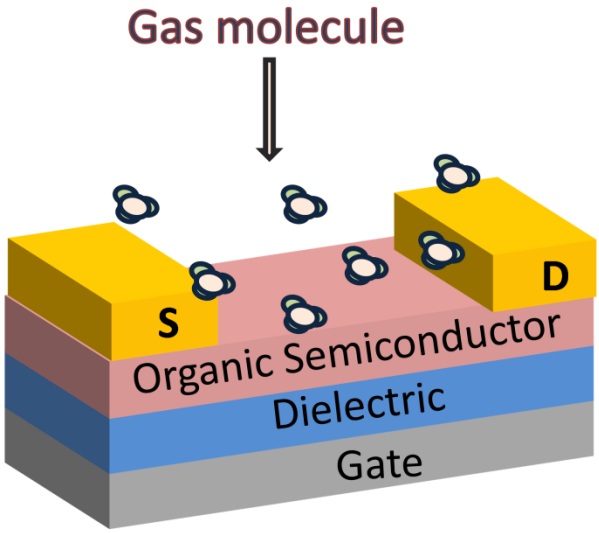

Fig.1.7. BGTC OTFT assembly with gas molecule interaction.

At constant bias conditions, in which the gate bias (V_G) and source-drain bias (V_{DS}) are fixed to facilitate current flow across the channel, are commonly used to monitor the transformation of the drain current during the exposure of analyte gas to the channel. The interaction or binding of gas molecule with the CPs of the channel that varies the source-drain current (I_{DS}), is eventually dependent on the gas concentration, and bias conditions of the OTFT [92]. Therefore, some of the important characteristics of the sensor depend on the rate of variation in drain current (I_{DS}) with analyte gas concentration under certain bias conditions that determines the quality of the sensors. The gas response of the OTFT sensor is dependent on the variation in drain current before and after the exposure of the analyte gas and is represented as:

$$R = \frac{|I_{DS,Air} - I_{DS,Gas}|}{|I_{DS,Air}|} \times 100\% \quad (1.7)$$

An advantage of transistors over conventional two-terminal chemi-resistors is the presence of an additional gate electrode, which modulates the conductivity of the sensing material and provides

an active sensing window along with integrated signal amplification. Multi-parametric analysis is also a further beneficial feature of the drain current modulation. This implies that changes in a number of parameters, including threshold voltage (V_T), conductivity, On/Off ration and mobility (μ) can be employed to monitor the analyte event.

The semiconductor film morphology, which works as the active site for the gas molecule interaction of the OTFT is a key player in gas sensing applications. Till date a number of techniques for depositing the organic semiconductor layer have been identified including the two important processes as thermal evaporation and spin coating [93]. In the case of a thermal evaporator system, the morphology of the deposited film is influenced by several deposition parameters such as substrate temperature, deposition rate, and film thickness, which have a major impact on the film properties and consequently, affect the performance of the OTFT sensor [94, 95]. However, in solution based coating the key variables that affect the film's morphology are the solvent, concentration of the polymer solution, and temperature etc.

1.7. Motivation of the thesis on Ammonia sensor

Ammonia (NH_3) is a pungent and colorless gas, which is commonly found in agricultural, industrial, and environmental contexts. It is toxic and hazardous compound that poses significant health and safety risks. When it released into the atmosphere in large quantities, can contribute to air pollution and environmental degradation. On the other hand, Ammonia, is a key chemical used in many industrial processes, including fertilizer production, and has significant potential as an energy carrier, especially for use in fuel cells or as a hydrogen carrier. Any leaks or exposure can be harmful to workers and the surrounding environment. Thus, effective detection of

ammonia is important for mitigating its harmful effects and ensuring compliance with environmental and health safety standards.

1. Environmental and Health Impact of Ammonia

Nowadays, human activity is the primary source of direct or indirect ammonia emissions into our atmosphere. Major artificial sources include intensive livestock farming, where manure decomposition releases significant amounts of ammonia and industrial processes, particularly in the production of fertilizers and refrigeration systems. Ammonia is flammable at high concentrations, which is a major disadvantage. Inhaling lower concentrations of this gas can cause soreness in the nose and coughing due to its suffocating odor. At higher concentrations, it can also cause burning sensations in the throat and nose. In severe circumstances, it might completely harm the respiratory system and can cause long-term health issues. Vytenis published documentation of an actual NH_3 explosion that occurred in West Texas in 2013, leaving 200 persons injured and 15 dead [96].

Agriculture-related emissions of atmospheric ammonia (NH_3) are a major cause of acidification. NH_3 directly affects the respiratory health of people who engage in handling animals. These health effects may include a decline in eye and throat discomfort, rise in coughing and phlegm production and lung function. According to current research, agricultural ammonia may have a direct impact on young children's early onset of asthma [97]. Ammonia is a major component of fine particulate matter ($PM_{2.5}$), which contributes to respiratory problems and other health issues. When ammonia enters water bodies, it can lead to eutrophication, which degrades water quality and harms aquatic life. Ammonia (NH_3) gas undergoes an exothermic reaction with water,

resulting in ammonia-induced corrosion in various metals, including copper (Cu), zinc (Zn), and their alloys.

2. Industrial Relevance

The global need for green hydrogen is set to expand as it plays a key role in reducing emissions, enhancing energy security and driving the transition to a sustainable low-carbon economy. In the context of green hydrogen, ammonia is often considered as a possible storage and transport medium due to its high hydrogen content. Many countries are exploring ammonia as a means to import and export hydrogen, as ammonia is easier to liquefy, store, and transport than hydrogen in its pure form. However, the production, storage, and transportation of ammonia come with safety risks, particularly related to its toxicity and potential environmental impact. This is where the global need for ammonia sensors is likely to grow significantly in the coming years and play a vital role in the widespread adoption of ammonia-based hydrogen storage technologies [98]. The importance of ammonia sensing in hydrogen storage can be understood in several key areas:

- **Safety Concerns:** If ammonia leaks into storage or transportation systems, it poses significant safety risks. Ammonia is toxic and corrosive, and its presence could lead to hazardous working conditions, so early detection and monitoring is critical to prevent accidents. By regularly sensing ammonia concentrations, it is possible to detect leaks early and reduce the risk of more severe system failures.
- **Optimizing Hydrogen Storage Systems:** Ammonia as a hydrogen carrier can be stored and transported at relatively low pressures or even in liquid form at moderate temperatures. Ammonia is synthesized and then decomposed to release hydrogen when

needed. Ammonia sensing helps to monitor the integrity and efficiency of the storage system and ensures that ammonia is released at the appropriate time for hydrogen usage.

- **Regulatory Compliance:** Many countries have stringent environmental and safety regulations for ammonia emissions, especially in industrial settings where hydrogen is stored or used. Low-concentration ammonia sensing ensures compliance with these regulations by providing real-time data on ammonia concentrations, which is necessary for reporting and controlling emissions.

Ammonia is also widely used in industrial processes, including in the production of fertilizers, explosives, refrigeration systems and in various chemical manufacturing operations. In many of these industries, ammonia is handled in large quantities, creating potential safety hazards and ammonia sensors will help in real-time monitoring of ammonia concentrations for ensuring the safety of workers and preventing accidents.

In summary, the growing need for reliable ammonia detection technologies driven by environmental concerns, industrial applications, and safety regulations, there is a need for cost-effective, portable and real-time ammonia sensors that are sensitive, selective and capable of continuous monitoring in a variety of environments. Therefore, this thesis work broadly explores and motivates the development of room temperature operating OTFT based high performance ammonia gas sensors fabricated by a low cost solution process technique. This work explores the ammonia-sensing capabilities of organic/heterojunction and homojunction based OTFTs based sensors. Moreover, the thesis chapters thoroughly examined the sensitivity, selectivity, stability and plausible mechanism of the sensor in response to ammonia gas concentrations at room temperature.

Chapter 2

Experimental Techniques and Instrumentations

2.1. Introduction

This chapter summarizes detailed explanation of the experimental techniques required for the material synthesis, and fabrication of the OTFT devices sensor along with the apparatus and instruments used for fabrication and characterization. To examine the optical, structural, and morphological features of the quantum dots, polymer and polymer/nano-composite based thin films, a brief summary of the experimental setup and characterization techniques has been explained. The optical properties of materials are examined using room temperature ultraviolet-visible (UV-Vis) spectroscopy and Fourier transform infrared spectroscopy (FTIR). For structural, and morphological investigations Transmission electron microscopy (TEM), and Atomic force microscopy (AFM) have been used.

2.2. Material Synthesis

In this thesis, a hybrid material combination, polythiophene (PTh) based conjugated polymer with transition metal dichalcogenides (TMDs) based Quantum dots (QDs) were adopted for the fabrication of OTFT based ammonia sensors. PBTTT-C14 [Poly(2,5-bis(3-tetradecylthiophen-2yl)thieno(3,2-b)thiophene] have garnered significant attention from the research society because of its advanced structural and electrical properties, which provides solution processability and crystallization for significant charge transportation in organic electronic devices. Pure conducting polymers typically exhibit low sensitivity toward the target gas. TMDs based QDs are also potential material for their adaptable surfacial functionality and distinctive feature. Both materials can be combined to develop a hybrid OTFT ammonia sensor with exceptionally high sensitivity.

In this thesis work, PBTTT-C14 (Mol. Wt. >40,000), brought from Sigma-Aldrich Pvt. Ltd, has

been utilized as CPs for OTFT fabrication. Besides, for the synthesis of MoS_2-QDs and WS_2-QDs, the hydrothermal method has been used, since this process is most frequently used for the synthesis of the TMDs based QDs and other nano-materials also. The primary focus of this thesis work is to develop an organic/inorganic hybrid p-n hetero-junction and homo-junction based high performing ammonia sensors, which can work at room temperature. Therefore, to identify a better composition of p-n organic/inorganic heterojunction that improves charge transport through the film in which hydrothermally synthesized QDs contributes as the n-type semiconductor in the polymer/QDs based heterojunction that highly enhances the overall sensitivity of the device. The hydrothermal synthesis of QDs is detailed in the respective chapters.

2.3. Device Fabrication

In OTFT device based gas sensor fabrication, the semiconductor channel plays an important role as the sensitive layer for the gas detection. In this work, an economical and facile technique called the Floating Film Transfer Method was chosen. This method requires no specialized instruments and generates minimal material waste. Before film fabrication, the substrates were cleaned by sequential sonication for 20 minutes each in deionized water, acetone, and isopropyl alcohol followed by a drying process. Fig. 2.1 displays the schematic of FTM technique. This FTM combines the Langmuir-Schaefer method with drop casting. This process involves casting a film over a liquid surface and then manually transferring the cast film over cleaned solid substrates. The FTM method requires a very high concentration solution of the material. To cast a film via FTM method, a polymer needs to dissolve in a volatile solvent (such as chloroform) which is required to float onto a non-volatile solvent that has a high boiling point. A micropipette is used to deposit a small amount (about 15 µl) of polymer solution onto the surface of a non-

volatile blend of glycerol and ethylene glycol. Chloroform immediately evaporates after spreading across the liquid blend surface. The contrast between a liquid spreading on a surface and its adherence and cohesiveness determines how the solvent spreads. During this process, it is possible to calculate the spreading coefficient (S) of a solvent over a water surface in the following way:

$$S = \gamma_{Liquid} - \gamma_{Solvent} - \gamma_{Solvent\text{-}Liquid} \quad (2.1)$$

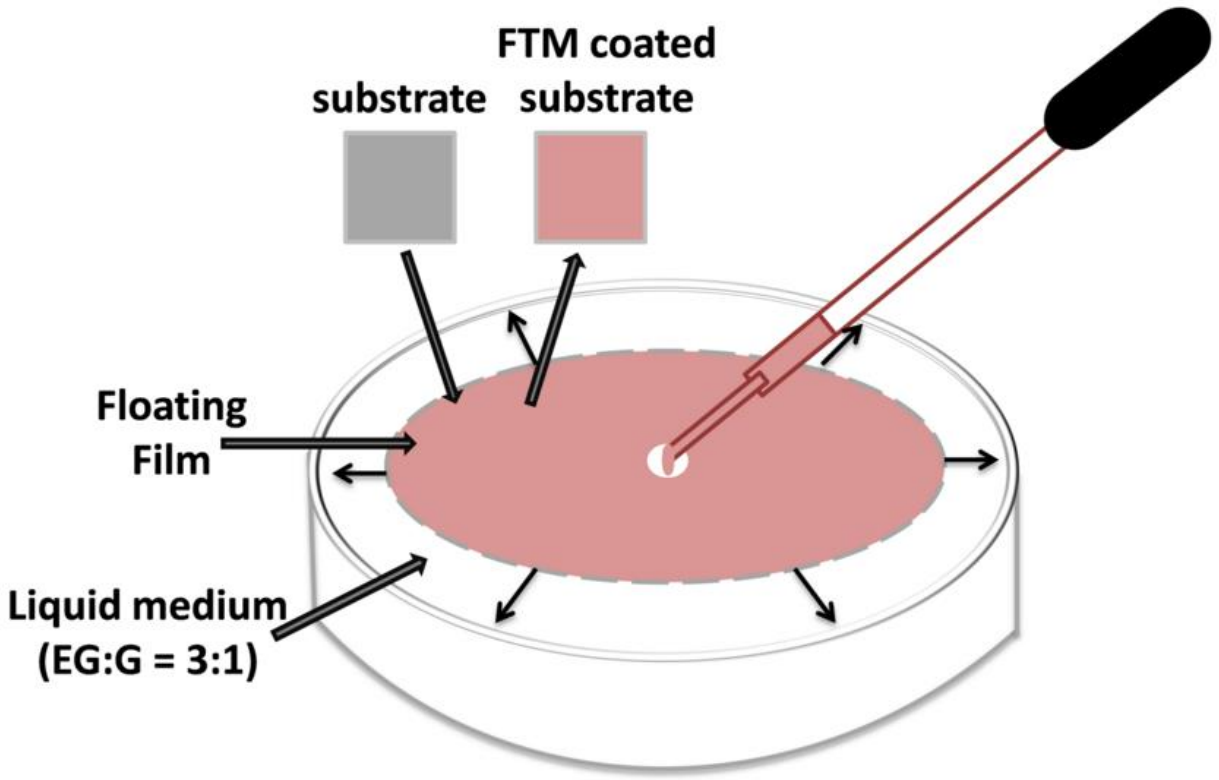

Fig. 2.1. Schematic representation of floating film transfer method (FTM) for film deposition.

where γ_{Liquid}, $\gamma_{Solvent}$, $\gamma_{Solvent\text{-}Liquid}$ are the surface tension of water, the surface tension of the solvent, and the interfacial tension between the two liquids, respectively. The spreading process is spontaneous when the spreading coefficient is positive. The spreading coefficient (S) of

chloroform can be modified by changes in temperature or by altering the solvent. After the evaporation of chloroform, the polymer molecules stay on the surface due to its immiscibility in non-volatile solvents like glycerol and ethylene glycol, and this entire process results in the production of a good film.

2.4. Characterization Techniques

2.4.1. Ultraviolet-Visible Spectroscopy

UV-Vis spectro-photometry is an analytical technique that determines the absorption or reflectance of light in the ultraviolet and visible sections of the electromagnetic spectrum (typically from 200 nm to 900 nm). A schematic figure of UV-Vis spectrophotometer is depicted in Fig. 2.2. In this process the absorption of radiation in the UV-Vis region causes atomic excitation or the transition of a molecule from a low-energy ground state to an excited state. The interaction of light with matter provides crucial information regarding the electronic structure of chemical compounds. Conjugated polymers containing alternating single and double bonds in their backbone display unique UV-Vis absorption spectra, resulting from π-electron transitions within the conjugated system. The absorption maximum in the UV-Vis spectrum is proportional to the length of the conjugated system; longer conjugation moves absorption to longer wavelengths (lower energy). This characterization technique is important for understanding its electronic properties and potential applications in photo-detectors or solar cells.

When polymers are blended with nano-particles or other materials, (for example, in nano-composites) UV-Vis spectroscopy can be employed to monitor changes in absorption spectra indicating component interactions or dispersion within the blend. In general, for polymers this

technique is very useful in assessment of functional groups, analysis of polymer blends and composites monitoring, degradation and stability etc.

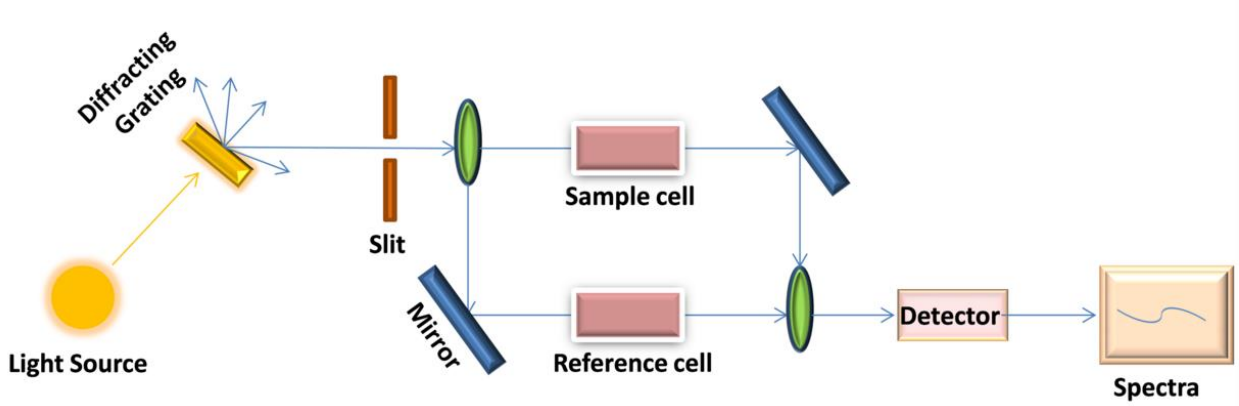

Fig. 2.2. Schematic illustration of UV-Vis spectro-photometer.

2.4.2. Fourier Transform Infrared Spectroscopy

The fundamental concept of FTIR is molecules absorb infrared light at certain frequencies that matches the modes of vibration of their bonds (C-H, C=O, N-H, etc.). The IR region is divided into three parts: near-IR, mid-IR, and far-IR. The mid-IR wave-numbers ranges from 4000-400 cm^{-1}. An absorption spectrum is produced when a sample is exposed to infrared light and its bonds absorb particular wavelengths. The Michelson interferometer (Fig. 2.3.), which includes a beam splitter, a stationary mirror, a moving mirror, a laser source, and a detector is the primary part of FTIR. Light from a source is split into two paths with the help of a beam splitter; one of the paths leads to an immovable mirror, while the other path leads to a moving mirror. An interference pattern is produced when the two beams are reflected from the mirrors and recombined at the beam splitter. This pattern is then transferred to the detector.

In Polymer Compositions**,** FTIR can be used to confirm the presence of specific monomers or additives in polymer blends or composites.

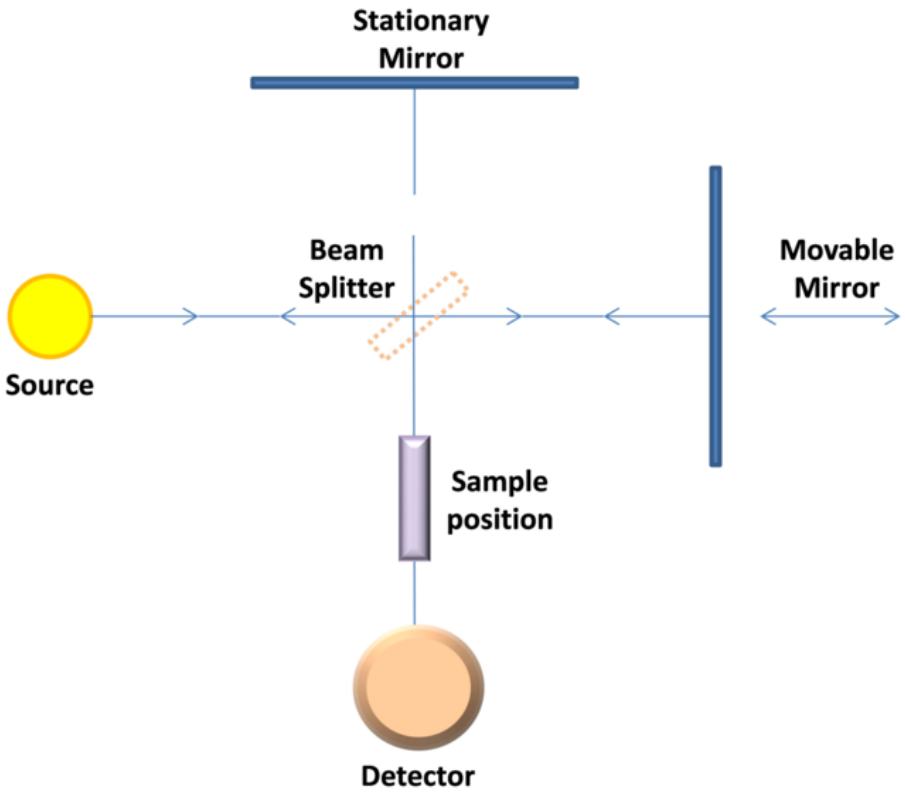

Fig. 2.3. Schematic representation of Michelson Interferometer.

2.4.3. X-ray diffractometer (XRD)

X-ray diffraction (XRD) analysis is a technique used in materials science to determine a substance's crystallographic structure. It measures the intensities and scattering angles of X-rays when a material is exposed to incident X-rays (Fig. 2.4). The results enable one to calculate the atomic distances inside the specimen's crystal lattice. XRD helps in understanding the crystalline arrangement of polymers to explain their properties. For example, polymers with a higher degree of crystallinity typically have higher tensile strength and stiffness. In polymer blends or composites, XRD can help identify interactions between different phases, phases with different

crystallinities, or new crystalline phases formed by the combination of materials. Polymers can be measured in the form of thin films, powders, or fibers. Sample preparation might involve cooling or heating to study temperature-dependent structural changes. A typical XRD scan for polymers might cover a 2θ range from 5° to 60° or more, depending on the polymer and the desired resolution. Overall, XRD is a versatile procedure for studying both the crystalline and amorphous regions of polymers, and can provide insights into their molecular structure, crystallinity, and processing behavior.

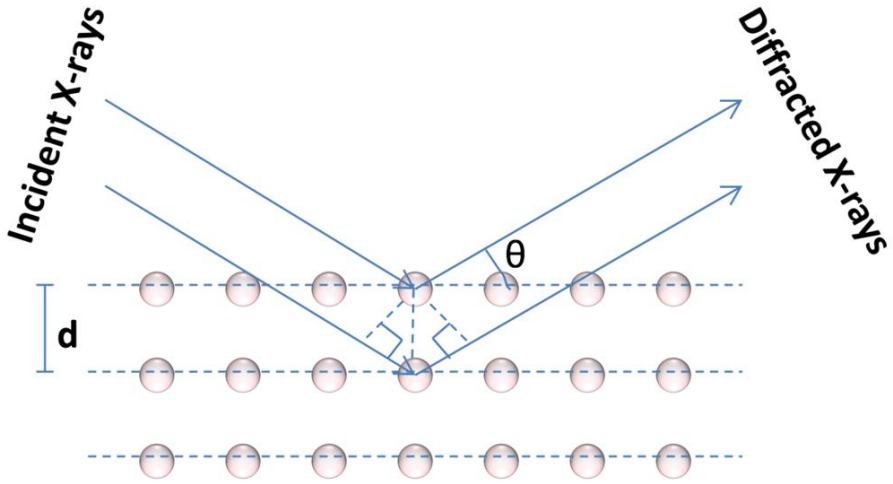

Fig. 2.4. Schematic diagram for X-ray diffraction

2.4.4. Atomic Force Microscopy (AFM)

AFM is a powerful tool for investigating the surface properties of materials at the nano-scale. AFM offers complete insights into the surface morphology, mechanical features, and nano-mechanical behavior of samples. AFM operates by scanning a sharp tip (typically made of silicon or silicon nitride) across the surface of a sample in a controlled manner. The interaction between the tip and the sample's surface is measured through the deflection of a cantilever. AFM

can be performed in several modes, each providing different information about the sample's surface. A tapping mode AFM schematic is displayed in Fig. 2.5.

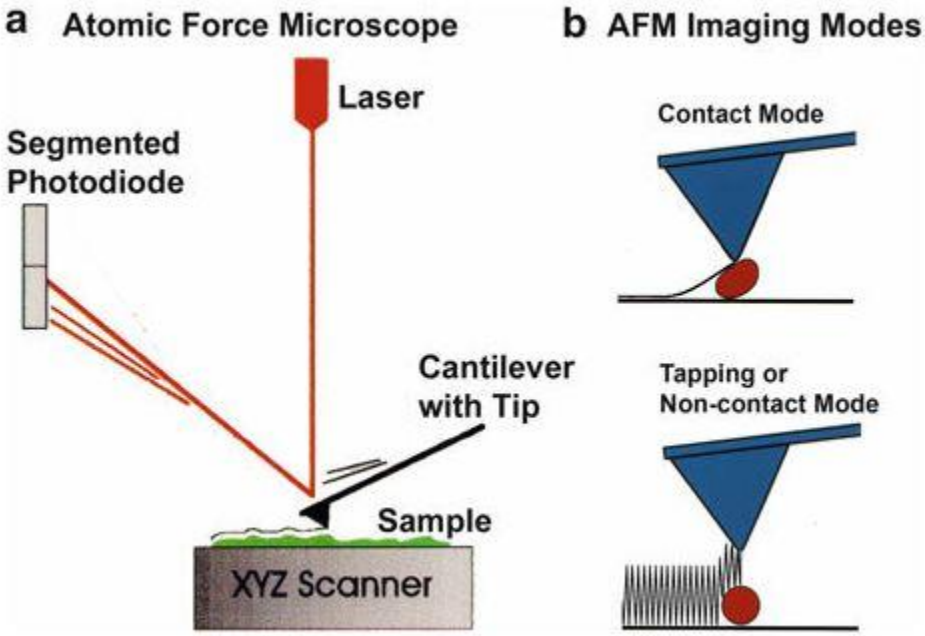

Fig. 2.5. Schematic of tapping mode AFM used for surface roughness measurements (image credit) [99].

Tapping Mode AFM is the most widely used study for polymer surface, in which the tip taps the surface without remaining in constant contact that reduces the likelihood of damaging soft or delicate polymer surface. This mode is particularly useful for studying soft polymers, allowing for the observation of surface topography without excessive force. These AFM micrographs can distinguish micro-phase separated regions in polymer blends, copolymers or nano-composites providing insights into the domain structure, size and distribution of components. Besides, AFM micrographs can reveal crystalline regions in semi-crystalline polymers by observing the periodic structures on the surface, such as lamellae. Therefore, an AFM is a useful instrument in

assessing the surface roughness, thin film morphology and adhesion features of polymer films and coatings, which is important for applications like organic electronics and photo-voltaics.

2.4.5. Transmission Electron Microscopy (TEM)

Transmission Electron Microscopy (TEM) is a powerful microscopy technique, which is used in material science for the analysis of the microstructure of materials at the atomic or nanoscale level. TEM provides high-resolution images and allows for the examination of the internal structure of materials, including phases, defects, crystallography and interfaces. In TEM, a beam of electrons is transmitted through a thin sample. These electrons interact with the material and are scattered, forming an image based on the density and atomic arrangement of the material. A TEM instrument is commonly equipped with EDX detectors, allowing for elemental investigations of the sample by detecting characteristic X-rays emitted from the material when it is bombarded with electrons. TEM can also perform electron diffraction, enabling the study of the crystallographic structure and orientation of materials. This provides important information about grain boundaries, dislocations, and other structural features.

Samples for TEM must be extremely thin (typically less than 100 nm), which often involves complex sample preparation techniques. For this thesis work, I performed TEM study of the polymer and polymer composites for their structural analysis. The thin films of the polymer or composite materials have been transferred onto the carbon coated Cu grid via FTM methods, to understand the detailed microstructure of the film that is used for OTFT fabrication.

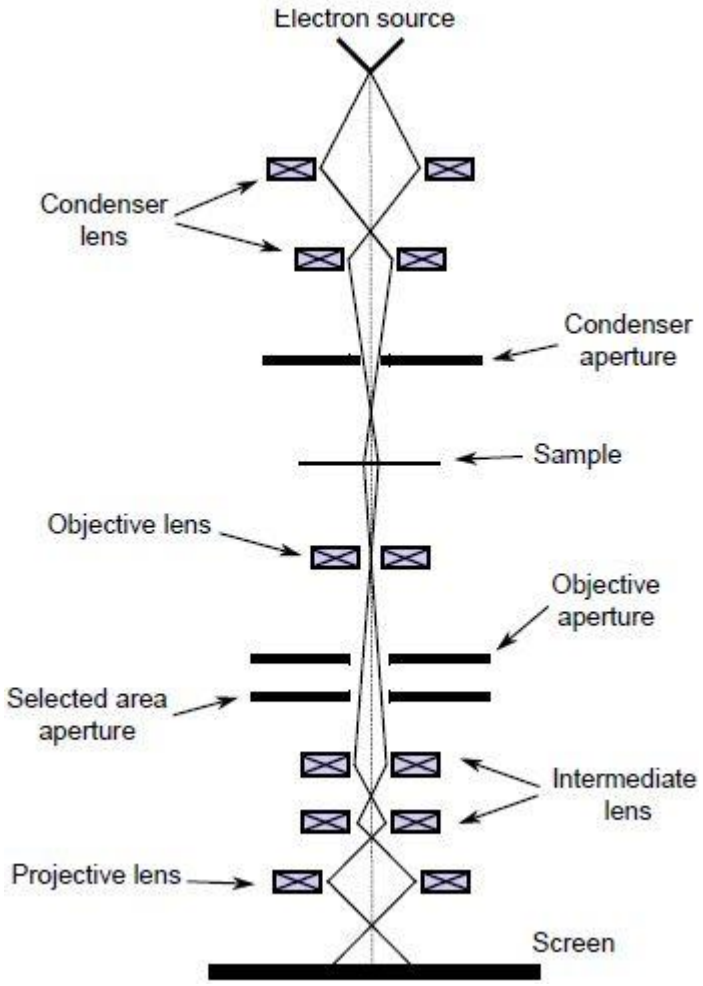

Fig. 2.6. Ray diagram of transmission electron microscope in image mode (image credit) [100].

2.5. Device fabrication

The Gas sensor device fabrication is done in the bottom gate top contact (BGTC) mode transistor configuration. The gas sensitive film is fabricated via FTM method over the Si/SiO_2 substrate while source-drain contact electrodes are deposited by thermal evaporator. These processes consist of following steps;

2.5.1. Substrate Cleaning

The Si/SiO_2 substrates were used where 300 nm SiO_2 works as a gate dielectric of the device. Before polymer or composite film deposition, the substrates are cleaned with soap solution and sonicated in an ultrasonic bath cleaner for 20 minutes sequentially in deionized-water, acetone and iso-propanol followed by the drying process in nitrogen atmosphere.

2.5.2. Polymer or composite thin film depositions

After the drying process, the polymer or polymer-composite layer is deposited via the pre-explained FTM method as described earlier.

2.5.3. Source-Drain electrode deposition

Thermal evaporation is one kind of physical vapor deposition, which is used to deposit thin films of materials onto surfaces, such as glass, metal, or plastic. This is done by evaporating the material by heating the substance to its boiling point or sublimation point in a vacuum chamber and then condensing the vapor onto the surface. This process requires careful control of temperature, pressure, and other factors. This technique can be used to deposit a large range of materials, including metals, insulators, and semiconductors. The thickness of the film or coating is in Angstroms to microns range and can be a single material or multiple layers of the different materials. Fig. 2.7 represents a schematic diagram of vacuum chamber of a thermal evaporation system.

In this method, materials are heated to an elevated temperature on the filament in order to evaporate them at lower pressure of about 10^{-6} Torr. An electric variac (current controller) is employed to monitor the filament's temperature. The vacuum inside the chamber is created by

diffusion pump, backed by a rotary pump. A quartz crystal micro balance is utilized to regulate the film's thickness. Thermal evaporation can produce high-purity materials with minimal contamination. This instrument has been used to deposit gold electrodes on polymer or composite thin film that works as source drain of the OTFTs.

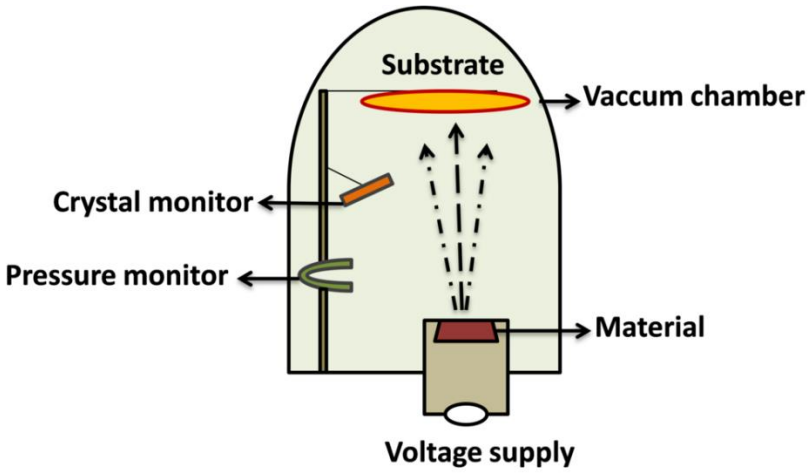

Fig. 2.7. Schematic of vacuum chamber of thermal evaporations system.

2.5.4. Gas Sensing Set-up

A controlled atmosphere gas sensing assembly is designed for the investigations of the ammonia sensing properties of the fabricated OTFT device sensors. A schematic presentation of this set-up is shown in Fig. 2.8. There are two inlets and one outflow on the gas assembly. Ammonia gas is injected through the first inlet, while dry air is injected through the second. Mass flow controllers (MFC) are used for the controlled circulation of the gases in chambers. There is a gas mixing chamber for the mixing of gases. A semiconductor parameter analyzer (Keysight, B1500A) is connected to the gas chamber via a probe station. The purpose of the exhaust pump is to flushing out air from the chamber. Ammonia gas with different concentrations is injected into the gas

chamber under the controlled flow of dry air, and the consequential variations in drain current are measured using electronic measurements.

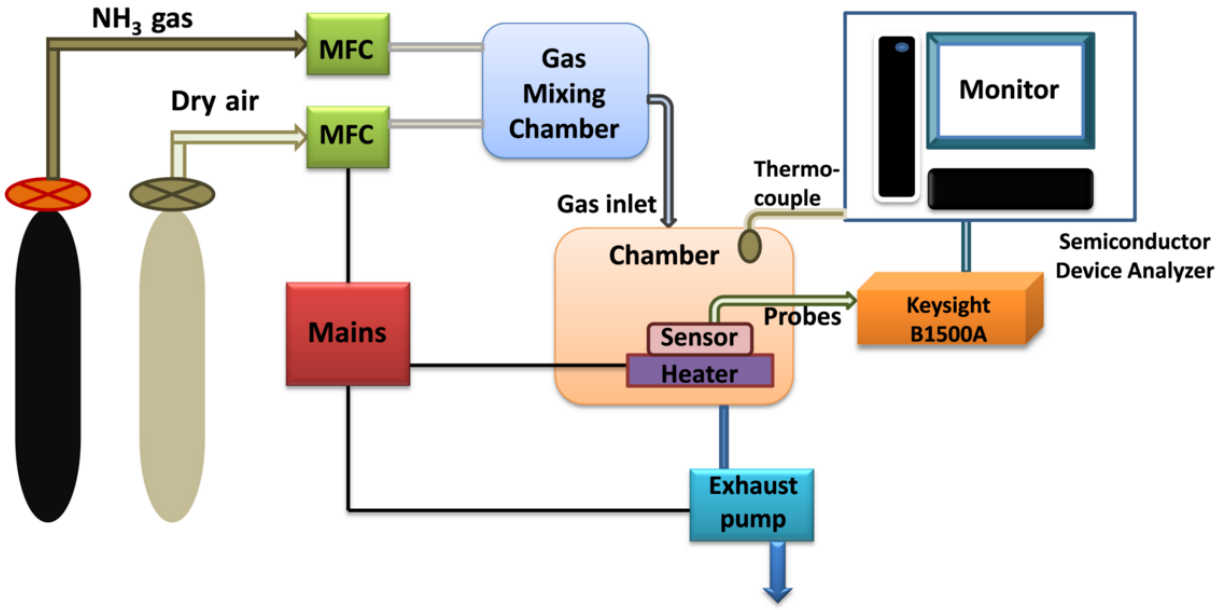

Fig. 2.8. Schematic diagram of Gas sensing set-up.

By analyzing a range of parameters with the help of gas sensing set-up, we can evaluate the performance and characteristics of gas sensors under different environmental conditions. The key parameters for gas sensing are:

- **Sensitivity** - The ability of a sensor to detect low concentrations of a specific gas. High sensitivity is essential to detect trace gases.
- **Selectivity** - The sensor's capability to detect a target gas in the presence of other interfering gases. A high selectivity ensures the sensor responds mainly to the gas of interest and not to other substances.
- **Response Time** - The time taken by the sensor to respond to a gas concentration change. A short response time is crucial for real-time monitoring of gases.

- **Recovery Time** - The time required for the sensor to return to baseline or normal readings after the gas exposure is removed. A quick recovery time is desirable for continuous monitoring and avoiding signal drift.
- **Limit of Detection** - The lowest concentration of a gas that the sensor can reliably detect. This determines how sensitive the sensor is at detecting very low levels of a gas.
- **Stability and Long-Term Performance** - The ability of a sensor to maintain its performance over time, especially under varying environmental conditions.

The above parameters help in evaluating the sensor's sensitivity, accuracy and response to various gases. These parameters collectively determine the performance and suitability of a gas sensor for different applications such as air quality monitoring, industrial safety, environmental monitoring and medical diagnostics.

Chapter 3

Depleted layer of PBTTT-C14/MoS_2-QDs heterojunction for enhanced ammonia gas sensitivity

Abstract

A highly sensitive, room temperature operating ammonia (NH_3) gas sensor has been fabricated by using PBTTT-C14/MoS_2-QDs heterojunction based organic thin film transistor (OTFT). Thin film of PBTTT-C14/MoS_2-QDs has been fabricated by low cost and high yield 'floating film transfer method' (FTM). Initially, hydrothermally synthesized MoS_2 quantum dots (QDs) were added in PBTTT-C14 polymer to make a composite ink, which was used for film fabrication. This polymer/QDs based film has been used as a channel of a top contact-bottom gated organic thin film transistor. Various concentration of NH_3 ranging from 0.5 to 50 ppm has been exposed on the channel to determine the sensitivity and the selectivity of the device. For comparison, a reference OTFT has been fabricated under the same condition by using pristine PBTTT-C14 thin film. It has been observed that the response of the polymer/QDs heterojunction device is ~ 85% at 50 ppm, which is ~ 3 times higher compared to reference device in higher concentration range of NH_3. This enhancement becomes possible due to the NH_3 sensitive depletion layer of polymer/QDs heterojunction. This OTFT sensor shows high selectivity to the NH_3 gas with good linearity to the concentration, which can fulfill basic requirements for practical utilization.

3.1. Introduction

Continuous monitoring of harmful gases produced from different industries and artificial resources becomes a major concern to control environmental pollution, particularly in high population zone [101-103]. Sometimes, human noses are ineffective for many toxic gases if they are odorless or exist in a very low concentration. A reliable gas sensor plays a vital role in monitoring the presence of harmful gases like H_2S, NO_2 and volatile organic compounds (VOCs) up to the human olfactory limit and makes the environment acceptable for the human survival [104, 105]. Among the many poisonous and hazardous gases, one of the most harmful and

colorless air contaminants is "ammonia" (NH_3) that has a severe impact on both human beings and the environment [106, 107]. Lower concentration of NH_3 may cause irritation in the eyes, nose, and throats of humans, and inhaling of an excessive amount of NH_3 vapors can lead to pulmonary edema [108, 109]. Consequently, it is crucial to monitor the existence of harmful NH_3 gas in the environment or in different workplaces. Till now, a number of inorganic oxides, different nanostructures and organic semiconductor based NH_3 gas sensors have been reported. Out of them, metal oxide based NH_3 sensors are very sensitive and show very good response. However, from the application point of view, their high operating temperature is a big concern. Single nano-crystal like nano-wire, 2D materials based gas sensor show very fast response with high sensitivity, but their fabrication cost, production yield, and tinny active area are the critical bottleneck for commercialization. On the other hand, organic semiconductor based sensor can be fabricated in larger area with high production yield and works at room temperature. Although, their long time stability, selectivity and poor response are the key issues. Therefore, a low-cost, reliable, highly sensitive and room temperature operating NH_3 gas sensor system is required for commercialization.

To opt the advantageous sides of organic, inorganic nano-structured materials, a numerous organic and inorganic nanostructure hybrids have been investigated up to this point as potential materials for gas detection [27, 110, 111]. Earlier, D. K. Bandgar et al. reported a flexible PANI/α-Fe_2O_3 based room temperature operating ammonia sensor with the response of 39% for 100 ppm with low detection limit (LOD) of 5 ppm [112]. Similarly, S. Han et al. have fabricated Poly(3-hexylthiophene)/polystyrene blends based OTFT with 52% response for 50 ppm and 5 ppm LOD [113].

In recent years, transition metal dichalcogenides (TMDs) became a very promising candidate for

chemical gas sensor study due to chemically active sites, room temperature operation, and lower power consumption [114, 115]. Among the TMDs, MoS_2 is a most widely known metal sulfide and is used as a charge donor or acceptor in several sensing applications. Higher specific surface area and strong surface chemistry improves their adsorption between it and the analyte gas, which makes them favorable material with prominent advantages for the gas detection [116, 117]. Quantum Dots (QDs) based materials on the other hand, are highly sensitive for gas sensing applications due to their distinctive properties like higher specific surface area, active edge sites, and quantum confinement effects. Its significant binding interaction with the gas molecules enhances the adsorption capability of the sensor and makes it a potential material for the detection of several kinds of hazardous gases [118, 119]. Instead of a good achievement of those organic/2D hybrid materials based chemical gas sensors, several issues need to be resolved including their faster response, higher stability, and selectivity.

In this study, a hybrid material combination of polythiophene (PTh) based conjugated polymer with TMDs based MoS_2-QDs has been adopted. PBTTT-C14 [Poly(2,5-bis(3-tetradecylthiophen-2yl)thieno(3,2-b)thiophene] attains immense interest from the scientific community due to its superior features like molecular self-ordering, π-π stacking, and alkyl side chains. These characteristics of the polymer provide solution processability in commonly available organic solvents and also induce crystallization, which offers significant charge transportation in organic electronic devices [120-122]. Compared to the other conjugated polymers PBTTT-C14 have relatively deep HOMO level resulting higher exhibition of air stability and mobility [123]. Generally, pure conducting polymers possess low sensitivity against the analyte gas. TMDs based MoS_2-QDs are also promising material for their unique functionality and adaptable surface chemistry. Merging of both the materials makes them suitable for the highly sensitive hybrid

based OTFT ammonia sensor.

Specifically, this study reports a PBTTT-C14/ MoS_2-QDs heterojunction based OTFT device for the detection of low concentration of ammonia. The chapter firstly described the synthesis of MoS_2-QDs and fabrication of the pristine polymer and hybrid polymer/QDs based OTFT device *via* facile and cost-effective technique floating film transfer method (FTM). To perform the sensing behavior, OTFT channels are exposed with 0.5 ppm to 50 ppm concentration of the ammonia that shows a very high sensitivity with excellent selectivity.

3.2. Experimental Section

3.2.1. Materials

Sodium molybdate dihydrate ($Na_2MoO_4 \cdot 2H_2O$) was obtained from Moly Chem India (purity ≥98%). L-cysteine ($HO_2CCH(NH_2)$- CH_2SH), Hydrochloric acid, and chloroform ($CHCl_3$) were attained from Merck, India. For the preparation of the reagents solution Milli-Q water is used. The organic conjugated polymer poly(2,5-bis(3-tetradecylthiophen-2yl)thieno(3,2-b)thiophene) PBTTT-C14 (Mol. Wt. >40,000) was brought from Sigma-Aldrich Pvt. Ltd. The polymer was used as received without additional purification. Ammonia gas was also purchased from Sigma Aldrich.

3.2.2. Synthesis procedure of MoS_2-QDs

In this work, the hydrothermal method was chosen for the synthesis of MoS_2-QDs, since this method is the most commonly used approach for the synthesis of the MOS_2-QDs and other nano-materials. The focus of this work is to develop an organic/inorganic hybrid p-n heterojunction based highly sensitive ammonia sensor. Therefore, MoS_2 dot was identified to form a better p-n organic/inorganic heterojunction in the composition. From that point of view, the MoS_2-QDs

have been synthesized *via* a facile and single-step hydrothermal route that can produce ligand free, chemically pure MoS_2 as represented in Fig. 3.1. For this, sodium molybdate dihydrate and L-cysteine (1:2 w/w) dissolved separately in 25 ml of Milli-Q water under constant stirring for 15 min. Afterward, both solutions were slowly mixed together under continuous stirring at a maintained temperature of 40°C to make a homogeneous solution. During this mixing, pH is maintained at ~3 with concentrated HCl.

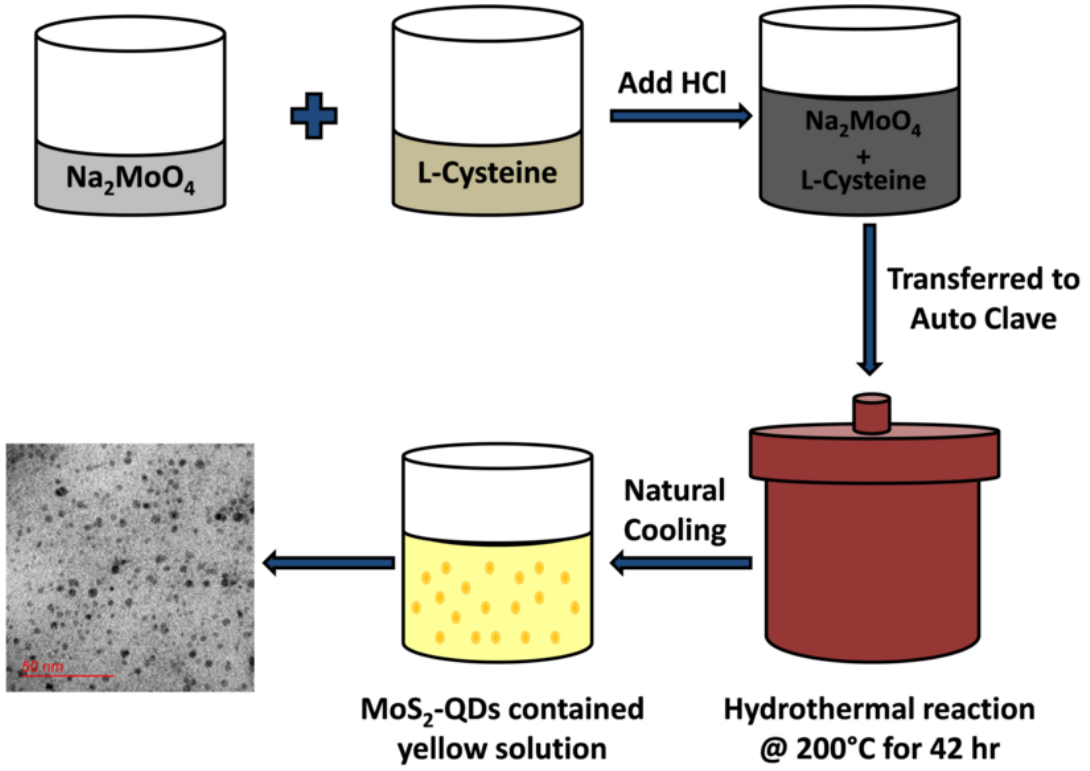

Fig. 3.1. Schematic demonstration of hydrothermal synthesis of MoS_2-QDs.

Subsequently, for the hydrothermal synthesis, this homogeneous solution is then transferred into a Teflon autoclave (100 ml capacity) lined with stainless steel and left for 42 hr at ~ 200°C in the oven. After completion of the process, the oven was allowed to cool down naturally at room temperature. Finally, a light yellowish colloidal solution of MoS_2-QDs was obtained. For the

purification process, the solution was dialyzed for about 3-4 days in a dialysis bag (Molecular Weight = 2000 Da).

3.2.3. Synthesis of PBTTT-C14/ MoS_2-QDs nanocomposite thin film

Prior to the synthesis of PBTTT-C14/MoS_2-QDs hybrid nanocomposite, the phase transfer method has been used to carry MoS_2-QDs from water to chloroform for the composite preparation, as shown in Fig. 3.2(a). The hydrothermally synthesized homogeneous aqueous solution of MoS_2-QDs is sonicated rigorously and then added with an equal amount of chloroform ($CHCl_3$). In this bi-phase immiscible solution of water and $CHCl_3$, the heavier $CHCl_3$ remains at the bottom and the aqueous dispersion remain at the top. To transfer QDs into chloroform, the immiscible solution is sonicated for 2-3 hr. After completing the sonication process, the aqueous solution has been taken out from the top and remained part is the transferred QDs in chloroform.

For the composite preparation, as shown in Fig. 3.2(a) 10 µl of the extracted solution of QDs/$CHCl_3$ was mixed in the anhydrous chloroform solution of 2 mg polymer with 10 mg ml^{-1} concentration. The composite solution is sonicated for the well dispersion of QDs in polymer. For the composite film casting, low cost and high yield floating film transfer method (FTM) has been used [124]. In this method, a small amount (~10 µl) of polymer/QDs blend was dropped at the center of a petri-dish with diameter of 15 cm, containing hydrophilic liquid substrate (ethylene glycol and glycerol with ratio of 3:1) in ambient conditions as shown in Fig. 3.2(b). As prepared film over the liquid substrate will be transferred to the desired cleaned Si/SiO_2 substrate and dried at 80°C under the flow of nitrogen for the fabrication of the OTFT.

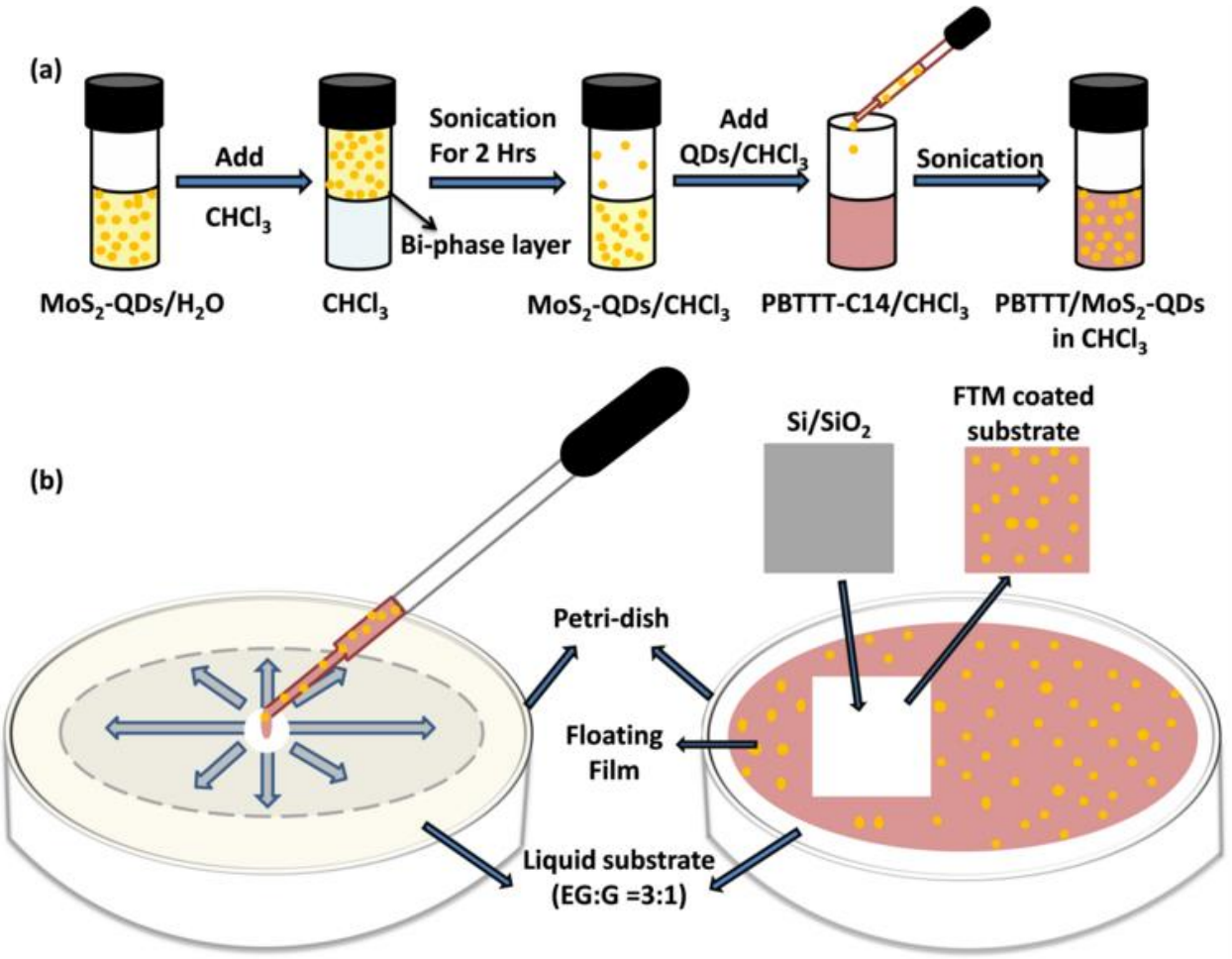

Fig. 3.2. Schematic illustration of (a) Phase transfer method to transfer MoS_2-QDs from water to chloroform; (b) FTM method for PBTTT-C14/MoS_2-QDs based hybrid film spreading on the nonvolatile liquid substrate (EG:G = 3:1) and stamping of the film on the substrate.

During this process, we have optimized the polymer/QDs solution for the film quality and the sensing performance of the device. Throughout this optimization, in our observation, higher ratio of MoS_2 leads to the breakage in the film that provides a poor device performance. Again, low concentration of MoS_2 reduces the sensitivity of the OTFT due to reduced depleted area of the film. The optimized ratio composite film over the liquid surface was transferred onto a carbon coated grid for the TEM study.

3.2.4. Device fabrication

For the bottom gate-top contact OTFT device fabrication, heavily p-doped silicon (p^+-Si) substrates are used with 300 nm thermally grown SiO_2 as the gate dielectric. Those p^+-Si/SiO_2 substrates are first properly cleaned using four different solvents, including soap solution, deionized water, acetone and isopropanol in an ultrasonic cleaner and dried at 80°C under the flow of nitrogen. After the cleaning process, the polymer/QDs layer (sensing layer) was transferred over the cleaned Si/SiO_2 substrate *via* pre described FTM technique. The formation of source-drain electrodes was subsequently deposited on the top of semiconducting film coated substrate by thermal vacuum evaporation of Au through an interdigitated shadow mask with the evaporation rate of 1.5 Å/s at vacuum 6×10^{-5} Torr. The length (L) and width (W) of the interdigitated channel were 50 µm and 18 mm, respectively.

3.2.5. Characterization

The TEM micrographs with selected area electron diffraction (SAED) patterns were obtained via TECHNAI $G^2$20 TWIN (New Zealand) over Cu grid. To achieve the absorption spectra of hydrothermally synthesized MoS_2-QDs, quartz cuvette (1 cm optical path length) was used in UV–Vis Epoch 2 micro-plate reader Biotech (USA) spectrophotometer. FT-IR analysis of QDs was done by Thermo Scientific Nicolet 6700 FTIR spectrometer (Germany). Lastly, the electrical (current-voltage) characteristics of the fabricated OTFTs were performed by a semiconductor device analyzer (Keysight B1500A). We have used a gas sensing chamber for the ammonia sensing measurement of the fabricated OTFT, as illustrated in the previous study [125].

3.3. Results and discussion

3.3.1. Characterizations of MoS_2-QDs and nanocomposite thin film

The MoS_2-QDs were synthesized through facial and single-step hydrothermal route by employing sodium molybdate and L-cysteine as the sources of molybdenum and sulfur, respectively. Synthesized water soluble QDs were characterized by TEM, SAED pattern, FT-IR, and UV-Vis spectroscopy. Fig. 3.3(a) and 3.3(b) represents the TEM images of the synthesized MoS_2-QDs, which indicates that the QDs are well dispersed in water and distributed homogeneously on copper grid. The average diameter of the synthesized QDs is 3.3 ± 0.86 nm as shown in the size distribution histogram (Inset, Fig. 3.3(a)). The SAED pattern at the inset of Fig. 3.3(b) suggests the crystalline nature of the QDs. Fig. 3.3(c) represents the FT-IR spectra of synthesized QDs, which exhibit a broad and strong peak at 3150-3500 cm^{-1} attributed to the -NH_2 and -OH stretching. A major frequency peak at 1633 cm^{-1} corresponds to the -C=O stretching vibration due to the presence of the –COOH group. The Smaller peaks at 1056 cm^{-1} and 1413 cm^{-1} were assigned to the –CN and –NH stretching vibrations of aromatic and aliphatic amines. Fig. 3.3(d) represents the UV-Vis spectra with the absorption peak at 272 nm of dialyzed MoS_2-QDs, which may be attributed to the excitonic feature of the MoS_2-QDs and also presents the surface absorbed functional group –NH_2, which can be confirmed from the FT-IR spectra [126]. The calculated band gap of MoS_2 is 4.2 eV, which is obtained from Tauc's plot (Inset, Fig. 3.3(d)). This value is higher than 2D single-layer MoS_2 (1.9 eV) and bulk MoS_2 (1.2 eV). The increment in the direct band gap energy with respect to the bulk and 2D monolayer MoS_2 is due to the strong quantum confinement effect that led to the enhanced band gap opening.

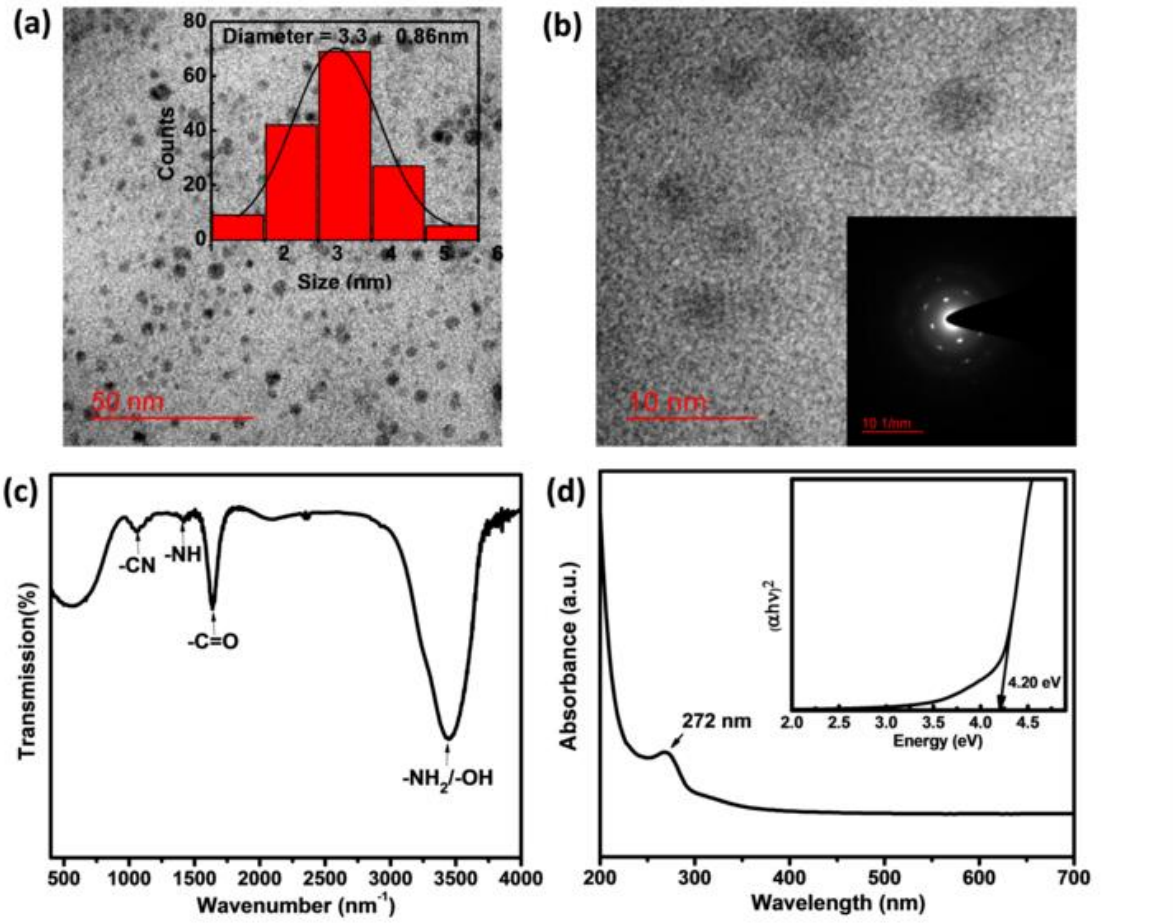

Fig. 3.3. (a) TEM image of synthesized MoS_2-QDs and size distribution histogram, (inset); (b) HR-TEM image and SAED pattern (inset); (c) FT-IR, and; (d) UV-Vis spectra and band gap (inset) of MoS_2-QDs.

For the PBTTT-C14/MoS_2-QDs hybrid nanocomposite based thin film characterization, TEM micrographs are shown in Fig. 3.4. The hybrid film has been lifted over the copper grid *via* predefined FTM method. As shown in Fig. 3.4(a), and 3.4(b), low and high resolution TEM images indicate that the QDs are homogeneously distributed on the polymer film. Fig. 3.4(c) represents the SAED pattern of the same, which is in the form of hazy ring pattern. This hazy ring pattern is due to the presence of excessive amount of polymer compared to the MoS_2-QDs.

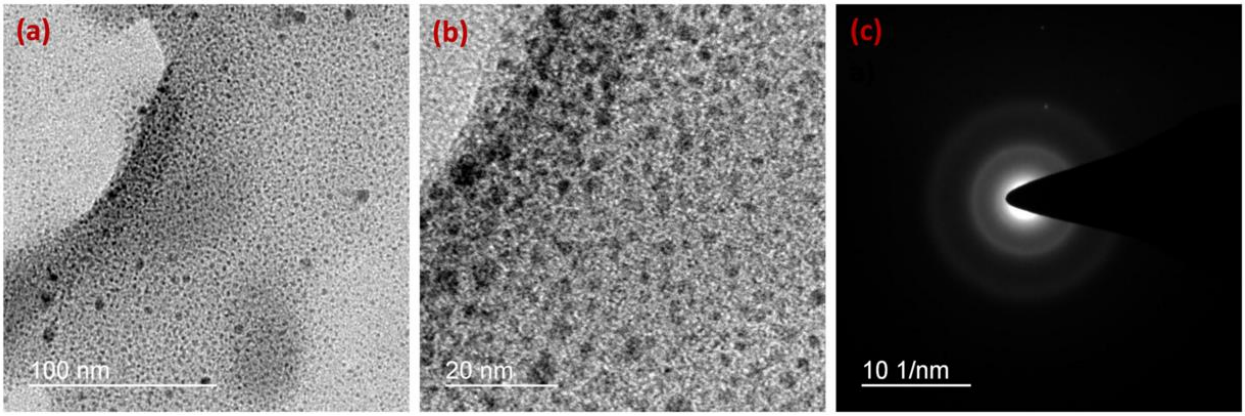

Fig. 3.4. TEM image (a) Low resolution, (b) High resolution; and (c) SAED pattern of PBTTT-C14/MoS_2-QDs FTM film casted over Cu grid.

3.3.2. Electrical Characterizations

Schematic of the assemblies, output (I_{DS}-V_{DS}) and transfer (I_{DS}-V_{GS}) characteristics of the fabricated pristine PBTTT-C14 (Device-1) and PBTTT-C14/MoS_2-QDs (Device-2) hybrid film based devices are shown in Fig. 3.5. The output characteristics (I_{DS}-V_{DS}) of the fabricated devices have been measured at 25°C (room temperature with 50% RH) under dark and plotted over the swept drain voltage range from 0 to -30 V with different constant bias gate voltages as represented in Fig. 3.5(c) and 3.5 (d). And it is found that at the fixed gate bias voltage, drain current is much higher in the polymer/QDs film based OTFT compared to the pristine polymer film. The improvement in the drain current is may be due to the intercalation of the MoS_2-QDs in the polymer matrix, which facilitates the charge transportation in the semiconducting (sensing) layer of the hybrid based OTFT. Moreover, presence of MoS_2 -QDs in polymer matrix also enhances the ammonia sensing capability of the hybrid film based transistor, which is discussed in the later section.

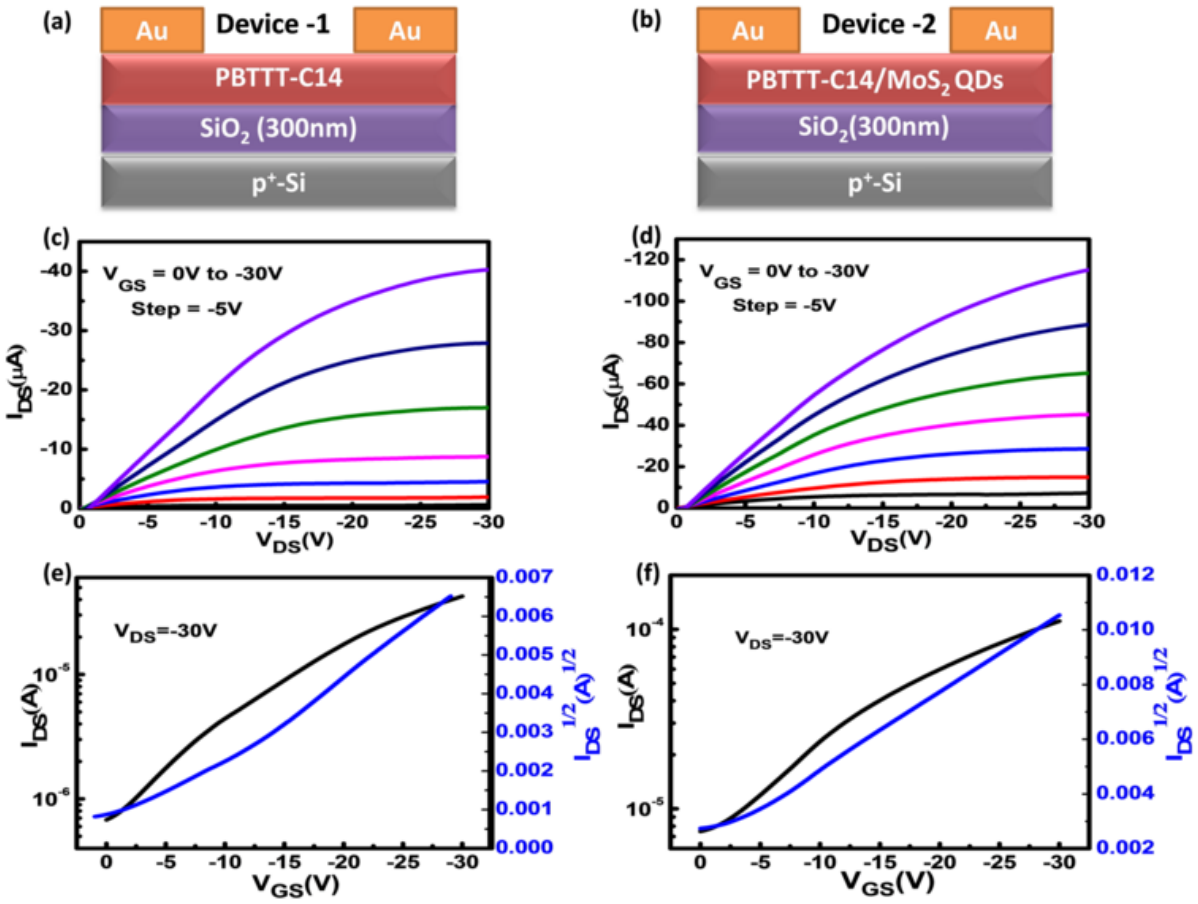

Fig. 3.5. Schematic representation of (a) pristine PBTTT-C14 OTFT (Device-1) (b) PBTTT-C14/MoS_2 -QDs OTFT (Device-2); Output characteristics (I_{DS}-V_{DS}) of as fabricated (c) Device-1 (d) Device-2; Transfer characteristics (I_{DS}-V_{GS}) of as fabricated (e) Device-1 (f) Device-2.

The transfer (I_{DS}-V_{GS}) characteristics of the fabricated OTFTs measured at constant drain voltage of -30 V over the swept gate voltage range from 0 to -30 V represented in Fig. 3.5(e) and 3.5(f). Transfer characteristics of OTFTs can be used to extract the important electrical parameters of the transistor as threshold voltage (V_{TH}) and mobility (μ). The key parameters of OTFTs can be calculated from the following equation [27]:

$$\sqrt{I_{DS}} = \sqrt{\frac{W\mu C}{2L}}(V_{GS} - V_{TH}) \quad (3.1)$$

Where I_{DS} represents the saturation drain current under pinch-off condition, L and W are symbolized as the length and width of the fabricated OTFT channel, respectively, and C is the capacitance per unit area of the oxide dielectric layer which was 10 $nFcm^{-2}$. The threshold voltage of the as fabricated OTFT can be calculated by extrapolation of the line corresponding to $I_{DS}^{1/2}$ versus V_{GS} curve at V_{DS} = -30 V.

3.3.3. Ammonia Sensing

The ammonia sensing experiment of the fabricated OTFTs has been performed inside a chamber as illustrated in the previous study [125]. Under the controlled flow of dry air mixed with analyte NH_3 gas, both pristine PBTTT-C14 and PBTTT-C14/MoS_2-QDs hybrid film based OTFT device channels are exposed with ammonia ranging from 0.5 ppm to 50 ppm at 25°C (room temperature) under ~ 50% relative humidity (RH) condition. For the sensing analysis, transfer characteristics (I_{DS}-V_{GS}) of the fabricated OTFTs are measured with various concentrations of ammonia. During this measurement, the gate voltage of the device swept in the range of 0 to -30 V with a fixed drain bias of -30 V. The transfer characteristics of Device-1 and 2 under different concentrations of NH_3 have been represented in Fig. 3.6(a) and 3.6(b) respectively. From the transfer characteristics it is observed that the drain current (I_{DS}) decreases as the concentration of the ammonia increases. The decrease in drain current is attributed to the chemical interaction between ammonia and the exposed active sensing material in the OTFT device channels, which is discussed later in the sensing mechanism section. The decrement in the drain current (ΔI_D) under fixed gate voltage can be calculated by taking the difference between the drain current before and after exposure of the gas. This ΔI_D also represents the response of the OTFTs due to

the exposure of the gas which is discussed in the following section. As shown in Fig. 3.6, the reduction in the drain current (ΔI_D) in the transfer characteristics (I_{DS}-V_{GS}) of Pristine PBTTT-C14 based OTFT is significantly lower as compared to the hybrid based PBTTT-C14/ MoS_2-QDs based OTFT. This result reveals the NH_3 sensitivity of this PBTTT-C14 OTFT can be enhanced notably by adding MoS_2-QDs.

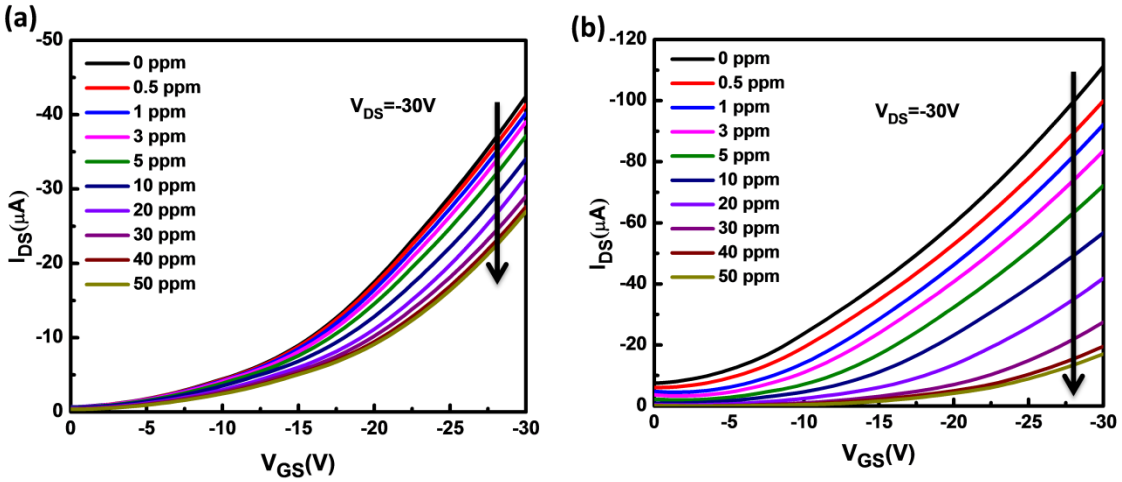

Fig. 3.6. Transfer characteristics (I_{DS}-V_{GS}) of as fabricated OTFT ammonia sensor at V_{DS} = -30V with various concentrations (0.5 ppm-50 ppm) (a) pristine PBTTT-C14 and (b) PBTTT-C14/MoS_2-QDs hybrid film based OTFT.

It is also noted that, in addition to the decrement in drain current (ΔI_D), various electrical parameters of OTFT, such as threshold voltage (V_{TH}), and effective carrier mobility (μ_h) changes due to the exposure of NH_3 gas. The variation in physical parameters of the PBTTT-C14/MoS_2-QDs based OTFT after the exposure of ammonia is given in the below Table-3.1.

Table-3.1: Variation of device parameters and the response of PBTTT-C14 (Device-1) vs. PBTTT-C14/MoS_2-QDs (Device-2) based OTFT sensors with different concentrations of NH_3.

NH_3 (ppm)	On current I_{on} (μA)		Effective Mobility μ_h ($cm^2V^{-1}sec^{-1}$)		Threshold voltage V_{TH} (V)		Change in Threshold voltage (ΔV_{TH})	Response (%)	
	Device -1	Device-2	Device -1	Device-2	Device -1	Device -2		Device -1	Device -2
0	42.48	-111.15	0.0302	0.0450	-2.5	7.56	0	0	0
0.5	41.35	-99.93	0.03	0.0441	-2.59	5.08	2.48	2.66	10.14
1	40.21	-92.08	0.0294	0.0438	-2.77	3.49	4.07	5.35	17.15
3	39.04	-83.31	0.0291	0.0430	-3.22	1.54	6.02	8.09	24.91
5	37.16	-72.23	0.0287	0.0426	-3.6	-1.13	8.69	12.52	35.08
10	34.08	-56.54	0.028	0.0414	-4.19	-3.22	10.78	19.76	48.99
20	31.68	-41.77	0.0268	0.0395	-4.48	-6.56	14.12	25.42	62.38
30	29.02	-27.46	0.0261	0.0346	-4.92	-10.59	18.15	31.69	75.30
40	27.60	-19.61	0.0245	0.0305	-5.18	-11.27	18.83	35.02	82.43
50	26.95	-17.30	0.024	0.0279	-5.72	-11.53	19.09	36.57	84.66

From the Table-3.1, it is clearly noticeable that the shift in the threshold voltage is huge as the increase in ammonia concentration, which is a good signature for the gas sensing application. Besides, the effective carrier mobility of the QDs based hybrid device also gradually decreases with the increasing concentration of ammonia.

3.3.4. Gas response and limit of detection

Fig. 3.7 illustrates the dynamic sensing response of the pristine PBTTT-C14 and PBTTT-C14/MoS_2-QDs hybrid film based OTFT sensor against various NH_3 concentrations ranging from 0.5 to 50 ppm. Ammonia gas is exposed on the fabricated OTFT channels and the response (R) of the sensor can be calculated by using equation [127]:

$$R = \frac{|I_{DS,Air} - I_{DS,Gas}|}{|I_{DS,Air}|} \times 100\% \quad (3.2)$$

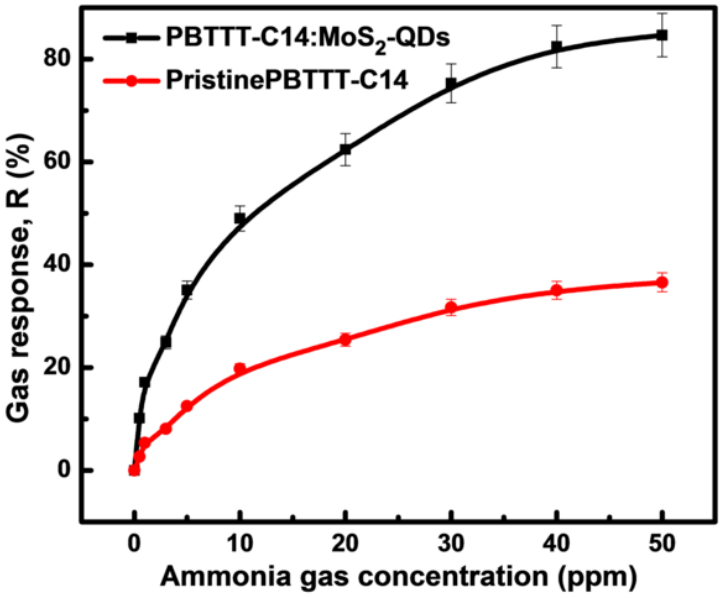

Fig. 3.7. Gas response graph of pristine PBTTT-C14 and PBTTT-C14/MoS_2-QDs hybrid based OTFTs for different NH_3 gas concentration (V_{DS} = -30 V and V_{GS} = -30 V).

The response graph of Device-1 and 2 presented in Fig. 3.7 suggests that the incorporation of QDs in polymer matrix created a remarkable improvement in the response data, particularly in the high concentration range of NH_3. At 50 ppm concentration of NH_3, the pristine polymer based OTFT sensor response (sensitivity) is 36.5%, while the polymer/QDs composite based OTFT sensor exhibits 84.66%. In addition, polymer/QDs based sensor shows quite good response even at lower concentration of ammonia.

The another important parameter of the fabricated sensor, called limit of detection (LOD), can be calculated by the following equation [128]:

$$Limit\ of\ detection\ (LOD) = \frac{3* \sigma_{rms}}{m} \tag{3.3}$$

Where σ_{rms} represents the root-mean-square deviation of the linear fitting of the curve and the baseline, and 'm' symbolizes the plotted curve's slope. The extracted value of LOD for the fabricated polymer/QDs based sensor has been found to be 0.317 ppm, which is extremely small and indicates its applicability up to a very low concentration limit of NH_3.

Besides, we perform the transient response of the OTFT for different concentrations of NH_3, which is given in Fig. 3.8. It has been observed that the variation of the drain current increases with analyte gas, but the rise time remains almost the same for all concentrations (~2 sec.). Besides, the sensor has good linearity in the response at lower concentrations of NH_3. But at higher concentration, after removing analyte gas, the decay time increases with NH_3 gas concentration. Most likely, it is due to the chemisorption of the NH_3 gas molecule with the semiconducting layer that takes longer time to recover.

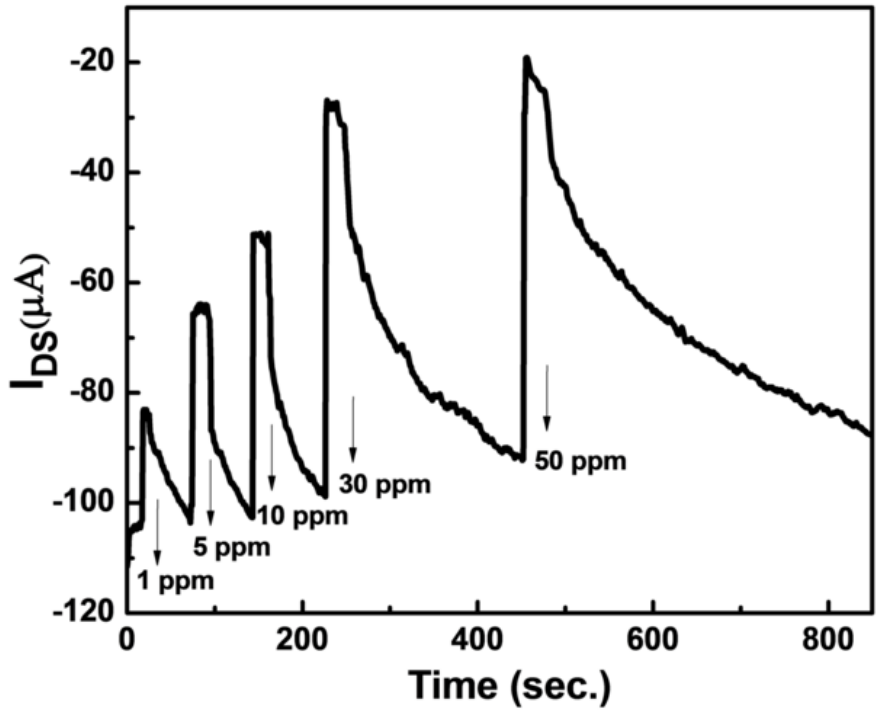

Fig. 3.8. Transient response curve (I_{DS}-t) of the OTFT sensor for various concentrations of NH_3.

3.3.5. Selectivity

Selectivity can be defined as the ability of the sensor to respond the specific gas in the existence of other commonly present interfering gases. The fabricated polymer/QDs film based OTFT sensor has negligible gas response towards 50 ppm of other oxidative, reductive and commonly available environmental interfering gases such as methane (CH_4), propane (C_3H_8), carbon dioxide (CO_2), carbon monoxide (CO) as shown in Fig. 3.9. For this measurement, the device channel has been exposed with individual interfering gas mixed with the controlled flow of dry air. Higher NH_3 response of the polymer/QDs film based sensor comparative to other interfering gases can be attributed to the high electron donating capability of the NH_3 gas. It is clearly

visible from the selectivity graph that the composite based sensor is highly selective for the low concentration of the ammonia.

For the selectivity analysis of the sensor, we have also investigated the effect of NO_2 gas. As NO_2 is a strong oxidizing gas, it will lead to a huge change in I_{DS} of the fabricated device in the negative direction to the NH_3 gas (reducing gas). We have examined the selectivity of the other gases at 50 ppm, similarly we have done this for the same concentration of NO_2 for the fabricated device. But in the presence of 50 ppm of this strongly oxidizing gas, the device gets damaged. Damaging of the device may be due to its highly oxidizing electron affinity effect, which is one limitation of this device.

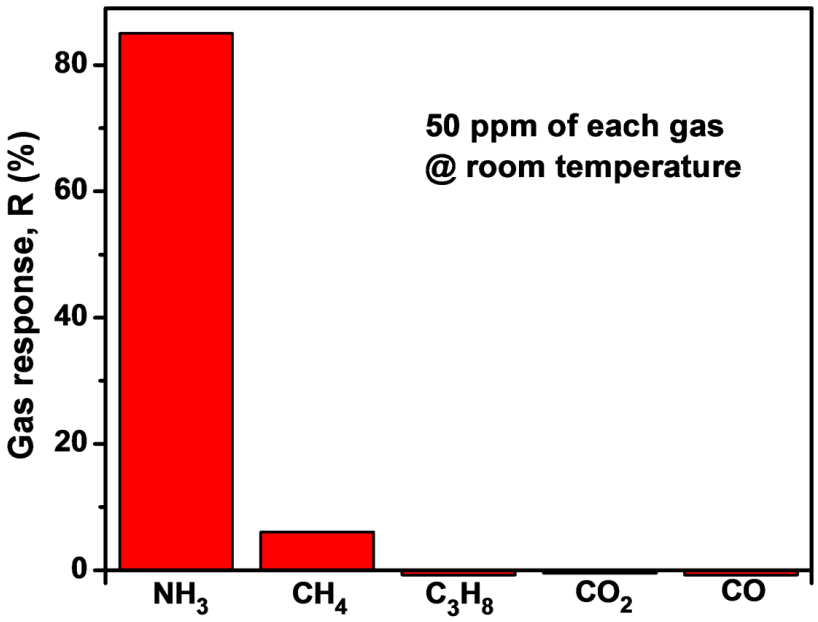

Fig. 3.9 Selectivity graph of PBTTT-C14/MoS_2-QDs hybrid based sensor over common interfering gases.

3.3.6. Reliability analysis

For the reliability test of the polymer/QDs film based OTFT ammonia sensor, the effect of RH on I_{DS} (with and without gas) has been investigated, and it has been observed that the response of the sensor is reduces by 8% when RH has been changes from 20% to 80% humidity range for 50 ppm concentration of ammonia as shown in Fig. 3.10, which is negligibly low variation w.r.t the overall NH_3 gas response of the device.

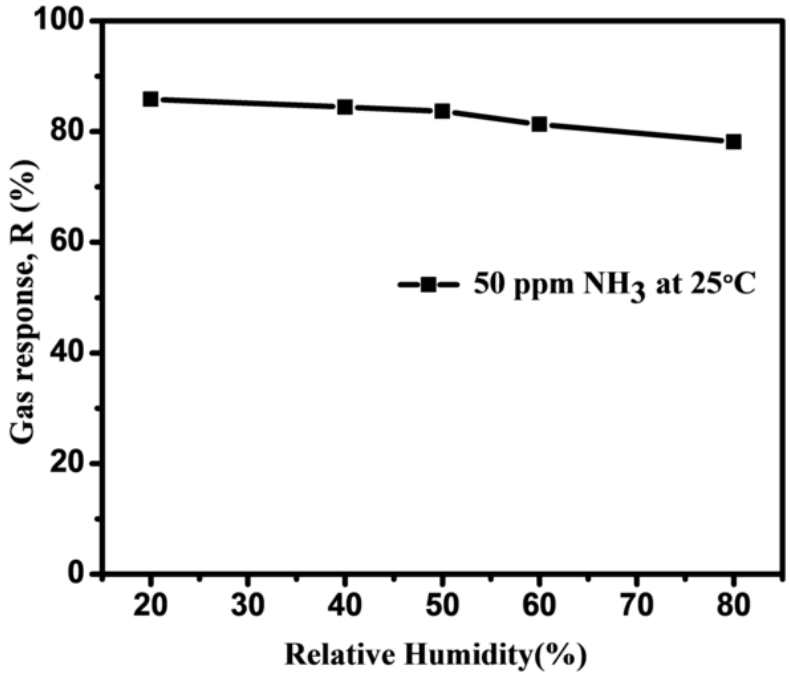

Fig. 3.10. Gas response of the PBTTT-C14/MoS_2-QDs hybrid based OTFT sensor with the variation of relative humidity.

Besides, we have examined two different types of stabilities. First one is the environmental stability, which has been tested for 25 consecutive days. During this study, we observed that I_{DS} reduces slowly, which is approximately only 7% of the initial responsivity of the sensor (Fig.

3.11 (a)). Further, we have also performed electrical stability of the fabricated sensor for 50 consecutive cycles at RH 50% and temperature 25°C. We have seen only 6% change in the response with respect to the first cycle (Fig. 3.11 (b)).

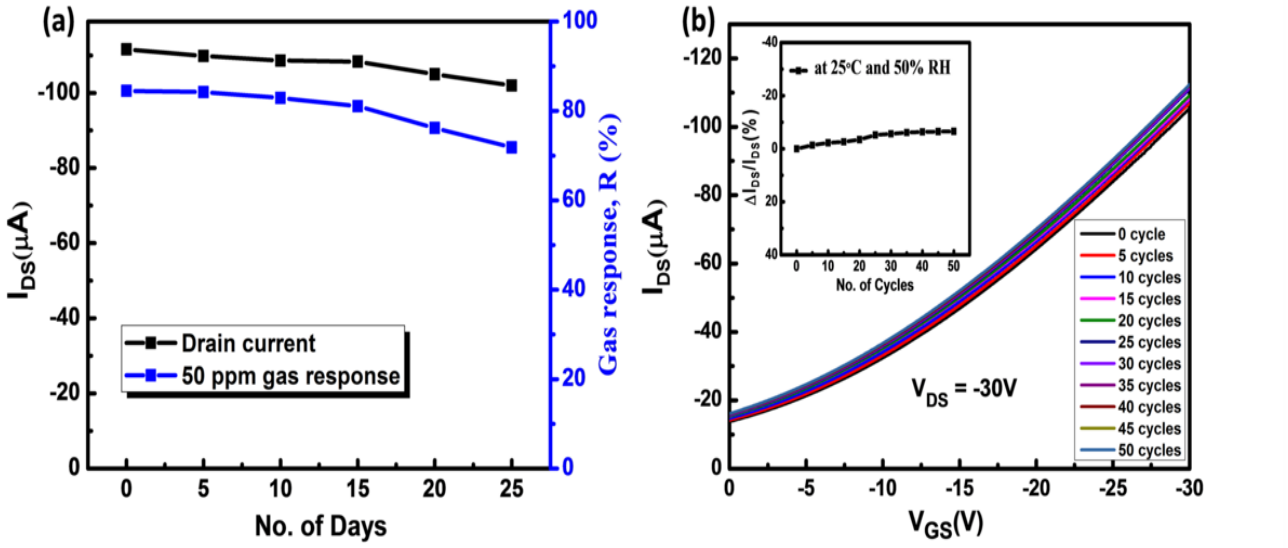

Fig. 3.11. (a) Environmental stability of the OTFT sensor and; (b) Electrical stability for 50 consecutive cycles at RH 50% and temperature 25°C.

The following findings demonstrate that the PBTTT-C14/MoS_2-QDs based OTFT sensor has quite good stability, which can be an excellent choice for the detection of ammonia at around room temperature within a wide range of relative humidity.

A comparative performance of the PBTTT-C14/MoS_2-QDs based OTFT sensor w.r.t the earlier reports are given in the Table-3.2.

Table-3.2: Comparative performance of the NH_3 sensor w.r.t the earlier reports.

Sensing material	Film deposition technique	Device configuration	Gas concentration	Response	Remark
PQT-12	Drop cast	MSM	100 PPM	Very low	Low sensitivity [129]
P3HT/Poly-styrene	Spin coat	Transistor	50 PPM	51%	Poor response [113]
Pentacene	Thermal evaporation	Transistor	100 PPM	14.8%	Poor response and recovery [130]
P3HT	Air-brush deposition	Transistor	100 PPM	19%	Low sensitivity [131]
PQT-12	FTM	Transistor	80 PPM	56.4%	Slower response [125]
PBTTT/MoS_2 -QDs (This work)	FTM	Transistor	50 PPM	Acc. Mode res.- 84.66% (50 ppm), dep. Mode (Off current factor)- 3X 10^3	Cost-effective, Highly sensitive, Quick response

3.3.7. Sensing mechanism

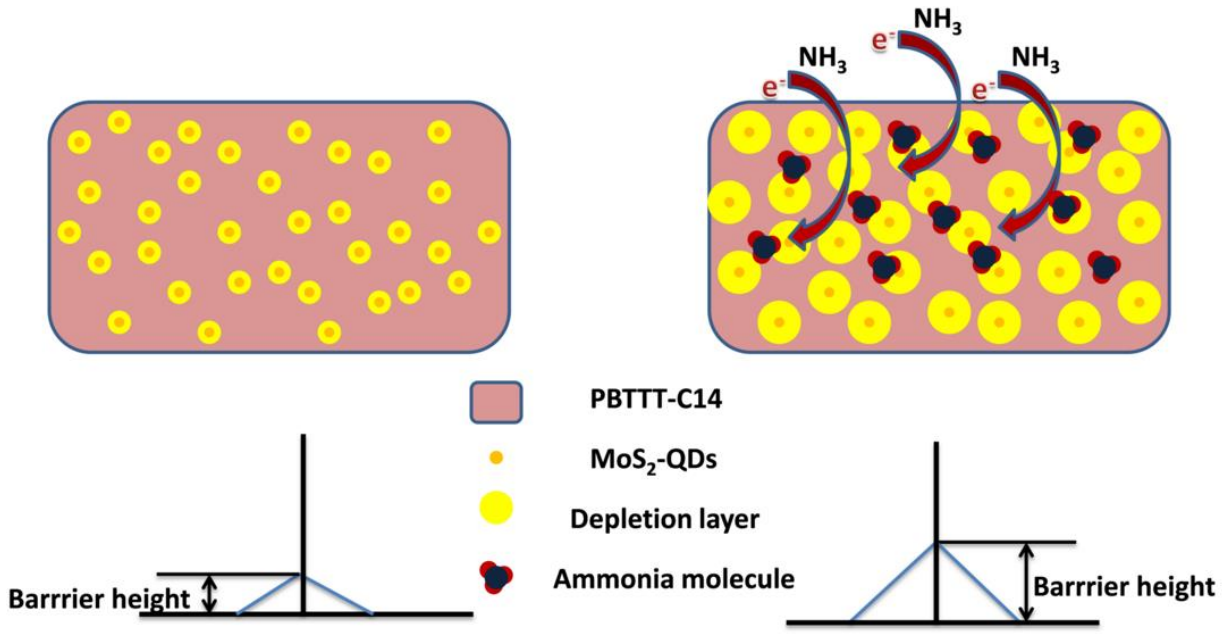

Fig. 3.12 Ammonia sensing mechanism of the PBTTT-C14/MoS_2-QDs hybrid based OTFT sensor.

The enhancement of the NH_3 sensing of the fabricated PBTTT-C14/MoS_2-QDs hybrid film based OTFT sensor can be realized from the enhancement of depletion layer and the potential barrier height of PBTTT-C14/MoS_2-QDs heterojunction. Since PBTTT-C14 and MoS_2-QDs are p- and n-type semiconductor respectively [132, 133], therefore their heterojunction will form a depletion by transferring hole from PBTTT-C14 to MoS_2-QDs and electron from MoS_2-QDs to PBTTT-C14 until their Fermi level comes in the same level. This depletion layer will form a barrier height during charge transfer (hole) through this composite thin film. As NH_3 is a reductive (electron-donating) gas [134, 135], it will reduce the hole concentration of exposed area of the PBTTT-C14 film which will lead to the enhancement in depletion layer width in the exposed surface part of the film (Fig. 3.12). Therefore, net mobile charge carrier concentration of the PBTTT-C14 polymer will decrease and the overall sheet resistance of the PBTTT-

C14/MoS_2-QDs channel will increase. Besides, barrier height of the mobile charges will also increase due the enhancement of the depletion layer width of the PBTTT-C14/MoS_2-QDs heterojunction.

Moreover, this will lead to the change in various OTFT parameters including ON/OFF ratio, threshold voltage (V_{Th}) of the device and effective carrier mobility (μ). It is known that the OFF current of an OTFT depends on two primary factors. One is the gate leakage current and the other one is the sheet resistance of the semiconductor channel. Assuming the gate leakage current of the OTFT will remain the same during gas sensitivity study, if sheet resistance of PBTTT-C14/MoS_2-QDs hybrid film increases, the OFF current of the OTFT should be reduced. Fig. 3.13(c) shows that the OFF current of the device gradually decreases with concentration of NH_3 which supports the enhancement of the depletion layer of the PBTTT-C14/MoS_2-QDs heterojunction. Fig. 3.13(d) shows the 'off current factor' (ratio of OFF current in absence to presence of NH_3 gas) of the devices. This data indicates that the variation of OFF current factor in case of hybrid device is ~ 3×10^3 when the NH_3 gas concentration changes from 0 to 50 ppm. This variation is several orders larger than the ON current variation of the device. Moreover, it has a good linearity >1 ppm concentration of NH_3. Though, the variation of this factor is almost negligible in case of Device-1compared to the Device-2. Besides, due to this enhancement of the depletion layer, depleted charge accumulation in the dielectric/semiconductor increases, this leads to a shifting of V_{Th} of the OTFT device. Fig. 3.13(a) shows that the Device-2 has a shift of V_{Th} of ~19 V when the concentration of NH_3 changes from 0 to 50 ppm. However, this shifting of V_{Th} in case of pristine PBTTT-C14 based OTFT is only ~1.5 V, which simply indicates that enhancement of depletion layer of PBTTT-C14/MoS_2-QDs heterojunction in presence of NH_3 is key reason for shifting of V_{Th} of the device. Besides, it has been observed from the Fig. 3.13(b)

the effective carrier mobility of the device also reduces from 0.045 to 0.028 cm^2 $V^{-1}sec^{-1}$ when the concentration of NH_3 changes from 0 to 50 ppm. Although, μ varies from 0.03 to 0.024 cm^2 $V^{-1}sec^{-1}$ in case of Device-1 (Fig. 3.7b). The larger reduction of μ in case of polymer/QDs hybrid film is due to the enhancement of barrier height of the accumulated hole carrier of the channel.

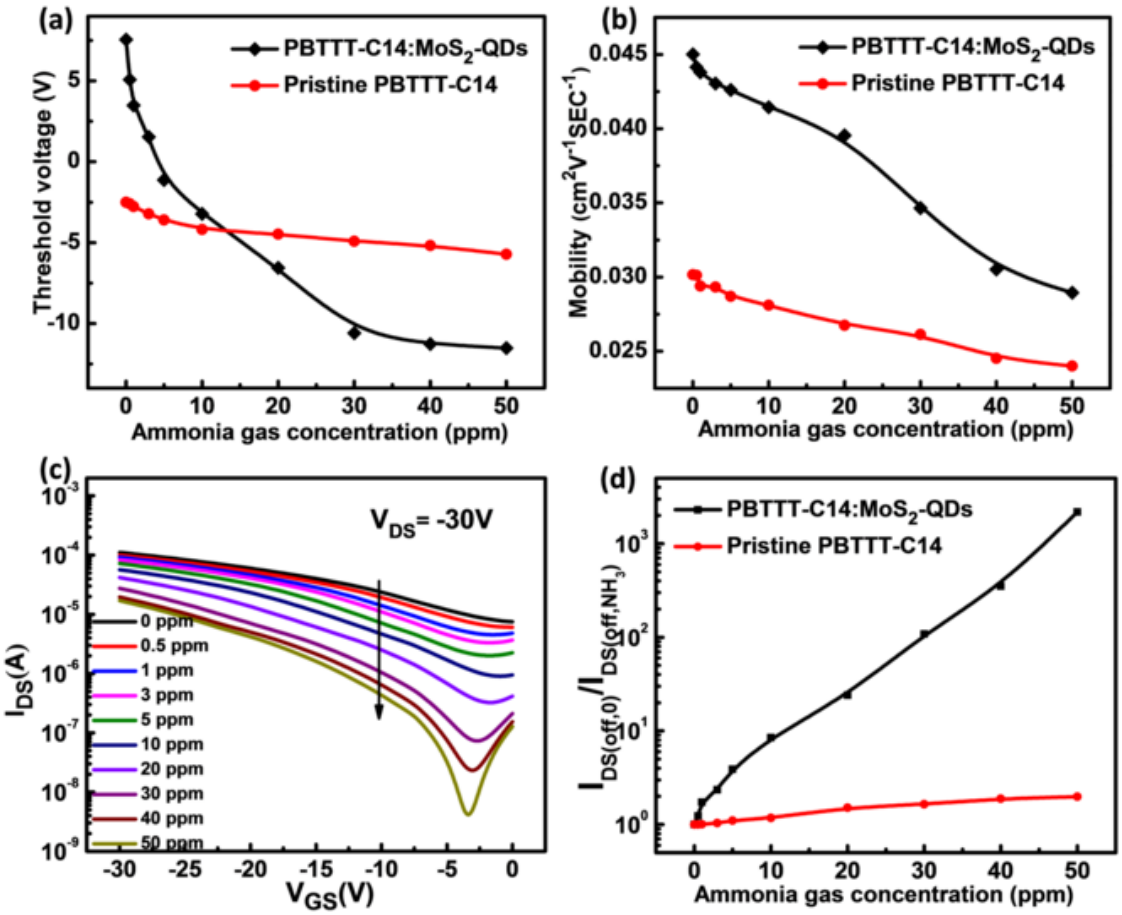

Fig. 3.13. Schematic representation of variation in (a) Threshold voltage, (b) mobility; (c) off current variation in PBTTT-C14/MoS_2-QDs heterojunction based OTFT, and (d) off current factor with the ammonia concentration ranging from 0 to 50 ppm.

3.4. Conclusion

A highly sensitive OTFT-based NH_3 sensor has been fabricated by using PBTTT-C14/MoS_2-QDs heterojunction thin film. Colloidal QDs of MoS_2 have been synthesized by a hydrothermal method, whereas heterojunction thin film has been deposited by a simple, low-cost and high yield 'floating film transfer method'. A reference OTFT of pristine PBTTT-C14 has been fabricated under the same condition. Our comparative study reveals that the depletion layer of PBTTT-C14/MoS_2-QDs heterojunction is extremely sensitive to the NH_3 gas which has been working as a hot-spot for this gas sensor. Due to a very small variation of gas concentration, a large variation of device parameters has been observed which enables us to reach a response of 85% at 50 ppm concentration of NH_3 that has been calculated from the ON current variation of the device. This value is ~3 times higher w.r.t the reference OTFT. However, the OFF current variation of this OTFT is much more sensitive and shows a variation of $\sim 3\times10^3$ times in presence of 50 ppm NH_3 which also becomes possible due to the large variation of the depletion layer of the heterojunction. Besides, this OTFT shows a very high selectivity with good linearity to the gas concentration. Moreover, this OTFT is capable of measuring low concentration of NH_3 up to the level of 500 ppb. Overall this polymer/QDs heterojunction based OTFT sensor that has been fabricated in a very easy and low-cost method is capable of fulfilling all basic features for its practical application as NH_3 sensor.

Chapter 4

Ammonia gas sensitivity and broadband photo-detection by depleted layer of polymer/QDs based thin film transistor

Abstract

An ambient temperature broadband photo-detector and ammonia (NH_3) gas sensor devices are developed with PBTTT-C14/WS_2-QDs heterojunction thin film. Gas and photo-sensitive semiconducting composite thin layer of PBTTT-C14 conjugate polymer and hydrothermally synthesized WS_2-QDs have been deposited by high yield and cost-effective 'floating film transfer method' (FTM), which works as a channel (p-type) of the thin film transistor (TFT). To determine the NH_3 sensing behavior of the TFT, different concentrations have been exposed of NH_3 (0.5-20 ppm) on the channel of the TFT, which shows the response of ~50% at 10 ppm ammonia concentration, which is significantly higher than PBTTT-C14 only TFT. This improvement is made possible by the NH_3-responsive depleted layer of polymer/QDs heterojunction, which varies widely in the presence of ammonia. As a consequence, the ON/OFF ratio, carrier mobility and threshold voltage (V_{th}) of the device changes in a wider range. Besides, this TFT based gas sensor is also highly selective to the other interfering gases. In addition to NH_3 gas sensitivity, this TFT also shows very high photosensitivity under white light illumination that enhances 'ON' and 'OFF' current of the device by ~2.2 and 70 times, respectively under one sun white light illumination, whereas V_{th} of the device is shifted by ~22 V. Besides, the device shows quite fast response/ recovery time under NH_3 gas exposure and light illumination.

4.1. Introduction

Environmental pollution caused by the production of nitrogenous fertilizers and other chemicals are the main source of typical atmospheric pollutant ammonia (NH_3), which is generated mostly by ammonification and combustion [136, 137]. Explosion of poisonous NH_3 gas can cause severe damage to an individual's health even at lower concentrations (ppb or ppm level). The corrosive

nature of NH_3 can cause damage to the lungs, eyes, skin and can induce pulmonary edema, blindness etc. Inhaling excessive amounts of this colorless with pungent odor gas can be a source of serious diseases like dyspnea and cancer [136, 138, 139]. This hazardous NH_3 is primarily produced in the production unit of nitrogenous fertilizers, industrial refrigerants, and manure from the natural breakdown of dead animals and plants [5, 6]. Therefore, it is important to design an ambient temperature operating, highly responsive, and economical NH_3 gas sensor. Besides, photo-detectors are widely used for various applications like optical fiber communication, wireless communication, image sensors etc [140, 141]. Thus, a low cost, highly sensitive, and reliable photo-detector is highly demanding [142, 143].

Till date, numerous types of materials have been used for the detection of NH_3 [144, 145]. Conventional metal oxide semiconductor (MOS) based sensors performed excellently as sensitive materials with good response, but their requirement of high temperature for the detection confines their application as sensing materials [146, 147]. Various types of conducting polymers have also been used for NH_3 detection at ambient temperature. However, pure conducting polymer based sensors possess low sensing response towards NH_3. Additionally, their low conductivity, poor stability and slow response times are the key issues. Therefore, researchers have investigated the strategy of making organic/inorganic hybrid nano-composite based materials by combining metal oxides or noble metals with conducting polymers to make them more efficient sensor devices [83, 148, 149]. Recently, quantum dot (QD) of different 2D materials like; reduced graphene oxide (RGO), MoS_2, WS_2 based materials achieved more attention in recent times as a photo-detector and chemical sensor application due to their high in extinction coefficient and chemically active sites [114, 150]. Although the sensitivity of those 2D-QD only devices are limited [151]. Relatively hybrid materials of 2D-QD with other classes

of semiconductors like; organic, metal oxide or silicon are getting more attention due to their enhanced photo and gas sensitivity [152-155].

To explore the beneficial sides of organic polymers and quantum dots, I have prepared PBTTT-C14/WS_2-QDs nano-heterojunction based TFT and systematically investigated its ammonia gas and photo sensing capabilities. PBTTT-C14 is a polythiophene based π-conjugated polymer which can be a good choice for higher air stability with high carrier mobility due to its relatively deep HOMO level [123]. Besides, WS_2 is a widely studied sensor material for its exciting photoelectric and gas sensing capabilities. Keeping in view of the above facts, in this work, our main approach is to determine the NH_3 gas sensitivity of PBTTT-C14/WS_2-QDs nano-heterojunction based thin film transistor (TFT) sensor at room temperature. Besides, a broadband photosensitivity of this TFT has been investigated. This composite based TFT was successfully fabricated *via* a cost-effective and facile procedure floating film transfer (FTM) method and the capability of ammonia and broadband photo sensing of this device are systematically investigated. The TFT channels of the prepared sensors are exposed with different ammonia concentrations (0.5 - 20 ppm), which shows fast response and recovery times with exceptional sensitivity and repeatability. In our previous study, it was observed that the PBTTT-C14/MoS_2-QDs composite based TFT sensor had quite higher sensitivity with respect to the pristine PBTTT-C14 based TFT sensor, which reveals the benefit of using organic/inorganic nano-heterojunction[156]. The key improvement of this PBTTT-C14/WS_2-QDs nano-heterojunction based TFT w.r.t the earlier work is the level of sensitivity which is several-fold higher than earlier. Besides, it was observed that the PBTTT-C14/MoS_2-QDs based sensor had a relatively poor recovery time towards NH_3 gas. However, sensor based on PBTTT-C14/WS_2-QDs exhibited prompt responsiveness to the NH_3 gas and demonstrated rapid response and recovery

following each gas pulse. The duration of the recovery is estimated to be between 5 and 6 s with exhibiting acceptable repeatability in terms of analyte concentrations. Further, the origin of the sensing mechanisms for the improvement of the device sensitivity has been discussed. In addition to its application as NH_3 gas sensor, this manuscript has also demonstrated its application as a visible range broadband photo-detector with a satisfactory sensitivity.

4.2. Materials and experimental methods

4.2.1. Synthesis of WS_2-QDs

Highly pure sodium tungstate dihydrate ($Na_2WO_4 \cdot 2H_2O$), L-cysteine, and hydrochloric acid precursor materials acquired from Merck, India have been used for the hydrothermal synthesis of WS_2-QDs.The procedure is similar as shown in previous chapter 3. At the beginning of this process, sodium tungstate dihydrate and L-cysteine (2:1 w/w) were stirred separately for 20 min in 25 ml of DI water. After that, both solutions were mixed and stirred with an added amount of concentrated HCl at a maintained value of pH ~3. And finally, the as-prepared solution was transferred into a 100 ml capacity Teflon autoclave walled with stainless steel and kept for approx 42 hours at ~ 200°C in the oven. After cooling down to room temperature, the WS_2-QDs contained light yellowish solution was obtained.

4.2.2. Synthesis of PBTTT-C14/WS_2-QDs nano-composite

The poly (2,5-bis (3-tetradecylthiophen-2yl) thieno (3,2-b) thiophene) PBTTT-C14 (Sigma-Aldrich Pvt. Ltd, Mol. Wt. > 40,000) has been used for PBTTT-C14/WS_2-QDs nano-heterojunction thin film fabrication that works as semiconducting channel materials of TFT. On the other hand, hydrothermally synthesized WS_2-QD has been dispersed in a chloroform ($CHCl_3$) solution. To transfer WS_2-QDs from the aqueous solution to the $CHCl_3$, we have used the phase

transfer technique, as reported in our earlier work [156]. In this method, aqueous solutions of QDs were sonicated rigorously for 2-3 hours with the same quantity of $CHCl_3$. In this immiscible solution of chloroform and water, the aqueous dispersion will remain at the top, and heavy $CHCl_3$ will remain at the bottom. After the completion of the sonication procedure, from the top, the aqueous solution was discarded, and the remaining solution will contain the QDs in chloroform.

After transferring QDs in $CHCl_3$ solvent, for the PBTTT-C14/WS_2-QDs nano-composite synthesis, 10 µl of $CHCl_3$/QDs dispersion was mixed in 2 mg polymer/chloroform solution with 10 mg ml^{-1} concentration. For the uniform mixing of QDs in polymer, the composite solution is sonicated and used for organic/inorganic hybrid semiconductor thin film deposition via FTM method, as described in our previous publication [24]. During this thin film deposition, a small drop of PBTTT-C14/WS_2-QDs solution was dropped under ambient conditions onto an aqueous mixture (ethylene glycol and glycerol in 3:1) containing petri-dish. Subsequently, nano-composite solution spread over the liquid medium without mixing into it and stabilized as a floating film on the liquid. Then, as prepared film on the surface of the liquid has been transferred onto the cleaned Si/SiO_2 substrate and heated at ~85°C. During this procedure, the quantity of nano-composite solution was optimized to obtain a good quality film that can be utilized to fabricate high performance TFT devices. This nano-composite film over the aqueous medium has been transferred onto the carbon coated TEM grid and Si/SiO_2 substrate for the TEM and AFM characterization purposes, respectively.

4.2.3. Device fabrication

For the TFT fabrication, highly doped silicon (p^+-Si) substrates with a SiO_2 (thermally grown) layer of 300 nm (C_{ox}, capacitance per unit area, 10 $nFcm^{-2}$) are used as the gate dielectric. Before PBTTT-C14/WS_2-QDs thin film deposition, Si/SiO_2 substrates were properly cleaned with soap solution. Afterward, substrates were cleaned in a sequence with DI water, acetone, and isopropanol by using an ultrasonic bath followed by the drying process. After the completion of the cleaning process, the composite (semiconducting) layer was deposited via pre-explained FTM method onto the cleaned Si/SiO_2 substrate followed by the drying process at ~80°C before the electrode deposition. Finally, around 60 nm source–drain Gold (Au) electrodes were subsequently deposited by thermal deposition onto the nano-composite film coated substrate with the rate of evaporation 1 Å/s to 2 Å/s at vacuum level 6×10^{-5} Torr. The interdigitated shadow masks (length (L) and width (W) of 50 µm and 18 mm, respectively) were used for the electrode deposition.

4.2.4. Characterization tools

For the characterization purpose, the absorption spectra of WS_2-QDs were obtained by UV–Vis spectrophotometer (UV-2600, Shimadzu). Electron micrographs and selected area electron Diffraction (SAED) pattern of polymer/QDs film were obtained via transmission electron microscope (TEM) study [TECHNAI $G^2$20 TWIN (New Zealand)]. The roughness study of the film was done by Atomic force micrograph (AFM) using NT-MDT "NTEGRA Prima" (Russia). Lastly, the ammonia sensing behaviors of the fabricated TFT were carried out by a controlled atmosphere gas sensing assembly. The gas assembly has two inlets and one outflow. The first inlet is for ammonia gas injection, while the second inlet and exit are for air flushing into and out of the chamber. A probe station connects a semiconductor parameter analyzer (Keysight,

B1500A) to the gas chamber. Ammonia gas with concentrations ranging from 0.5 ppm to 20 ppm is fed into the gas chamber at 27°C with 50% RH under the controlled flow of dry air, and the resulting changes in drain current are detected using electrical measurements. Similar procedure was obtained for the other sample gases preparation for selectivity analysis [125]. Photosensitivity of the device has been investigated by doing electrical characterization of the TFTs under white light illumination. Xenon lamp has been used as a source of white light.

4.3. Results and discussion

4.3.1. Characterization of WS_2 -QDs

The characteristics of synthesized WS_2-QDs were examined by TEM and UV-Vis spectroscopy. TEM image of the well dispersed QDs in water is shown in Fig. 4.1(a) and indicates that QDs are homogeneously distributed on a carbon coated Cu grid. Fig. 4.1(b) shows HR-TEM the SAED pattern (inset), which suggests that QDs are polycrystalline in nature. The size distributions of the QDs are in the range of 4-6 nm, which is observed from the histogram presented in Fig. 4.1(c). Fig. 4.1(d) demonstrates the UV-Vis spectra of WS_2-QDs with two absorption peaks at 305 nm and 383 nm. This absorption data demonstrates the excitonic characteristic of the synthesized WS_2-QDs [157, 158]. The band gap of the synthesized QDs calculated by the tauc's plot is 3.79eV represented in the inset of Fig 4.1(d).

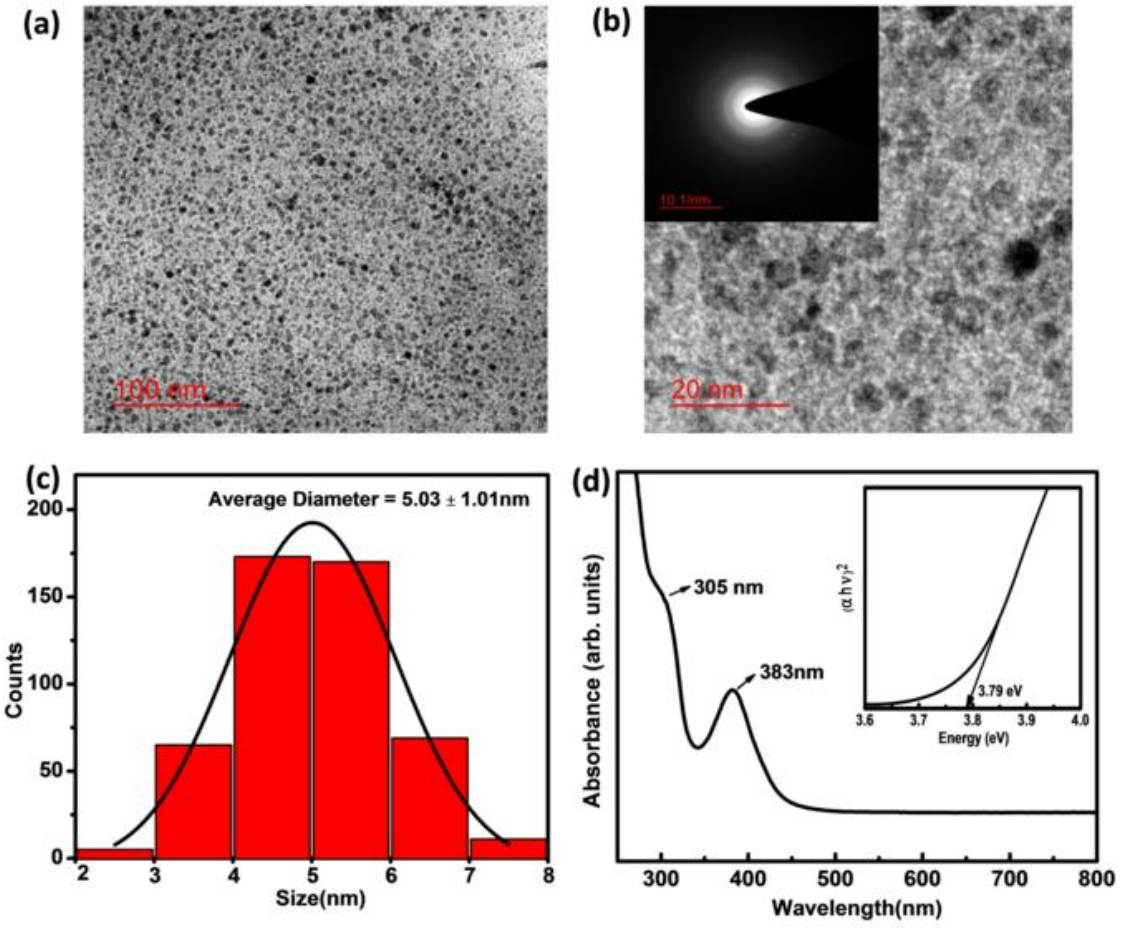

Fig. 4.1. (a) TEM image, (b) HR-TEM image and SAED pattern (inset), (c) size distribution histogram, and (d) UV-Vis spectra and Tauc's plot (inset) of synthesized WS_2-QDs.

4.3.2. Characterizations of PBTTT-C14/WS_2-QDs nano-composite thin Film

For the TEM micrograph and SAED pattern of PBTTT-C14/WS_2-QDs nano-composite, thin film has been transferred via pre-described FTM method onto the Cu grid. The TEM image of the nano-composite indicates that the QDs are distributed equivalently on the matrix of polymer, as shown in image Fig. 4.2(a). The hazy ring pattern in the SAED pattern of the nano-composite presented in Fig. 4.2(b) is due to the polymer matrix present in the nano-composite material.

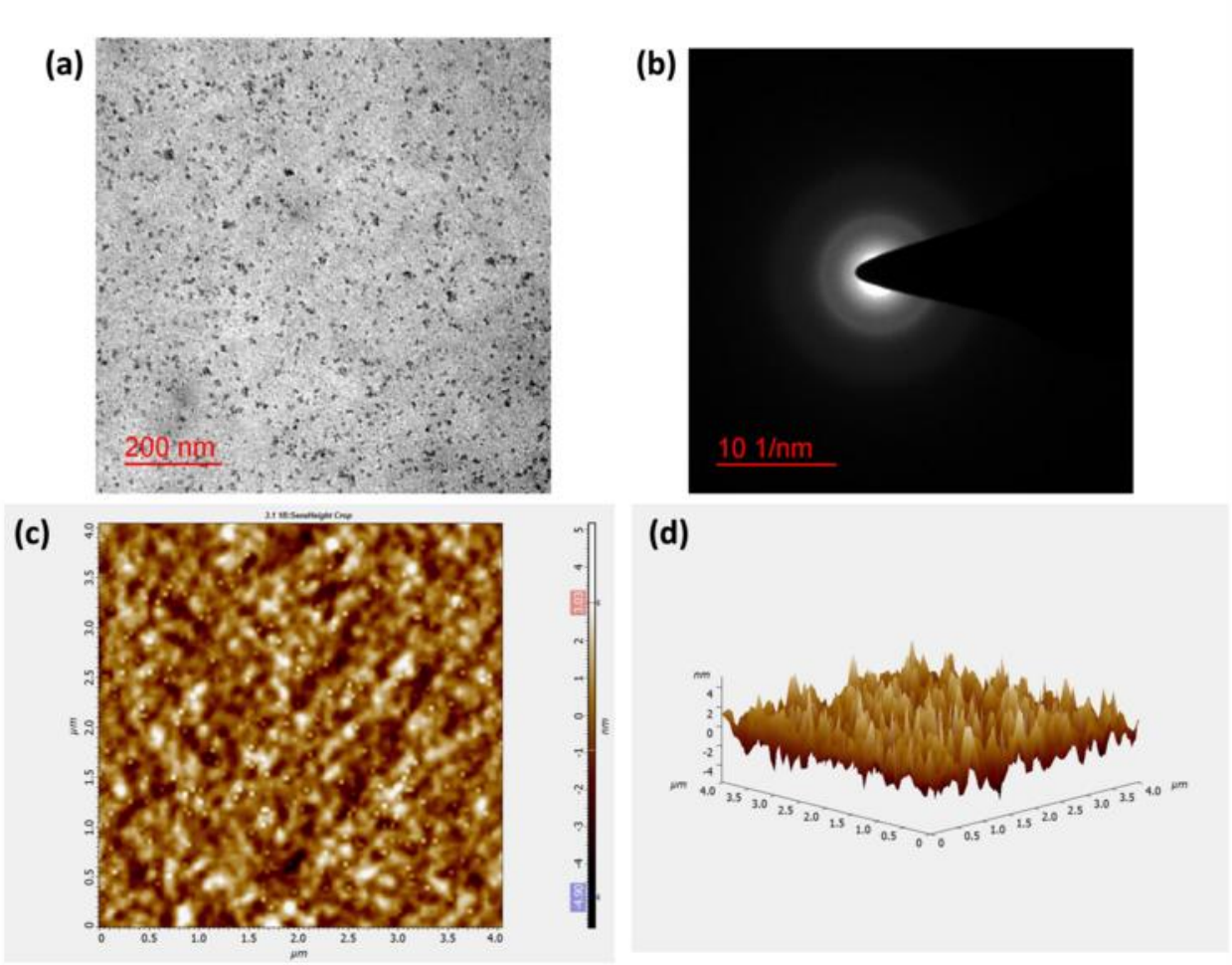

Fig. 4.2. (a) TEM micrograph and (b) SAED pattern ;(c) 2D and (d) 3D AFM image of PBTTT-C14/WS_2-QDs FTM film.

An AFM measurement has been used to analyze the surface roughness of the nano-composite film. Fig. 4.2(c) and 4.2(d) represent 2D and 3D AFM images of the polymer/QDs nano-composite film, indicating the root-mean-square (R_{rms}) roughness nano-composite film is 1.28 nm. Brighter spherical spots of this film are the WS_2-QDs, which are ~9 % surface coverage of the film, has been estimated from Image-J software (Fig. 4.2(a)). It can be noted that the WS_2-QDs have been distributed throughout the film uniformly.

4.3.3. Electrical Characterizations

For the electrical characterization of the fabricated TFT (Fig. 4.3(a)), the output (I_{DS}-V_{DS}) and transfer (I_{DS}-V_{GS}) characteristics were measured at 27°C (room temperature) with 50% relative humidity (RH) and represented in Fig. 4.3(b) and Fig. 4.3(c), respectively. Output characteristic of the TFT was examined by sweeping the drain voltage (0 to -30 V) with different constant bias gate voltages. Whereas, the transfer characteristic was estimated at a constant drain voltage of -30 V and a gate voltage sweep from 0 to -30 V.

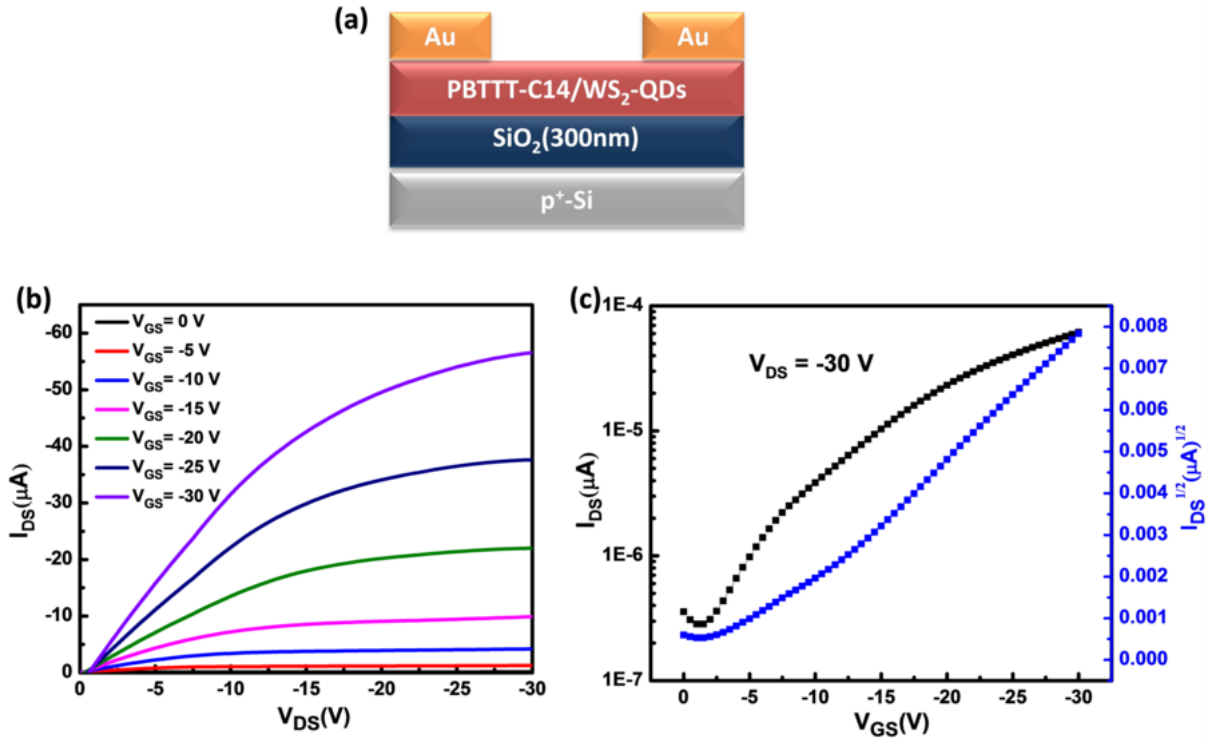

Fig. 4.3. (a) Schematic diagram, (b) Output characteristics, and (c) Transfer characteristics of PBTTT-C14/WS_2-QDs based TFT.

From the transfer characteristic, the parameters of the TFT can be extracted by using the subsequent equation (3.1).

4.3.4. Ammonia Sensing

For the gas sensing measurement, a fabricated TFT device is exposed with different concentrations of NH_3 gas ranging from 0 ppm to 20 ppm at 27°C under the controlled flow of dry air inside a sealed chamber with 50% RH. During the sensing measurement, the gate bias (V_{GS}) is swept from 0 to -30 V under a constant drain voltage (V_{DS}) of -30 V, as shown in Fig. 4.4(a). It is observed from the transfer characteristic that as soon as the concentration of NH_3 increases, the drain current (I_{DS}) of the TFT decreases gradually. The reduction in the I_{DS} (ΔI_{DS}) at constant V_{GS} can be determined by taking the difference between the I_{DS} data before and after exposure of the ammonia.

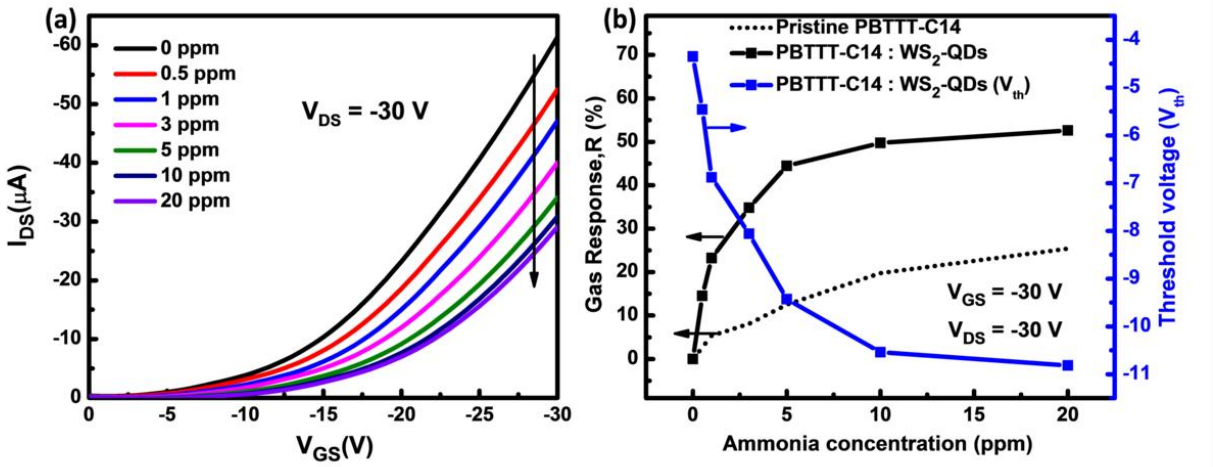

Fig. 4.4. (a) Transfer characteristics of PBTTT-C14/WS_2-QDs nano-composite film based TFT based sensor at V_{DS} = -30V and (b) Gas response (V_{GS} = -30 V, and V_{DS} = -30 V) and threshold voltage (V_{th}) shift with different concentrations of ammonia (0 ppm-20 ppm). (Response data for pristine PBTTT-C14 based TFT sensor has been added as reference (dotted line)).

Table - 4.1: The Summary of variation in TFT parameters and the sensitivity of PBTTT-C14/WS_2-QDs with different concentrations of NH_3.

NH_3 (ppm)	**On current I_{on} (μA)**	**Effective Mobility μ_h ($cm^2V^{-1}sec^{-1}$)**	**Threshold voltage V_{th} (V)**	**Change in Threshold voltage (ΔV_{th})**	**Response (%)**
0	-61.39	0.0536	-4.35	0	0
0.5	-52.47	0.0496	-5.46	1.11	14.53
1	-47.13	0.0481	-6.88	2.53	23.23
3	-40.02	0.0456	-8.06	3.71	34.81
5	-34.09	0.0431	-9.43	5.08	44.46
10	-30.86	0.0428	-10.54	6.19	49.73
20	-29.08	0.0425	-10.82	6.47	52.62

Besides, various electrical parameters of the device also change upon exposure of NH_3 gas, such as mobility (μ_h) and threshold voltage (V_{th}), as represented in Table - 4.1. These large variations in the electrical parameters of the fabricated TFT indicate its potential for NH_3 gas sensing application. Fig. 4.4(b) depicted the dynamic ammonia gas response (V_{GS} = -30 V, and V_{DS} = -30 V) and the corresponding shift in the V_{th} of the fabricated TFT against different NH_3 concentrations ranging from 0 to 20 ppm. Besides, response data of reference pristine PBTTT-C14 based TFT has been presented in a dotted black line. From Fig 4.4(b), it can be observed that the improvement of response w.r.t the pristine TFT is several folds higher throughout the range. This data also shows a shift of $V_{th,}$ for the nano-composite material, which is more than 6 V during the variation of NH_3 concentration that has good linearity up to 10 ppm. Besides, the

effective carrier mobility of the fabricated sensor is also reduced from 0.054 to 0.043 $cm^2 V^{-1}sec^{-1}$, which is ~20% of its original value.

4.3.5. Response, Detection limit, and Transient response

Fig. 4.5(a) depicted the dynamic ammonia gas response of the fabricated TFT based gas sensor against the different concentrations ranging from 0 to 20 ppm. The gas response (V_{DS} = -30 V and V_{GS} = -30 V) over some ammonia concentration of the fabricated TFT sensor can be extracted by the equation (3.2). From the response graph, it is clearly visible that the nano-composite based sensing layer illustrates the remarkable sensitivity in lower as well as higher concentration ranges of ammonia. However, this gas sensor has a relatively higher response of 52.62% in lower concentration range up to 20 ppm of ammonia.

The detection limit, which is one key figure of merit of the sensor, is defined by the lowest concentration of the analyte gas that can be detected, and estimated from the equation (3.3). The calculated LOD value of this sensor is ~0.44 ppm, indicating its applicability in lower concentration range of NH_3.

Fig. 4.5(b) represents cycles of the real-time transient response of the fabricated gas sensor (V_{DS} = -30 V and V_{GS} = -30 V) against the different concentrations of ammonia at 27°C. The response of the fabricated TFT sensor increases in a stepwise trend with the increasing concentration of ammonia. From this transient response curve, the response/recovery characteristics of the fabricated sensor can be determined. This data indicates that the fabricated nano-composite based TFT sensor exhibits a response time of ~2 sec, which is sufficiently fast as an NH_3 gas sensor, and the fabricated device shows a recovery time of ~6 sec for full recovery. However, it was observed that in our earlier report, the PBTTT-C14/MoS_2-QDs based sensor had a relatively poor recovery time towards NH_3 gas.

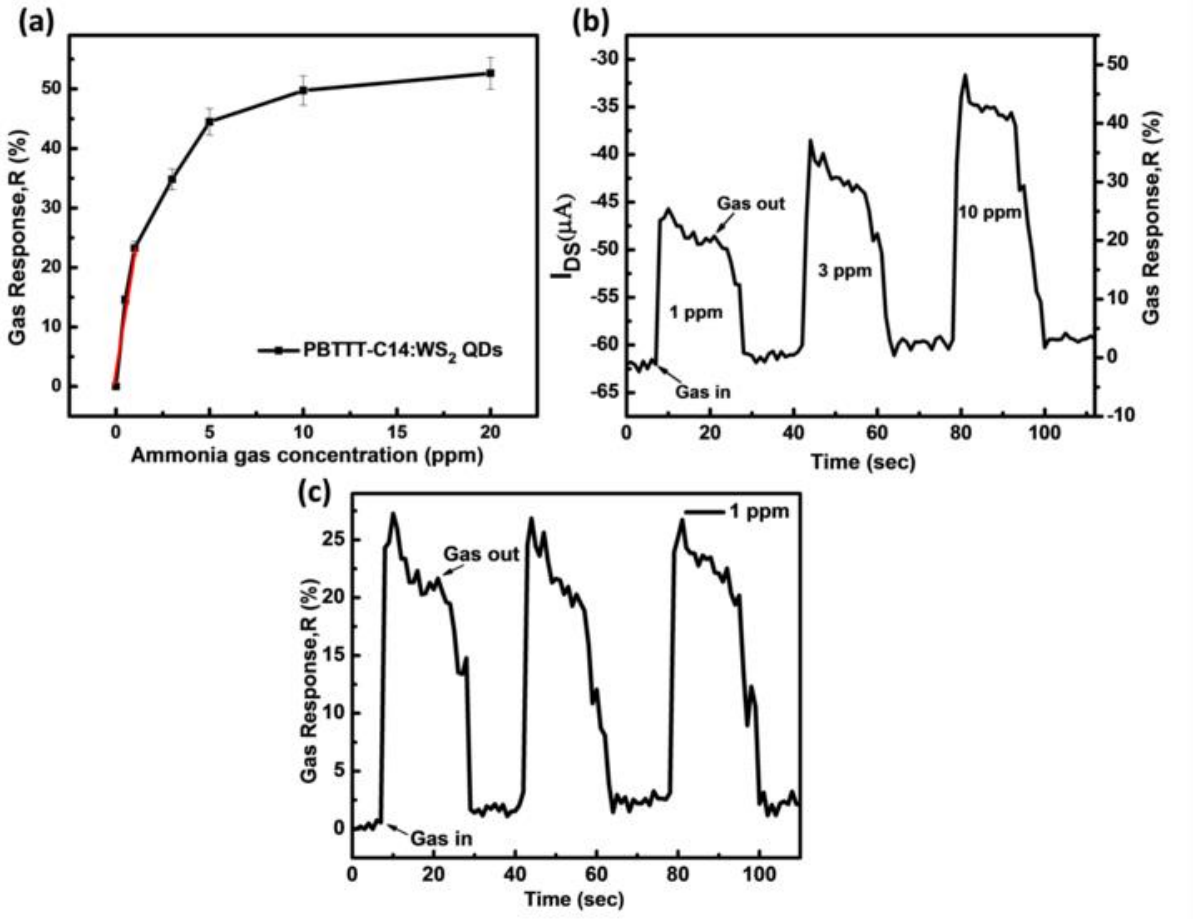

Fig. 4.5. (a) Estimation of detection limit (linear fitting of Gas response/calibration curve (red line)), (b) Transient gas response, and (c) repeatability of the TFT-based gas sensor at various concentration analyte gas at V_{DS} = -30 V and V_{GS} = -30 V.

In addition, the PBTTT-C14/WS_2-QDs based sensor has been tested for its reversibility characteristics, which is performed by repeated NH_3 flow with a fixed concentration in a certain time interval. Fig. 4.5(c) represents the transient response (V_{DS} = -30 V and V_{GS} = -30 V) for 1 ppm concentration of ammonia, which shows almost similar gas response in each cycle. These characteristics illustrate the good repeatability of the device, indicating its high reliability for practical application. A comparative performance of the PBTTT-C14/WS_2-QDs based OTFT sensor w.r.t the earlier reports are given in the Table-4.2.

Comparative performance of the PBTTT-C14/WS_2-QDs heterojunction based TFT sensor w.r.t the earlier reports are given in the Table-4.2.

Sensing material	**Device Type**	**Gas concentration**	**Response**	**Response/ Recovery time**	**Remark**
PQT-12	MSM	100 PPM	8%	8s/103s	Poor sensitivity [24]
Tips - Pentacene	OTFT	10 PPM	25%	200s/400s	Poor response/ recovery [159]
P3HT/RGO	OTFT	100 PPM	0.8%	5min/5min	Very low sensitivity [160]
PBTTT/MoS_2 -QDs	OTFT	50 PPM	Acc. Mode res.- 84.66% , dep. mode (Off current factor)- 3X 10^3	2s/-	Not sensitive for lower concentrations [161]
PBTTT/WS_2 -QDs (This work)	OTFT	20 PPM	Acc. Mode res.- 52.62%, dep. mode (Off current factor)- ~ 10^3	2s/6s	Quick response and recovery

4.3.6. Selectivity and Humidity Analysis

The selectivity study of the gas sensor is a crucial issue that helps us to recognize that particular analyte if it is mixed in with a similar type of analyte. Alternatively, it can be defined as the sensor's ability to detect a particular gas in presence of the other oxidative, reductive, and other common interfering gases. Fig. 4.6(a) represents the selectivity data of this heterojunction nano-composite based ammonia sensor. This data implies that the TFT based sensor having a higher response (positive) at 20 ppm NH_3 concentration compared to the other interfering gases, such as carbon dioxide (CO_2), carbon monoxide (CO), methane (CH_4), and propane (C_3H_8), which have been investigated up to 50 ppm of concentrations. In the characteristics, CH_4 gas possess positive response but with a negligible value. However, the other gases as CO_2, CO, and C_3H_8 are showing negative response (negligible) toward the sensor. This comparative data is ascribed to the high electron-donating capacity of the NH_3 gas, as discussed in the later mechanism section. However, for the other, gases the response value of the sensor either positive or negative, which depends on the electron-donating or capturing capability of the analyte gas [156, 162, 163].

Besides, it is very important to examine the influence of relative humidity on this ammonia sensor. For this investigation, the sensor has been exposed with 3 ppm concentration of ammonia in different RH ranges, and the findings are displayed in Fig. 4.6(b). This data implies that the variations in RH have a very mild effect on the sensor's response (V_{DS} = -30 V and V_{GS} = -30 V) as the drain current changes only 5% during the variation of RH from 20 to 80% as illustrated in the inset of Fig. 4.6(b). These outcomes suggest that the PBTTT-C14/WS_2-QDs heterojunction based TFT ammonia sensor is an excellent choice for NH_3 detection within a broad humidity range at room temperature.

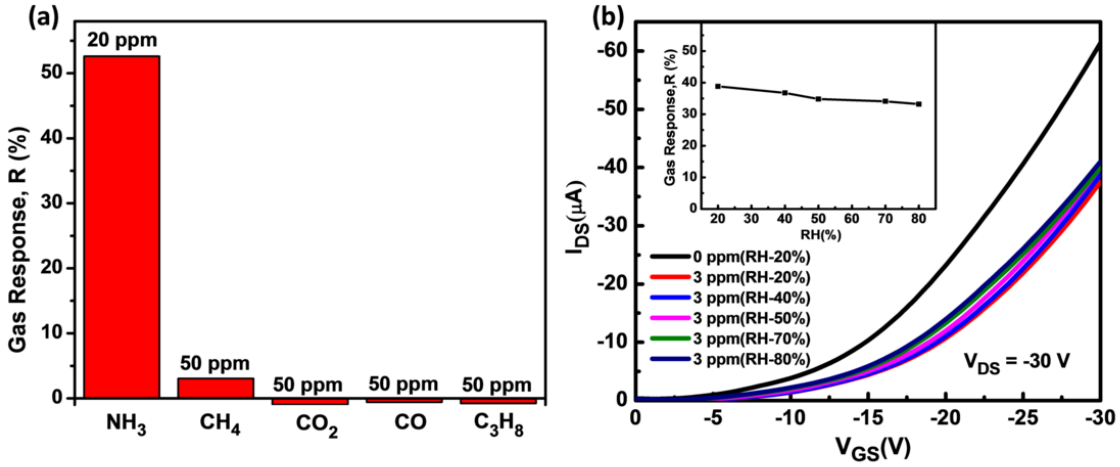

Fig. 4.6. (a) Selectivity analysis of sensor among various interfering gases, (b) Gas response of the TFT sensor with the variation of RH.

4.3.7. Ammonia sensing mechanism

The mechanism of ammonia detection by this PBTTT-C14/WS_2-QDs heterojunction based TFT sensor can be recognized from the variation of depletion layer and associated barrier height of polymer/QDs heterojunction. In this heterojunction WS_2-QDs and PBTTT-C14 works as n- and p-type semiconductors that forms a depletion layer around the junction where 'holes' transfer from the polymer to the QDs and 'electron' in a reverse way until their Fermi level achieved thermal equilibrium. As a consequence, a potential barrier will form at the heterojunction through this charge transfer (Fig. 4.7(b)). This uniformly distributed depleted part of this film exists throughout this nano-composite thin film (Fig. 4.7(a)). Electron-donating (reductive) NH_3 gas [135], decreases the hole concentration in the exposed polymer film, resulting in an extended depletion layer of the heterojunction, as shown in Fig. 4.7(c). Consequently, the PBTTT-C14 polymer's net mobile charge carrier concentration decreases, resulting in an enhancement of the total sheet resistance of the TFT channel. The potential barrier height of the mobile charges also

likewise increases (Fig. 4.7(d)). As a result, effective mobile carrier concentration of the polymer/QDs heterojunction thin film reduces.

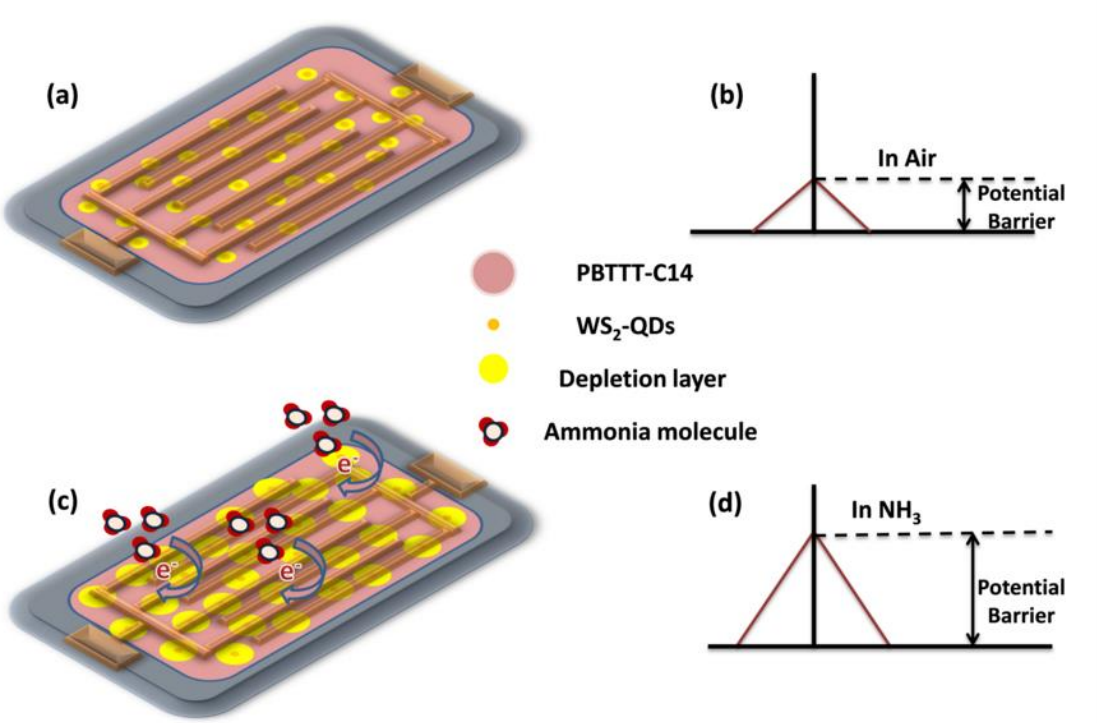

Fig. 4.7. Sensing mechanism of the TFT based sensor before and after the exposer of NH_3 gas.

As a consequence, TFT parameters, such as the ON/OFF ratio, carrier mobility (μ), and threshold voltage (V_{th}) changes continuously with gas concentration. There are two key factors that influence the OFF current of a TFT. The first is the gate-leakage current, and the second is the channel's DC conductance. If conductance of the polymer/QDs film decreases during the gas exposure and the gate leakage current of the TFT remains unchanged, then the off current of the TFT should decrease. Figure 4.8(a) demonstrates the OFF current variation of the TFT sensor, which diminishes gradually with increasing NH_3 concentration, supporting the enhancement of the polymer/QDs heterojunction depletion layer. Therefore, the 'OFF current factor' (ratio of OFF current before and after the exposer of NH_3) of the device, which is depicted in Fig. 4.8(b)

increases with gas concentration. Moreover, the variation in OFF current factor for device is ~10^3 orders greater than the device's on current variation. Besides, the semi-log presentation of this 'OFF current factor' has a good linearity with the analyte gas concentration. It can be noted that the variation of this 'OFF current factor' in the concentration range of 0-20 ppm is ~10^3, whereas in our earlier work, within this range it was only ~20 time, which indicates the level of improvement of this current work [156]. On the other hand, this sensor is capable to detect NH_3 gas within 20 ppm concentration and above of this range, variation of this 'OFF current factor' is very less.

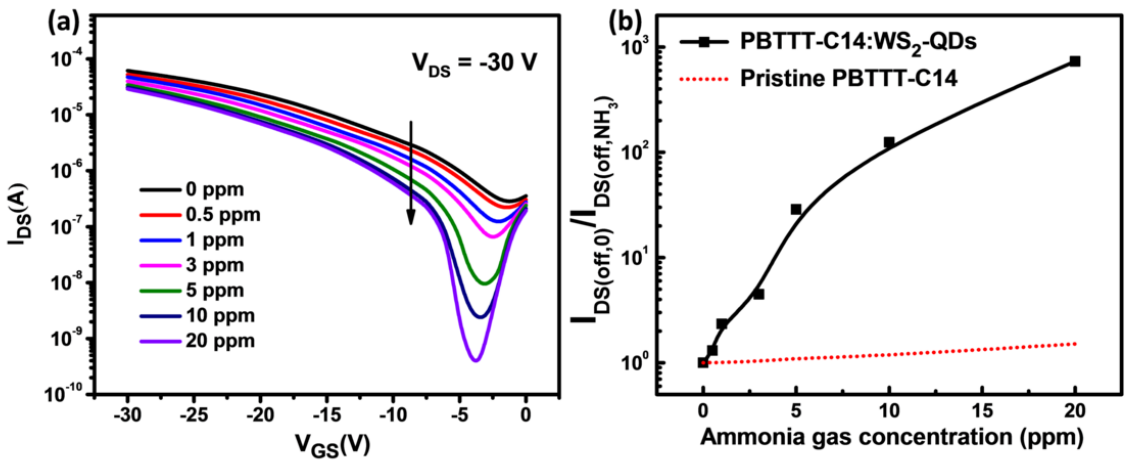

Fig. 4.8. (a) OFF current variation in nanocomposite based TFT sensor, and (b) variation of 'OFF current' factor with the NH_3 concentration in pristine PBTTT-C14 and PBTTT-C14/WS_2-QDs based TFT sensors.

In contrast, the earlier reported device is capable of measuring up to 50 ppm concentration by maintaining its good linearity [156]. Besides, off current factor data of reference pristine PBTTT-C14 based TFT has been presented in a dotted black line. From Fig 4.8(b), it can be observed that the improvement of off current factor w.r.t the pristine TFT is several orders

higher throughout the range. In addition to the OFF current variation of the device, the enhanced depletion layer enhances the depleted charge accumulation at the interface of dielectric and semiconductor, resulting in a shift in the V_{th} of the device by 6 V. As a consequence of this depleted charge accumulation of the polymer/QDs heterojunction, the effective carrier mobility of the TFT likewise decreases from 0.054 to 0.043 $cm^2 V^{-1}sec^{-1}$.

4.3.8. Broadband photo sensing properties

In addition to the NH_3 sensitivity, we also investigated the photo-sensing properties of fabricated polymer/QDs heterojunction based TFT under white light illumination in ambient conditions. A relative energy band diagram of this p-n heterojunction has been presented in Fig. 4.9(a) that represents a type-II heterojunction. Fig. 4.9(b) represents the UV-Vis absorption spectra of the pristine PBTTT-C14 and PBTTT-C14/WS_2-QDs nano-composite thin films, within the range of 300 to 1600 nm (QE-R quantum efficiency system (ENLITECH)). From these comparative absorption spectra, it can be noted that the absorption of the PBTTT-C14/WS_2-QDs film is mostly due to the PBTTT-C14 and is limited within 350 to 600 nm. The signature of the WS_2-QDs is quite invisible due to the lower concentration of the QDs in the polymer. However, these WS_2-QDs have a big role for the enhancement of photosensitivity that forms a depletion layer in the interfaces of the heterojunction as described earlier. Therefore, the performances of the polymer/QDs based phototransistors were investigated under white light illumination.

Fig. 4.10(a) shows the electrical characteristics of fabricated polymer/QDs based phototransistors under various white light intensities varied from dark to 650 W/m^2. This electrical data implies a large improvement in both (ON and OFF) the currents and is due to the photocurrent generation

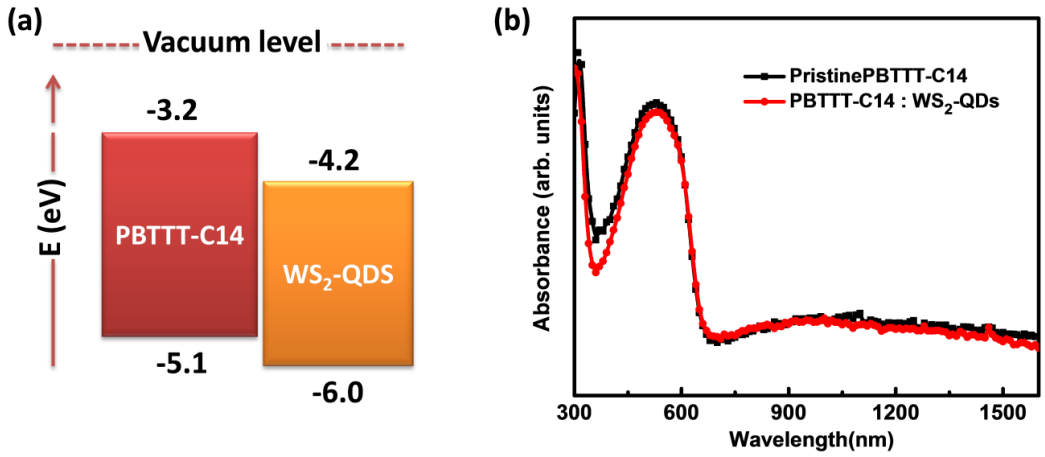

Fig. 4.9. (a) Energy level diagram of PBTTT-C14/WS_2-QDs, (b) UV-Vis spectra of PBTTT-C14 and PBTTT-C14/WS_2-QDs nano-composite.

in the hybrid channel of TFT. This data also indicates that there is ~ 70 times enhancement of OFF current under 650 W/m^2, whereas ON current of the device has been increased only 2.2 times (Fig. 4.10(c)). This data suggests that OFF current variation of this TFT is larger, which is due to the formation of depletion layers at the interfaces of nano-composite heterojunction. The photo-generated carrier in this depleted area then transfers to the PBTTT-C14 polymer which causes a large enhancement of channel conductivity, resulting in a larger variation of the OFF current of the device. Besides, a large positive shift of threshold voltage has been observed which originated due to the enhancement of carrier concentration of the channel. Fig. 4.10(b) displayed the threshold voltage shift of the phototransistor under various white light intensities. The threshold voltage Shift is as large as ~22 V corresponding to the light intensity of 650 W/m^2.

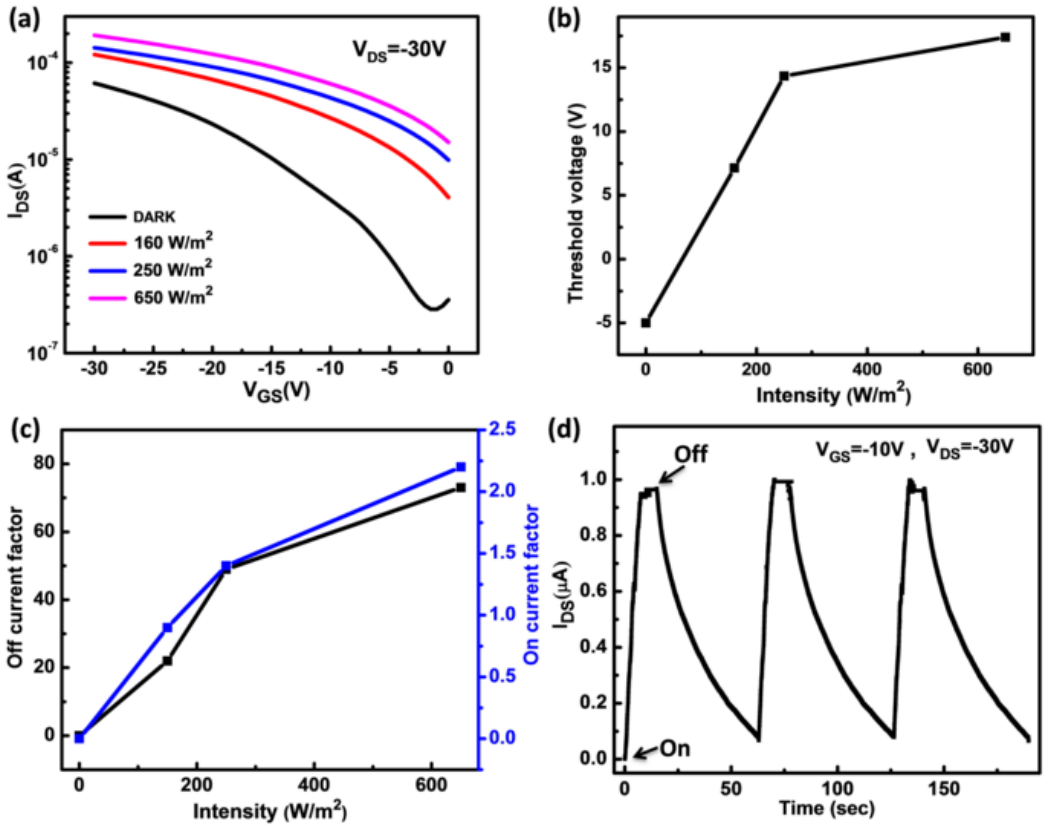

Fig. 4.10. (a) Output characteristics of heterojunction phototransistors (V_{DS} = -30 V) in dark and under various intensities of white light illumination, (b) Threshold voltage shift of the phototransistor under various white light intensities, (c) ON-state and OFF-state current factor and (d) Transient photo current response of the fabricated phototransistor at V_{DS} = -30 V and V_{GS} = -10 V.

The transient photo response of the heterojunction based phototransistor is represented in Fig. 4.10(d), which indicates the device has a faster response but a longer decay time. The primary reason of this longer decay time depends on the transit time of photo-generated carrier, which depends on two primary factors. One is the channel length of TFT and the other one is the carrier mobility of the semiconductor. This PBTTT-C14/WS_2-QDs has relatively poor carrier mobility.

Besides, the channel length is ~50 μm, which is quite high. Therefore, decay time is also very long. For this particular PBTTT-C14/WS_2-QDs semiconductor based TFT, the decay time can be faster if we reduce the channel length.

4.4. Conclusion

A highly sensitive PBTTT-C14/WS_2-QDs nano-heterojunction TFT based NH_3 sensor and broadband photo-detector has been fabricated by a simple, economical and high yield 'FTM procedure'. Hydrothermally synthesized WS_2-QDs and PBTTT-C14 blend based thin film has been used as the active NH_3 sensing layer of the TFT device. A considerable change in the ON current of the device has been noticed due to the small variation in gas concentration, which leads to the significant change in device parameters and consent to get a response of 50% at 10 ppm NH_3 concentration. Additionally, sensor based on PBTTT-C14/WS_2-QDs exhibited rapid response and recovery following each gas pulse with exceptional sensitivity and repeatability. Again the variation of this 'OFF current factor' in the concentration range of 0-20 ppm is ~10^3, whereas in our earlier PBTTT-C14/MoS_2-QDs work, within this range, it was only ~20 times with poor NH_3 recovery mechanism, which indicates the level of improvement of this current work. This TFT also possesses superior selectivity and can detect the low concentrations of NH_3 up to the detection limit of 0.44 ppm. Besides, around 70 times OFF current variation of this TFT has been observed under 650 W/m^2 white light illumination, indicating its very high photosensitivity under white light. In short, this PBTTT-C14/WS_2-QDs nano-heterojunction based TFT acquires very high sensitivity with fast response/recovery times with a wide range of detection capabilities, and is meeting most of the fundamental requirements for its practical implementation as an NH_3 sensor and broadband photo-detector.

Chapter 5

Organic homo-junction based thin film transistor for ammonia sensing applications

Abstract

An extremely sensitive ammonia (NH_3) sensor was developed using an aligned nanowires/thin film hybrid channel of an organic thin film transistor (OTFT). Conjugated polymer poly(2,5-bis(3-tetradecylthiophen-2yl)thieno(3,2-b)thiophene) (PBTTT-C14) has been used as semiconductor channel that has been fabricated via 'floating film transfer method' (FTM). The crystalline fibrillar microstructure within the liquid phase of the polymer has been developed by mixed solvent, which has been self-assembled on the air-liquid interface through the FTM method. This hybrid structured film was then transferred on a cleaned Si/SiO_2 substrate, whereas Au was used as source-drain electrodes of this OTFT. To investigate the ammonia sensing behavior of the designed OTFT, various low concentrations of the NH_3 have been exposed on the channel ranging from 0.2 ppm to 5 ppm. From the accumulation mode drain current variation, it was observed that the sensor is extremely sensitive towards ammonia gas with a response of about 75% at 5 ppm, whereas the limit of detection (LOD) is ~0.67 ppm, which confirms its applicability at the lower concentrations. More interestingly, the depletion mode current of this OTFT reduces ~ 200 times during this investigation, which is ~40 times larger variation than accumulation mode current. Additionally, these current variations of this sensor have excellent linearity to NH_3 concentration. This fabricated sensor also exhibits excellent selectivity and sensitivity to NH_3 gas, which can satisfy requirements for real-world applications.

5.1. Introduction

Chemical gas sensors have gain significant interest due to their widespread applications in modern civilization. Electrical gas sensors can be fabricated using different inorganic nano-structured materials, organic/polymer based semiconductor, carbon nano-structured based materials etc.[164-166]. Among different materials organic semiconductor (OS) based chemical

sensors are getting more attention because of their considerable variety in molecular design, high sensitivity with excellent selectivity at ambient conditions [167-170]. However, pure conducting polymer based sensors acquire low sensitivity towards analyte gases. Earlier, different nanostructures OS and organic/inorganic hybrid nanostructure have been used to improve the sensitivity of gas sensors [161, 171]. Owing to the noticeable structure, several techniques have been devised to modify the OS nanostructures in order to investigate the links between nanostructure to the enchantment of gas sensitivity [83, 172]. Besides, device geometry also plays a key role to improve its sensitivity and reliability. Among them the utilization of organic thin film transistors (OTFTs) as gas sensors has received considerable interest due to its advantages like higher sensitivity, option of direct interaction of semiconductor channel with analyte, functioning at room temperature etc. [169, 173-175]. In order to enhance the sensor's overall performance, it is imperative to exert control over the morphology by inducing in-plane ordering within the polymer [168, 176]. Several procedures have been utilized to achieve long-range ordering of polymer chains, including vaporization induced self-assembly, poor solvent induced assembly, ageing, high temperature rubbing, lithography, electro-spinning, and epitaxial crystallization [56, 58, 177-180]. Among them, poor solvent induced ageing is an economically viable method that synthesizes long fibers and could be an ideal choice for low cost and large area fabrication [181, 182]. In a mixture of good and poor solvent of a polymer, the poor solvent component generates collapsed coils of the polymer chains that work as a driving force for the self-assembly of polymers [183-185].

Among different gas sensors, ammonia (NH_3) sensor is widely used, particularly for unavoidable exposure of different workplaces including industry, hospital, cold storage etc. Workplace NH_3 exposure has been set by the US Occupational Safety and Health Administration (OSHA) at 50

ppm for eight hours a day, 25 ppm for ten hours a day, and 40 ppm per week. For instance, the breath NH_3 content may be several hundred parts per billion higher than normal in a patient with liver disease or urea balance issues [174, 186]. Commercialization hence necessitates an inexpensive and extremely sensitive NH_3 gas sensitive system which operates at room-temperature [187, 188].

In this chapter, I am presenting an OTFT based NH_3 gas sensor fabrication that has an aligned nano-wires/thin film hybrid morphology of PBTTT-C14 polymer channel. This PBTTT-C14 polymer has been used widely as NH_3 gas sensor due to their higher air stability and high carrier mobility [156, 189]. A good-poor mixed solvent has been used to dissolve the PBTTT-C14 polymer that produces a fractional part of the film by crystalline fibrillar polymer nano-wire, which effectively forms this hybrid layer. A facial method called floating film transfer method (FTM) has been used to deposit this polymer channel. To investigate the room temperature NH_3 sensing behavior of this gas sensor, the channel of the OTFT was exposed with ranges of concentrations of the ammonia from 0.2 ppm to 5 ppm and recorded the change in the OTFT parameters for the investigation of the sensitivity, selectivity and other important parameters.

5.2. Experimental methods

5.2.1. Materials

Conjugated polymer, PBTTT-C14 with a molecular weight of more than 40,000 is acquired from Sigma-Aldrich, India. Both analytical-grade chloroform and toluene were attained from Merck, India.

5.2.2. Preparation of fibrillar PBTTT-C14 nanowires

By using the conception of solvent driven self-assembly of the polymer, PBTTT-C14 solution was prepared by the ageing of polymer dissolved in a pair of solvents of chloroform and toluene. In self-assembly of the polymer, pair solvent of chloroform and toluene were used as the good and poor solvents, respectively. For this procedure firstly, the mixed solvent volume ratio of chloroform and toluene has been taken 9:1 and then subsequently added with 5 mg/ml polymer concentration in a glass vial. This mixed polymer solution was then stirred on a magnetic hot plate at an elevated temperature of 90°C for 2 hours in a sealed glass vial for the complete dissolution. The heated solution was then left in closed chamber for 10 min allowing for the self-assembly of the polymer to form the nano-wires [182].

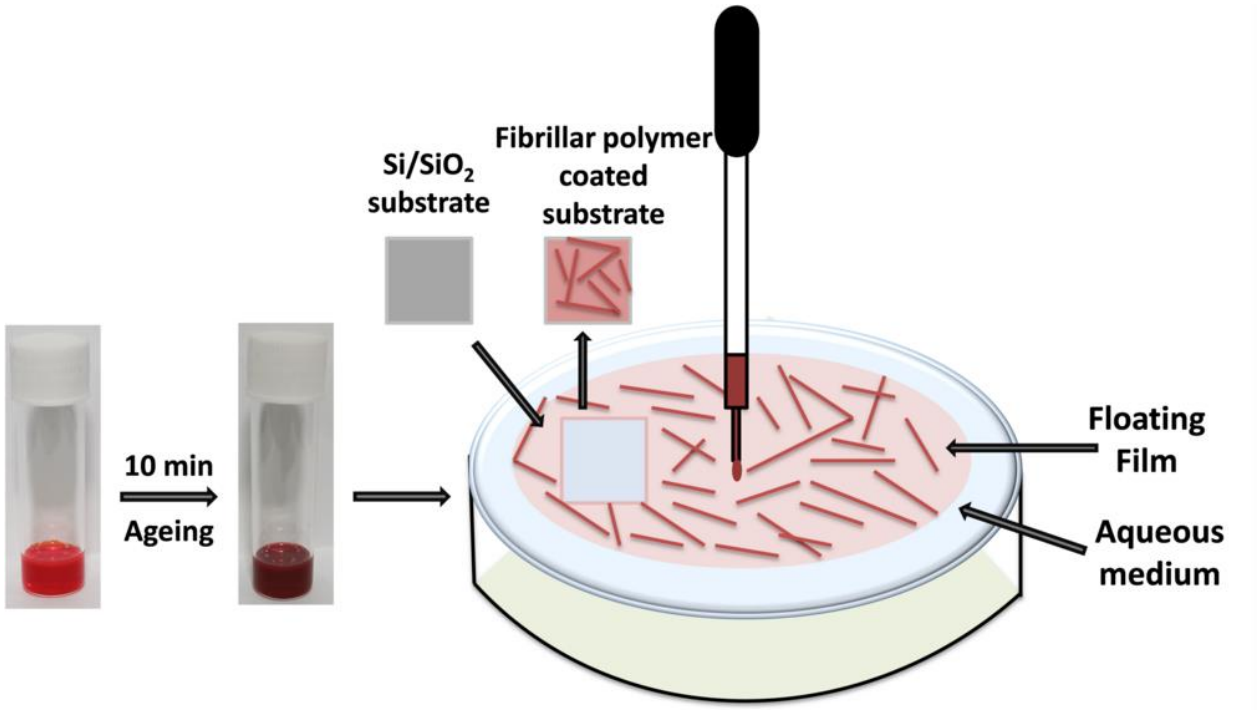

Fig .5.1. Demonstration of the self-assembly of the polymer and FTM method for the thin film fabrication.

In this mixed solvent, chloroform encourages polymer chain extension due to its high solubility, which enhances chain organization freedom and poor solvent creates unfavorable interactions with polymer chains, resulting in a driving factor for polymer self-assembly. Fig. 5.1 demonstrates as well-dissolved PBTTT ages, it creates fibers as it interacts with solvent molecules, and one prominent physical change that can be seen is the color changing from bright orange to dark brownish-purple as it goes through this transition. That aged solution has been used for thin film deposition via FTM method as shown in Fig .5.1. In which long-fibrous nano-wire polymer film is stamped onto the desired substrate for the sensing device fabrication.

5.2.3. Device fabrication

For the bottom contact top gated OTFT based sensor fabrication, commercially available highly doped p++ silicon substrates with a thermally grown SiO_2 (300 nm) layer are used as the gate dielectric. Initially, Si/SiO_2 substrates are thoroughly cleaned in an ultrasonic bath cleaner using distinct solvents: soap solution, deionized water, acetone, and isopropanol, and then dried at 80°C under nitrogen atmosphere. For the casting of the semiconducting/sensing layer on the cleaned substrate pre-described FTM method has been used, in which approximately 10 µl of the polymer solution was poured at the middle of a 10 cm diameter petri-dish containing hydrophilic liquid substrate (ethylene glycol and glycerol in a 3:1 ratio) under ambient conditions. In order to fabricate the OTFT, the formed polymeric fibrillar film over the liquid substrate was casted to the specified substrate as illustrated in Fig. 5.1, and dried in a nitrogen environment at 90°C. After that, a thermal vacuum evaporation unit with an interdigitated Ni shadow mask was used to construct source-drain electrodes of gold (Au) on top of a substrate covered with a semiconducting layer. The evaporation rate was 1.5 Å/s at vacuum 6×10^{-5} Torr. The

interdigitated channels were 50 µm in length and 18 mm in width, respectively. Semiconductor device analyzer was used to measure the electronic properties of the fabricated device.

5.2.4. Characterization

To obtain the absorption spectra of the FTM coated PBTTT-C14 and fibrillar PBTTT nano-wire based film, UV–Vis spectrophotometer (UV-2600, Shimadzu) was used. X-ray diffractometer (Rigaku) is used for the crystallinity analysis of the films. The TEM micrographs with selected area electron diffraction (SAED) patterns of the fibrillar polymer film over Cu grid were obtained via TECHNAI $G^2$20 TWIN (New Zealand). The roughness analysis of the film deposited substrate was performed by Atomic force micrograph (AFM) using NT-MDT "NTEGRA Prima" (Russia). Lastly, a controlled atmosphere gas sensing assembly was used investigate the ammonia sensing performances of the OTFT sensor. There are two inlets and one outlet in the gas assembly. The first inlet is for injecting NH_3 gas with the mass flow controller, while the second inlet and exit are for flushing air into and out of the chamber. A set of probes inside the test chamber are placed to connect devices with Keysight B1500A semiconductor parameter for their electrical characterization. Different concentrations of NH_3 gas are passed through the inlet line of the test chamber under ambient temperature (temperature ~ 25°C with RH of ~ 50%) with a regulated flow of dry air, and variation of electrical signal are observed using a parameter analyzer.

5.3. Results and discussion

5.3.1. Optical and structural characterizations of PBTTT-C14 nano-wire thin film

As mentioned earlier, the color of mixed solvent PBTTT-C14 polymer solution changes over the time from bright orange to dark brownish-purple as it performs this transition. The detailed kinetics of the variation of absorption w.r.t time has been discussed in earlier report [182]. Simultaneously, the viscosity of the solution also increases along with the fiber synthesis process. Changes in color and viscosity are correlated with the numbers of non-dissolved microfibers present in the polymer solution. Specifically, the development of optical absorption of the polymer solution serves as a direct indicator of the degree of π-π inter-chain contact, which is the driving force behind the production of nano-wires. The normalized absorption spectra of PBTTT-C14 films produced by FTM methods are shown in Fig 5.2(b). Both PBTTT-C14 films have single broad absorption band in their UV-vis spectra, which is typically present in polythiophene derivatives. The fibrillar PBTTT-C14 nano-wire film exhibits a more noticeable red-shift in its UV-vis spectrum, and its absorbance is higher than that of the isolated one. The higher energy absorption band (549 nm) appeared in both the cases due to π-π* transition. However, as the thiophene ring aged, an extra shoulder peak at lower energy 577 nm and 603 nm was observed as a result of the coupling of the π-π* transition to the C=C, as was also noted for P3HT.[190-192] Additional evidence for the molecular packing of PBTTT-C14 nano-wire films was investigated by XRD study (Fig. 5.2(c)). The diffraction peaks at 4.09, 8.30 and 12.42 are the results of the d-spacing (lamellar structure) of their crystal structure, which corresponds to the (100), (200) and (300) planes, respectively, indicating their structure towards

face-on orientation. These peaks moved toward higher 2θ values (that is, from 4.09 to 4.23 for (100) plane, from 8.30 to 8.42 for (200) plane and, from 12.29 to 12.56 for (300) plane), in comparison to its isolated akin. This behavior could be the consequence of face-on orientation leading to a decrease in d-spacing.

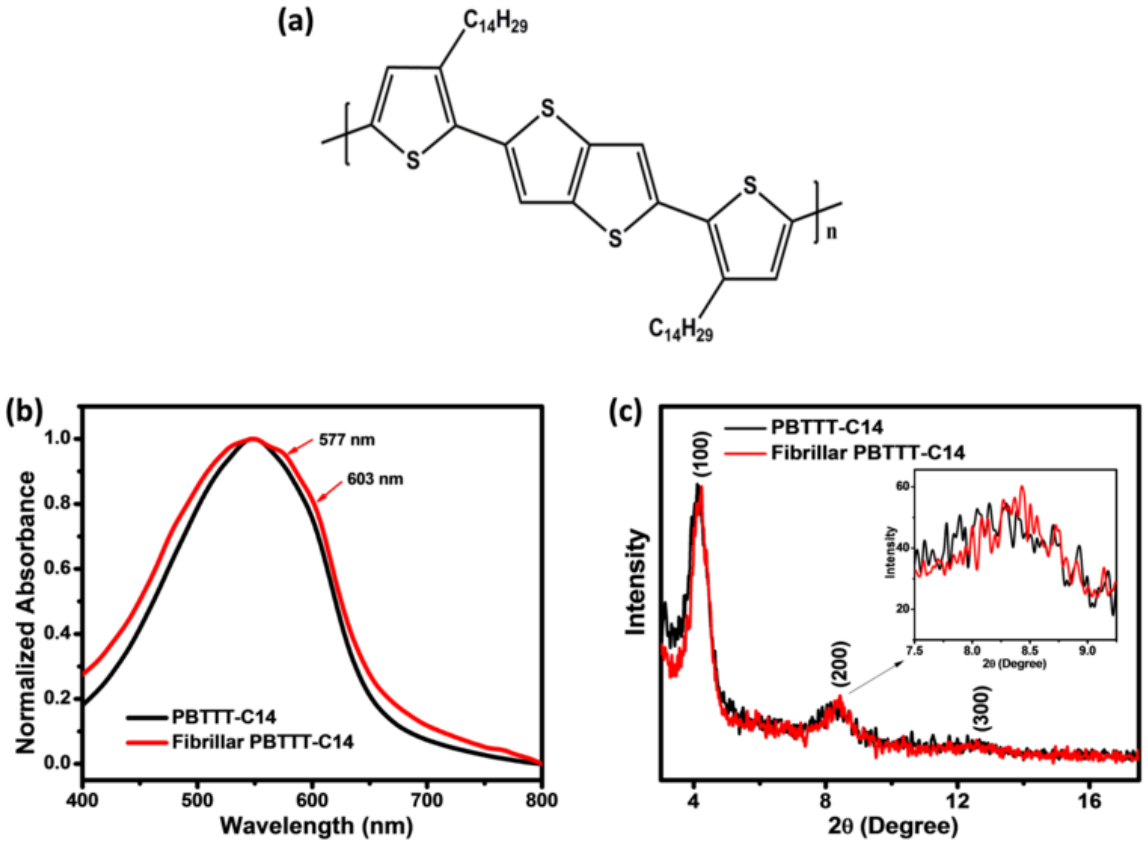

Fig. 5.2. (a) Chemical structure of PBTTT-C14**,** (b) UV-Vis spectroscopy of pristine and nano-wires/thin film hybrid PBTTT-C14 thin film, and (c) XRD pattern of pristine and nano-wires/thin film hybrid PBTTT-C14 (inset shows zoom view of (200) peak).

For the structural analysis of FTM coated fibrillar polymeric film, TEM analysis has been done by transferring the film via FTM method onto a carbon coated TEM grid. The TEM micrograph and SAED pattern of this polymer film is presented in Fig. 5.3(a) and 5.3(b), respectively. This

TEM micrograph clearly shows the aligned nano-wire formation over the area that is spread uniformly. Additionally, development of the SAED pattern indicates the nano-wires are crystalline in nature.

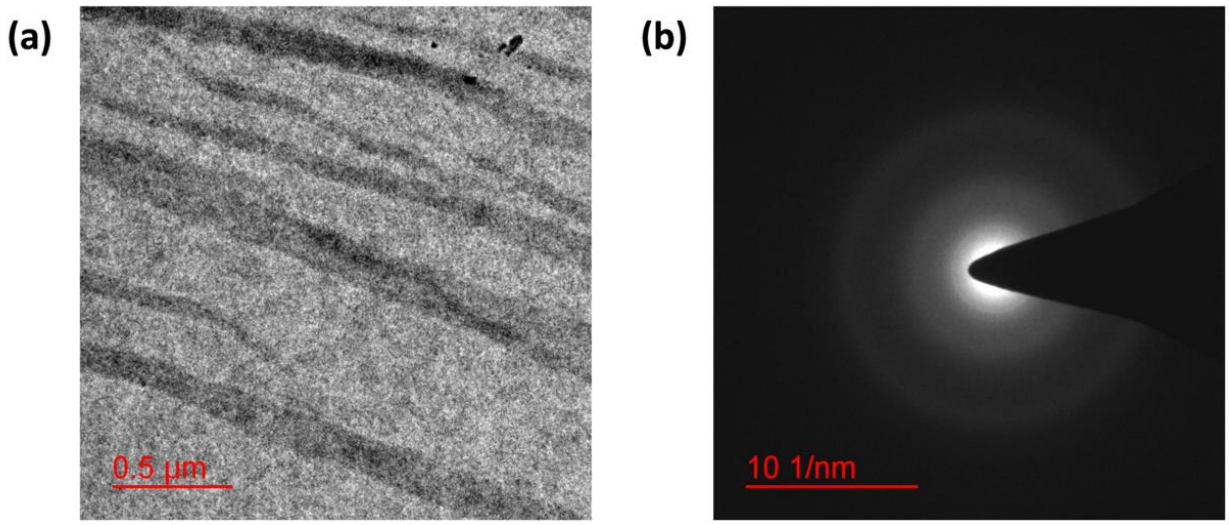

Fig. 5.3. (a) TEM image and, (b) SAED pattern of FTM coated PBTTT-C14 nanowire/thin film.

AFM characterization has been done by scanning 10 µm x 10 µm and 3 µm x 3 µm film regions, as illustrated in Fig. 5.4(a) and 5.4(b), which revealed the formation of polymeric fibrillar morphology consist of regular network of interconnected 1D nano-wires. The uniformity and self-alignment of these nano-wires are clearly visible in the micrographs. Fig. 5.4(c) shows the 3D structure that provides the regular height variation of the film due to this nano-wire formation, whereas Fig. 5.4(d) shows the height profile of the nano-wire, indicating its diameter and height are ~ 300 nm and 20 nm respectively. From careful AFM studies of different parts of the film, we measured the average coverage of such nano-wire in the film with the help of image J. This study indicates the nano-wire is covering ~26% of the film area.

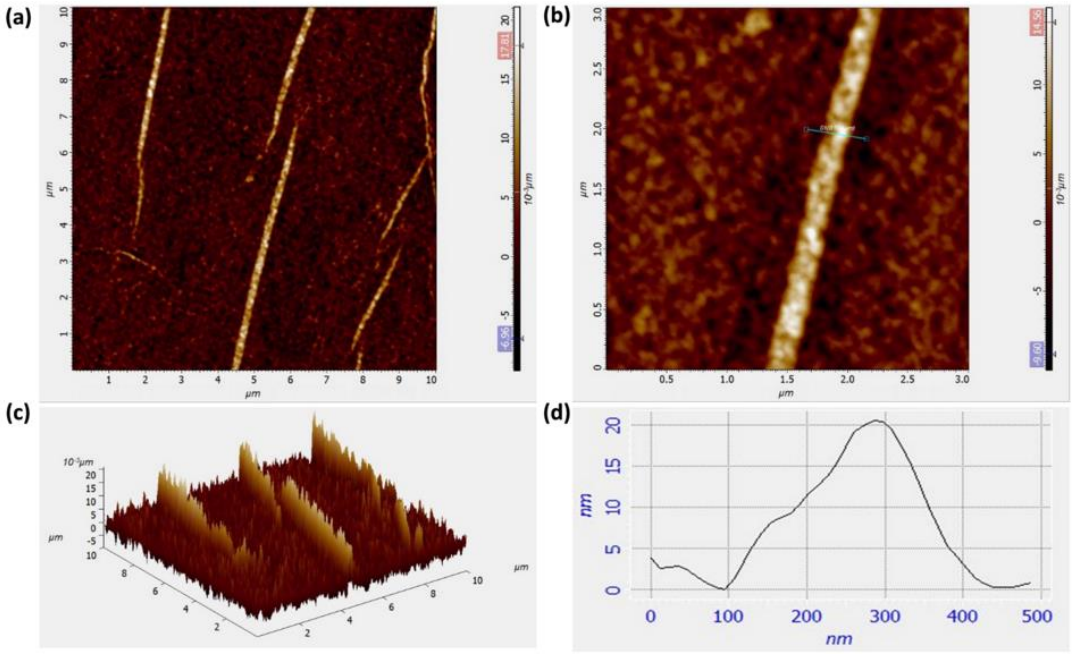

Fig. 5.4. (a), (b) AFM images of the FTM coated fibrillar PBTTT-C14 and, (c) corresponding 3D image and (d) AFM height profile of the film.

5.3.2. Electrical Characterization

Figure 5.5 illustrates the ambient condition (25°C with 50% RH) electrical characterization (current-voltage characteristics) of the designed top contact bottom gated transistor. The output (I_{DS}-V_{DS}) characteristics of the PBTTT-C14 nano-wire/thin film hybrid channel based OTFT are shown in Fig. 5.5(a). During this study, the drain voltage has been swept in the range of 0 to -30 V with various constant gate biases. Fig. 5.5(b) shows the transfer (I_{DS}-V_{GS}) characteristics in which gate bias has been varied from 0 to -30 V and keeping drain bias at -30 V. Important transistor electrical parameters, like mobility (μ_h) and threshold voltage (V_{TH}), are derived from transfer characteristics by using the equation (3.1). The fitted straight line that corresponds to the

$I_{DS}^{1/2}$ against V_{GS} curve at V_{DS} = -30 V is extrapolated to find the threshold voltage of the designed OTFT.

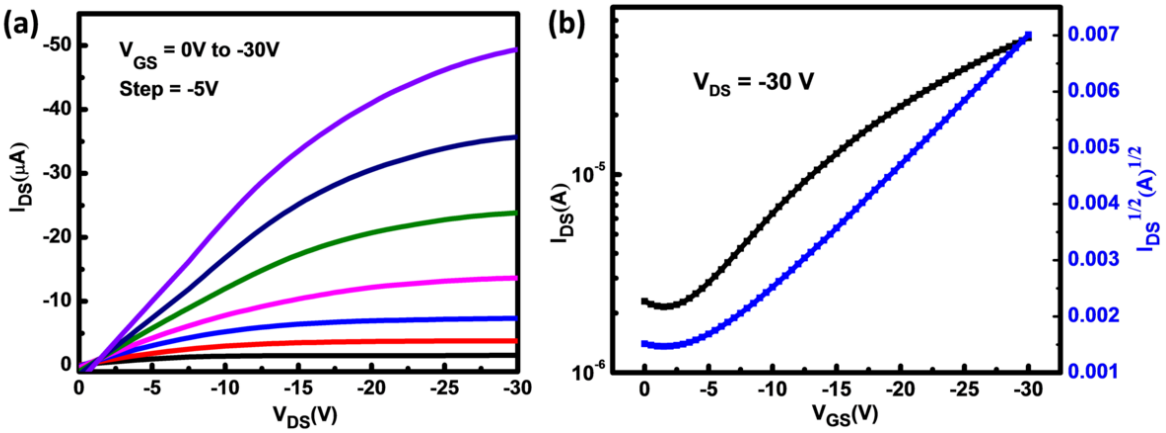

Fig. 5.5. (a) Output characteristics, and (b) Transfer characteristics of PBTTT-C14 nanowire/thin film hybrid channel OTFT.

5.3.3. Ammonia sensing analysis

For the purpose of NH_3 sensing analysis, OTFT channel is exposed to different concentrations of NH_3 gas, ranging from 0 ppm to 5 ppm, at 25°C under the regulated flow of dry air inside a sealed container with 50% relative humidity, as seen in Fig. 5.6(a). The gate bias (V_{GS}) is swept from 0 to -30 V throughout the sensing measurement, while the drain voltage (V_{DS}) is fixed to -30 V. The transfer characteristic shows that the drain current (I_{DS}) of the OTFT steadily drops as soon as the NH_3 concentration rises and almost saturates after being exposed to more than 5 ppm NH_3 gas concentration.

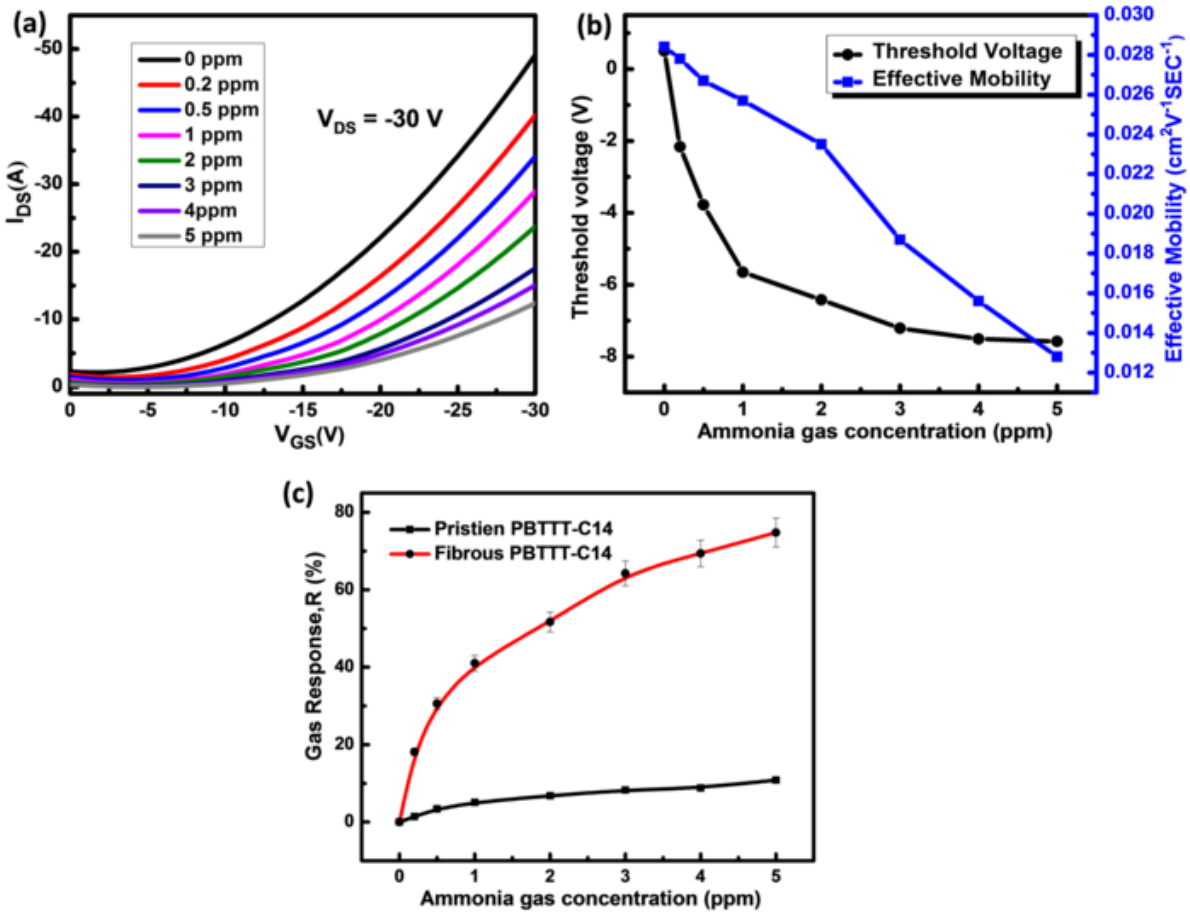

Fig. 5.6. (a) Transfer characteristics of PBTTT-C14 nano-wire/thin film hybrid channel OTFT sensor at V_{DS} = -30V, and (b) Corresponding Shift in threshold voltage (V_{TH}) and mobility (μ_h) with different concentrations of ammonia (0 ppm-5 ppm), (c) Gas response graph of the fabricated OTFT sensor at V_{DS} = -30 V (The data points with black line indicates the response of pristine PBTTT-C14 based OTFT device).

The decrease in drain current (I_{DS}) of the OTFT is associated with the reduction of effective carrier mobility (μ_h) and threshold voltage shifting (V_{TH}), which is due to the depletion of the channel caused by the NH_3 molecules. This depletion forms a layer of static charge in the

channel that reduces effective carrier density of the channel resulting in the reduction of the accumulation mode current. Besides, due to the addition of a static depleted layer (positive change) on top of the channel, V_{TH} of OTFT shifted towards a more negative direction. The variation in V_{TH} and μ_h of the devices as a function of NH_3 concentration is depicted in Fig. 5.6(b). The results demonstrate that there is a change of V_{TH} of more than 8 V during the exposure of various NH_3 concentrations, with high linearity up to 5 ppm. Additionally, the designed sensor's effective carrier mobility also decreases from 0.0284 to 0.0128 $cm^2 V^{-1}sec^{-1}$, which is about 50% of its initial value. We performed this NH_3 sensing study several times with the same device and found ~±2% variation of device parameters of these listed values. The reduction of accumulation mode drain current is used to determine the response (R) of the device. This R is define from the ratio of variation of drain current with respect to the original drain current as shown in the equation (3.2).

The response (sensitivity) of the PBTTT-C14 nano-wire/thin film hybrid channel OTFT at 5 ppm concentration of NH_3 is 74.8% (Fig. 5.6(c)), which is calculated at the constant value of V_{DS} = -30 V corresponding to the Fig. 5.6(a). It can be noted that the response of this device is ~8 times higher than the pristine PBTTT-C14 based OTFT (Fig. 5.6(c)). The limit of detection of the sensor was also estimated with the help of the following equation (3.3). The calculated LOD of the fabricated ammonia sensor is 0.67 ppm. It can be noted that the sensor exhibits a very acceptable response (~18%) even at the concentration of 0.2 ppm. The variation in V_{TH} and μ_h of the devices with various concentrations of ammonia gas is listed in Table-5.1

Table- 5.1: Variation in OTFT parameters and the sensitivity of the sensor with different concentrations of NH_3 gas.

NH_3 (ppm)	**On current Ion (μA)**	**Effective Mobility μ_h ($cm^2V^{-1}sec^{-1}$) $x10^{-2}$**	**Threshold voltage V_{th} (V)**	**Change in Threshold voltage (ΔV_{th})**	**Response (%)**
0	49.14	2.84	0.5	0	0
0.2	40.24	2.76	-2.16	2.66	18.11
0.5	34.10	2.67	-3.78	4.28	30.59
1	28.97	2.57	-5.65	6.15	41.03
2	23.75	2.35	-6.42	6.92	51.67
3	17.56	1.87	-7.21	7.21	64.26
4	15.05	1.56	-7.51	8.01	69.36
5	12.38	1.28	-7.58	8.08	74.80

It can be noted that as an NH_3 gas sensor, this fibrillar conjugated polymer based OTFT sensor provides various advantages such as room temperature operation with high sensitivity, rapid response to low-concentration analyte with the excellent selectivity to the NH_3 gas. Besides, this OTFT based sensor also offers both depletion and accumulation mode of operations, in which the variation of channel current is quite linear with NH_3 concentration, which is an important factor for practical application. Also, the manufacturing method of the sensor is pretty simple, which doesn't require any additional instrument for the NH_3 sensitive fibrillar polymer film fabrication. A comparative performance of the NH_3 sensor w.r.t the earlier reports are given in the Table-5.2.

Table-5.2: Comparative performance of the NH_3 sensor w.r.t the earlier reports.

Device Type	Sensing material	Deposition technique	Operating Temp.	Response (%)	Remark
Chemi-resistive	PANI/TiO_2	chemical poly-merization	RT	5.6% (117 ppm)	Poor response [193]
MSM	PDI-HIS	Drop casting	RT	35% (100 ppm)	Less Detection limit [128]
OTFT	P3HT	Spin coating	RT	100% (30 ppm)	High response time [194]
OTFT	PBTTT/MoS_2-QDs	FTM	RT	Accumulation Mode res.- 35.1% (5 ppm), depletion mode Off current factor- ~3.9	Slower recovery time/ not that sensitive for lower conc. [156]
OTFT	PBTTT/WS_2-QDs	FTM	RT	Accumulation mode res. – 44.5% (5 ppm), depletion mode Off current factor- ~28	Quite good for high detection limit, and low concentration NH_3 detection [195]
OTFT (This work)	PBTTT Nano-wire	FTM	RT	Accumulation mode res.- 74.8% (5 ppm), depletion mode Off current factor - ~10^2	High sensing response at lower conc. in both operating modes (this work)

5.3.4. Selectivity and Transient analysis

To identify the selectivity of this sensor, the electrical characterization of this OTFT was tested with other interfering gases such as methane (CH_4), propane (C_3H_8), carbon dioxide (CO_2), carbon monoxide (CO). The relative response of OTFT in presence of those gases w.r.t the NH_3 gas is presented in Fig. 5.7(a). It can be noted the response of the device at 5 ppm NH_3 is several orders higher than that of 20 ppm other interfering gases. These findings imply that the PBTTT-C14 nano-wire/thin film hybrid channel OTFT sensor exhibits notable improvements in selectivity, indicating its considerable potential for use in low-cost, portable ammonia sensors. The level of response difference of interfering gases that we achieve in this work is quite higher w.r.t most of those reports.

To investigate the transient performance of the fabricated sensor, various concentrations of the ammonia have been exposed ranging from 1-5 ppm, on the OTFT channel. A step-wise trend has been obtained with the variation in drain current of the OTFT sensor, as depicted in Fig. 5.7(b). The fabricated sensor follows the physisorption mechanism dominantly, and acquires a rapid response time of 2 sec. However, the recovery time of the sensor is ~12 sec which could be due to the slow desorption of NH_3 from the channel. Further, it can be reduced by reducing the channel length. Besides, in a fixed concentration of analyte, we tested ~ 10 successive cycles for its response behavior study that show quite repeatable cyclic behavior. However, above this range, the variation of I_{DS} slowly decays. After leaving this device for several hours, it works like a fresh device again. This type of fatigue behavior is very common for conducting polymer based sensors.

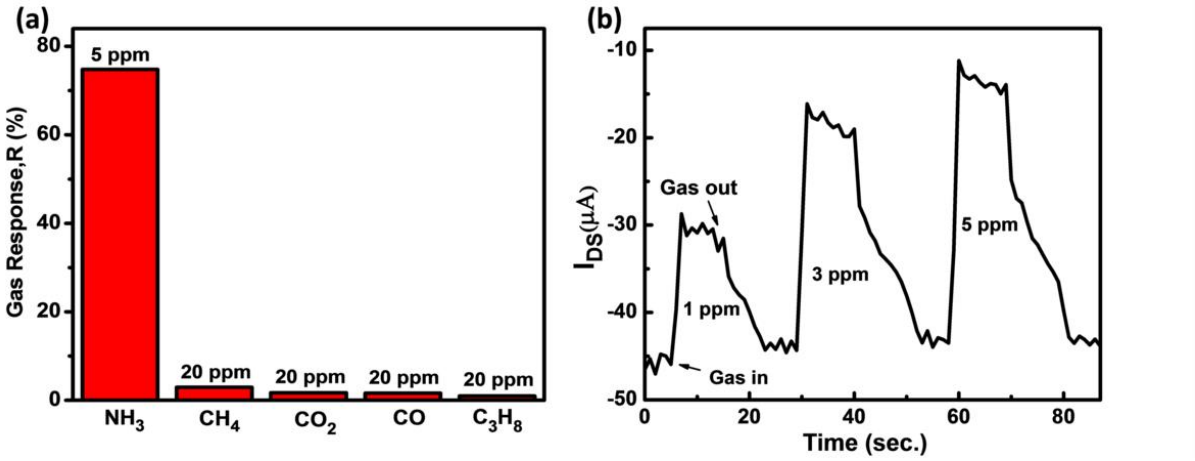

Fig.5.7. (a) Selectivity analysis, and (b) transient response of the OTFT sensor (V_{DS} = -30 V, and V_{GS} = -30 V).

5.3.5. Sensing mechanism

The variation of I_{DS} of this device in presence of analyte gas is primarily due to the reversible chemisorption or redox reaction. The organic PBTTT semiconductor is a p-type semiconductor and has provision to oxidize NH_3 by sharing H^+. During the exposure of NH_3 gas to the semiconductor channel, PBTTT is donating H^+ through chemisorption ($NH_3+H^+ \leftrightarrow NH^{4+}$), which is reversible phenomena. Besides, the preceding technique was designed to achieve a high NH_3 sensing performance through the polymeric fibrillar nano-wire/thin film hybrid morphology for its higher specific surface area, which offers additional active sites for the ammonia molecule interactions (Figure 5.8(a)). These fibrillar morphologies are quite thick and have significantly high conductivity w.r.t the pristine PBTTT-C14 film, which decreases the sheet resistance of the OTFT channel very extensively. As a consequence, the ambient condition off current (~2.15 μA) of this aligned nano-wires/thin film hybrid channel based OTFT is ~2 orders higher w.r.t the pristine film OTFT (~0.68 μA).

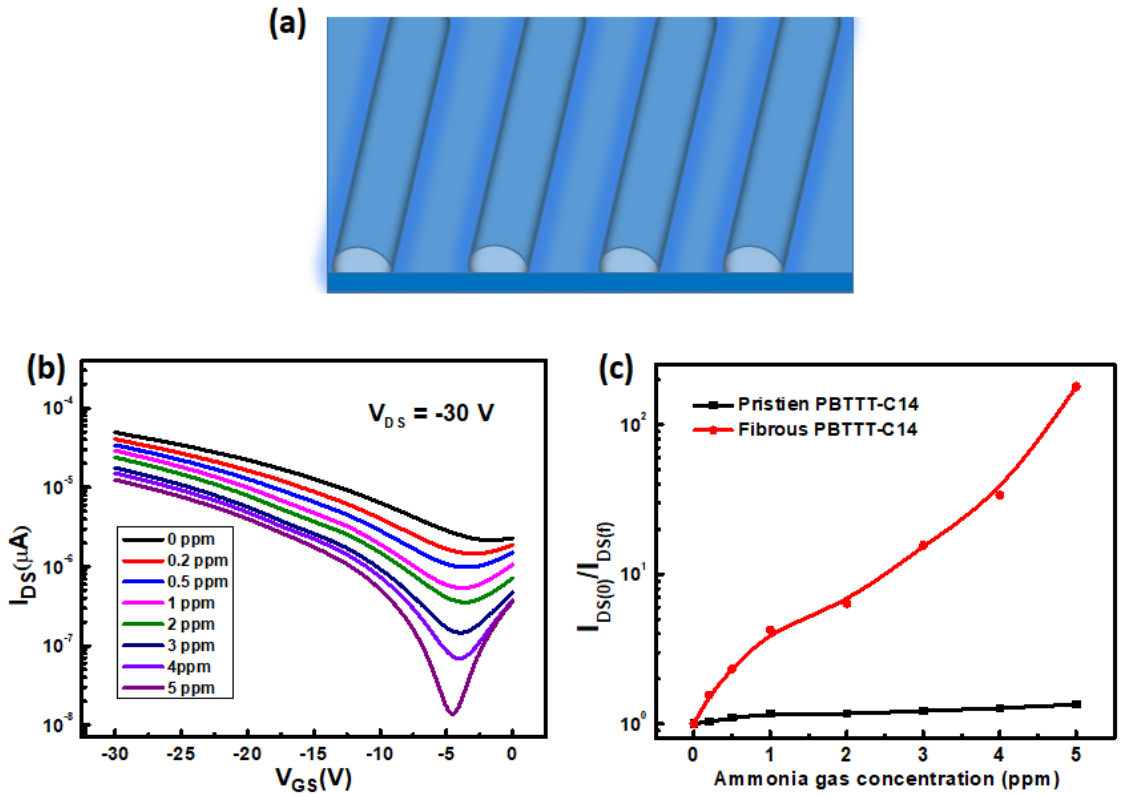

Fig. 5.8. (a) Schematic presentation of align nanowires/thin film hybrid channel, (b) variation in OFF current of the OTFT sensor, and (c) corresponding OFF current factor with the NH_3 concentrations (The data points with black line indicates the OFF current factor of pristine PBTTT-C14 based OTFT device).

When NH_3 gas enters the conductive channel of the OTFT, it interacts mostly with these nano-wires due to their higher effective surface coverage. During this process, the NH_3 gas diffuses into the fibrillar structure via chemisorption. Since PBTTT-C14 is a p-type semiconductor in which holes serve as the primary charge carriers, therefore as soon reductive NH_3 interacts, electrons are injected to the nano-wires. This electron injection causes a partial depletion of the channel that results in a large reduction of the I_{DS} both in accumulation and depletion mode [134, 156].

In the accumulation mode, the variation of I_{DS} is ~7 times larger compared to the pristine film OTFT [156]. As a result, the sensor's response also rises in the same ratio. Simultaneously, due to the deletion of the nano-wires, the sheet resistance of the nano-wires/thin film hybrid channel increases in a larger ratio which reduces the off current (also off current factor) of OTFT in a wide scale that result this OTFT very sensitive in depletion mode operation. Due to the variation of NH_3 concentration from 0 to 5 ppm, the OFF current reduces ~200 times which is shown in Figure 5.8(b). Again this variation of the off current of the OTFT, which is presented in term of the 'off current factor', the ratio of the off current of the device under ambient to NH_3 gas ($I_{D,\ off}{}^{amb}$/ $I_{D,\ off}{}^{NH3}$), varies quite linearly with NH_3 concentration as illustrated in Fig 5.8(c). It's worth to note that the off current variation of the sensor within the range of 5 ppm NH_3 concentration, is approximately ~40 times larger than the ON current variation, indicating its extremely high sensitivity in depletion mode operation.

5.4. Conclusion

P-type PBTTT-C14 polymer based aligned nanowires/thin film hybrid channel has been used in a top contact bottom gated organic field-effect transistor (OTFT). This OTFT shows an extraordinarily high sensitivity in the low concentration range (0.2 ppm to 5 ppm) of ammonia gas. The fibrillar polymer nano-wires have been grown from the solvent-driven polymer self-assembly, in which a mixed solvent of a good and poor solubility of PBTTT-C14 have been used to prepare the solution. This nano-wires/thin film hybrid film was deposited by the economical and efficient Floating film transfer method (FTM). Various concentrations of NH_3 were exposed on the fibrous polymer-based OTFT channel from 0.2 ppm to 5 ppm to explore the NH_3 sensing behavior of the constructed OTFT. In the accumulation mode operation, the sensor has achieved

~75% response at 5 ppm concentration of NH_3, which is unusually high in this low concentration range. More interestingly, in the depletion mode operation the variation of drain current is ~100 times higher than its accumulation mode current that results ~200 times off current variation due to the interaction of 5 ppm NH_3 gas. Both in depletion and accumulation mode of operation, variation of channel current is quite linear with NH_3 concentration, which is an important factor for practical application.

Chapter 6

Development of low-voltage operating organic thin film transistor for ammonia and photo sensing applications

Abstract

A low operating voltage (≤2 V) organic thin-film transistor (OTFTT) is developed in top contact bottom gated configuration using a fibrous conducting polymer channel for its application as NH_3 gas sensor. For, this device fabrication, fibrous film of PBTTT-C14 is transferred onto the Li-alumina (Li-Al_2O_3) gate dielectric by the economical and facial Floating film transfer method (FTM).This fibrous PBTTT-C14 thin film has been prepared, as of our previous study, by utilizing the conception of solvent driven self-assembly of the polymer. To examine the ammonia sensing performance of the fabricated OTFT, a range of concentrations of the NH_3 have been exposed on the fibrous polymer based OTFT channel from 0 ppm to 20 ppm. From the electrical characteristics behavior of the OTFT we have investigated the sensitivity, and selectivity of the sensor. It was investigated that the OTFT device based sensor is very sensitive towards the analyte gas with response of ~ 69% at 20 ppm concentration, with the detection limit of 0.41 ppm, which validates its applicability for the lower concentration detection of ammonia. This OTFT sensor not only exhibits great selectivity to NH_3 gas but also maintain good linearity to concentration. Additionally, this TFT exhibits extremely high photosensitivity under white light illumination with increasing the device's "ON" and "OFF" currents and shifting the threshold voltage by around 1.5 V.

6.1. Introduction

Organic thin film transistors (OTFTs) are appealing building blocks for economical electronic devices like radio-frequency identification (RFID) tags, sensors, electronic paper, and backplane circuits for active-matrix displays [1, 196, 197].These OTFTs have multiple device parameters that determine its performance, including threshold voltage, sub-threshold swing, and mobility [161, 198]. These OTFs are commonly fabricated on top of Si/SiO_2 substrate where SiO_2 works

as gate dielectric because of its advantages like low defect density, compatibility with CMOS technology, and good thermal conductivity. However, it requires a elevated operating voltage (>20 V) because of the low dielectric constant of SiO_2 (~3.9), restricting their application as portable electronics. [125, 161]. Besides, SiO_2 gate dielectric poses high tunneling current at low oxide thickness that causes a very significant static and dynamic power dissipation compared to high-k dielectric material-based OTFTs such as zirconium oxide (ZrO_2) [199], HfO_2 [200], and Ta_2O_5 [201]. The dissipation of power generates thermal energy, which raises the temperature. Such a situation can raise temperature quickly, especially in circuits with high-density OFETs. This may cause organic materials to gradually deteriorate and shorten the lifespan of the device [202].

Therefore, the development of gate dielectrics with a high areal capacitance is required for practical applications of OTFTs which can require few voltages to operate these devices [203, 204]. High-k oxide dielectrics are more susceptible to charge traps than SiO_2 due to defects states such as oxygen vacancies, poor surface roughness, and reduced band offset. These issues cause higher threshold voltage, decreased device mobility, and increased leakage current in the fabricated devices. Till date, several high-κ metal oxide dielectrics have been developed, which are appealing because of their compatibility with various organic semiconductors. The synthesis techniques of these high-κ dielectrics include metal anodization [47, 205], vacuum-based deposition [206, 207] and sol-gel technique [208].

This chapter explains the fabrication method of low operating voltage (≤2V) OTFT based NH_3 gas sensor by utilizing an ion-conducting gate dielectric and fibrous polymer thin film based semiconductor channel. During this fabrication an aligned nanowires/thin film of PBTTT-C14 polymer has transferred via economical and facial FTM method onto a Li-alumina (Li-Al_2O_3)

thin film which makes it work at lower voltage. This designed OTFT has been examined for the NH_3 gas detection application by exposing the channel to analyte gas. The change in the OTFT parameters was then recorded in order to investigate the sensitivity, selectivity, and other significant parameters. Additionally, I have also explored the photosensitivity of this device under white light, demonstrating its elevated photosensitivity to white light.

6.2. Experimental section

To synthesize dielectric lithium beta alumina (Li-β-Al_2O_3), 500 mM precursor solution is made by combining 98% pure aluminum nitrate nonahydrate [$Al(NO_3)_3$, $9H_2O$] (SDFCL) and >98% pure lithium acetate (CH_3COOLi) (TCI) in an 11:1 molecular ratio. After dissolving the combination in 2-methoxyethanol, it was stirred for around 6 hours. To encourage gelation, the prepared solution was aged for a full day. A 0.45 μm PVDF syringe filter was used to filter it before spin coating deposition on the desired substrate.

6.2.1 Device fabrication

Figure 6.2 (a) illustrates the fabricated bottom gate top contact geometry based OTFT device. Silicon substrates (p+-Si) were first cleaned with soap solution and then ultrasonically sonicated with DI water, acetone, and isopropanol before being dried in order to fabricate the device. Clean substrates were treated with oxygen plasma for 10-15 minutes prior to spin coating of the dielectric material in order to remove organic residue and make them hydrophilic. The fabrication of the gate dielectric thin film in TFTs requires a homogeneous, pinhole-free thin film, which hydrophilic substrates aid in coating. Then, the substrates were spin-coated with a 500 mM Li-Al_2O_3 precursor sol at 5000 rpm for 50 s, followed by 30 minutes of annealing at 350 °C. To obtain the appropriate thickness, the procedure was executed three times. Lastly, the

dielectric material coated substrates were annealed for 30 minutes in a preheated furnace at 500°C, resulting in a thick film of Li-Al_2O_3. To create a hydrophobic self-assembled monolayer, the dielectric film was then subjected to a vapor phase hexamethyldisilazane (HMDS) treatment. Afterward, the floating film of the active layer was stamped via FTM procedure as the previous study over the hybrid dielectric film that had been treated with HMDS and then annealed at 80°C [209]. A thermal evaporator was used for gold electrode deposition that works as source/drain contact of OTFT.

6.2.2 Characterization tools

TEM micrographs and SAED patterns of polymer films over Cu grid were acquired via TECHNAI $G^2$20 TWIN (New Zealand). The electrical characterizations and sensing measurements of the fabricated OTFTs were carried out by a semiconductor parameter analyzer (Keysight B1500A). In addition, the investigation of the Photosensitivity of the OTFT has been studied by electronic characterization of the OTFT in the presence of white light of different intensities by using a xenon lamp.

6.3. Results and discussion

6.3.1 Structural investigation of the Fibrillar PBTTT-C14

By transferring the film using the FTM process onto a carbon-coated TEM grid, TEM analysis was performed for the structural investigation of the FTM coated fibrillar polymeric film. Figures 6.1(a) and 6.1(b) shows the polymer film's TEM micrograph and SAED pattern, respectively. This figure clearly indicates a uniformly distributed aligned nanowire formation of polymer film that has an average width of ~300 nm. Additionally, formation of the SAED pattern shows the nano-wires are crystalline in form.

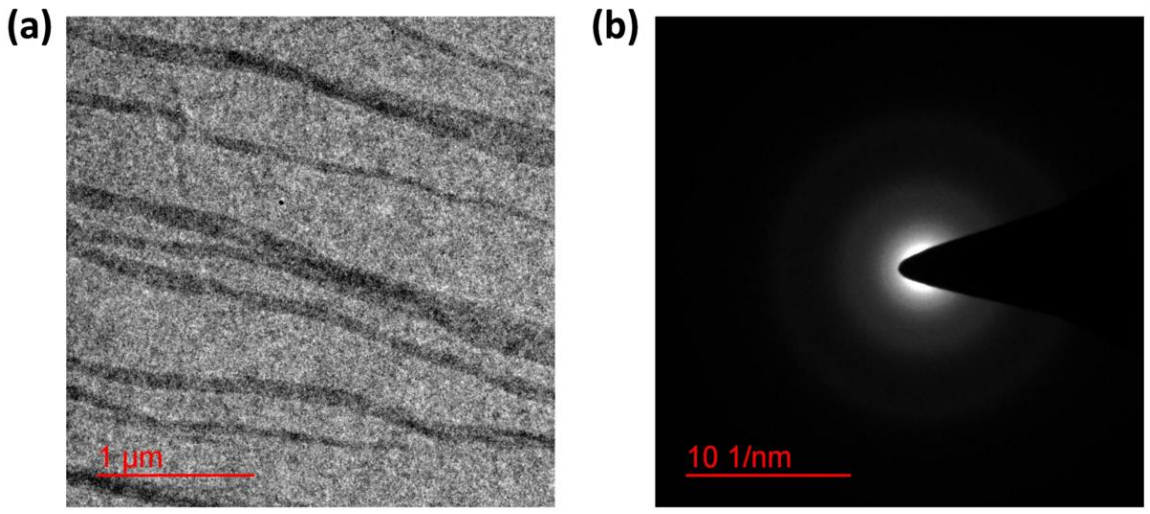

Fig. 6.1. (a) TEM image and, (b) SAED pattern of FTM coated fibrous PBTTT-C14 thin film.

6.3.2. Electrical Characterization

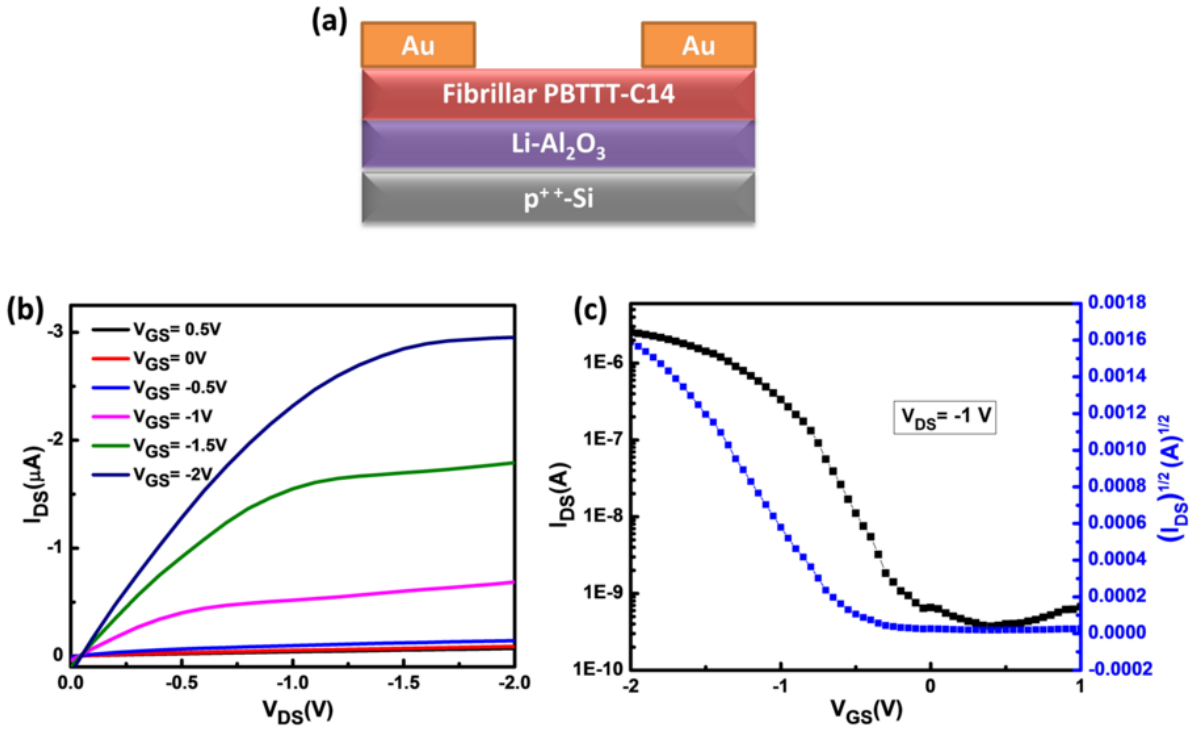

Fig.6.2.(a) Device schematic; (b) Output, and; (c) Transfer characteristics of fibrous homo-juntion based OTFT.

To investigate the electronic performance of the fabricated device, output and transfer characteristics have been studied. For the output characteristics drain voltage is swept from 0 V to -2 V with constant gate bias voltage ranging from 0.5 V to -2 V with a step of 0.5 V. The graphic of the device clearly displays the linear and saturated region of the output characteristics as displayed in Fig. 6.2(b), indicating the device can be operated with 2 V power supply. The transfer characteristic of OTFT is shown in Fig. 6.2(c), implying its ON/OFF ratio of **X**. During this study, the gate to source voltages is swept from - 0.2 V to 1 V keeping drain voltage constant at -1 V for both devices. Important transistor electrical parameters, like mobility (μ_h) and threshold voltage (V_{TH}), can be derived from transfer characteristics of the device by using the following equation (3.1).

6.3.3. Ammonia sensing

For NH_3 sensing measurement, the OTFT device is subjected to varying concentrations, from 0 ppm to 20 ppm of the NH_3 gas, at 27°C under the regulated flow of dry air inside a sealed container with 50% relative humidity, as seen in Fig. 6.3(a). Then, the gate bias (V_{GS}) is swept from 0 to -2 V throughout the sensing measurement while the constant drain voltage (V_{DS}) is set to -1 V. The transfer characteristic shows that the drain current (I_{DS}) of the OTFT steadily drops as soon as the NH_3 concentration rises and almost quenches after being exposed to 20 ppm NH_3 gas concentration.

With the decrement in current (I_{DS}) the corresponding OTFT parameters also tend to decrease with the ammonia concentration and that is caused by the NH_3 molecule's charge-trapping and charge-quenching effects on the positive charge carriers (holes) in the p-type OTFTs. The charge density in the conduction channel decreased as the injected NH_3 gas concentration increased. As

a result, the threshold voltage (V_{TH}) gradually shifted in the negative direction. The variation in threshold voltage (V_{TH}) and effective charge mobility (μ_h) of the devices as a function of NH_3 concentration is depicted in Fig. 6.3(b). The results demonstrate that there is a change of V_{th} of more than 0.5 V during the variation of NH_3 concentration, with high linearity up to 20 ppm. Additionally, the designed sensor's effective carrier mobility also decreases from 0.053 to 0.026 $cm^2\ V^{-1}sec^{-1}$, which is about 50% of its initial value (Fig.6.3(c)).

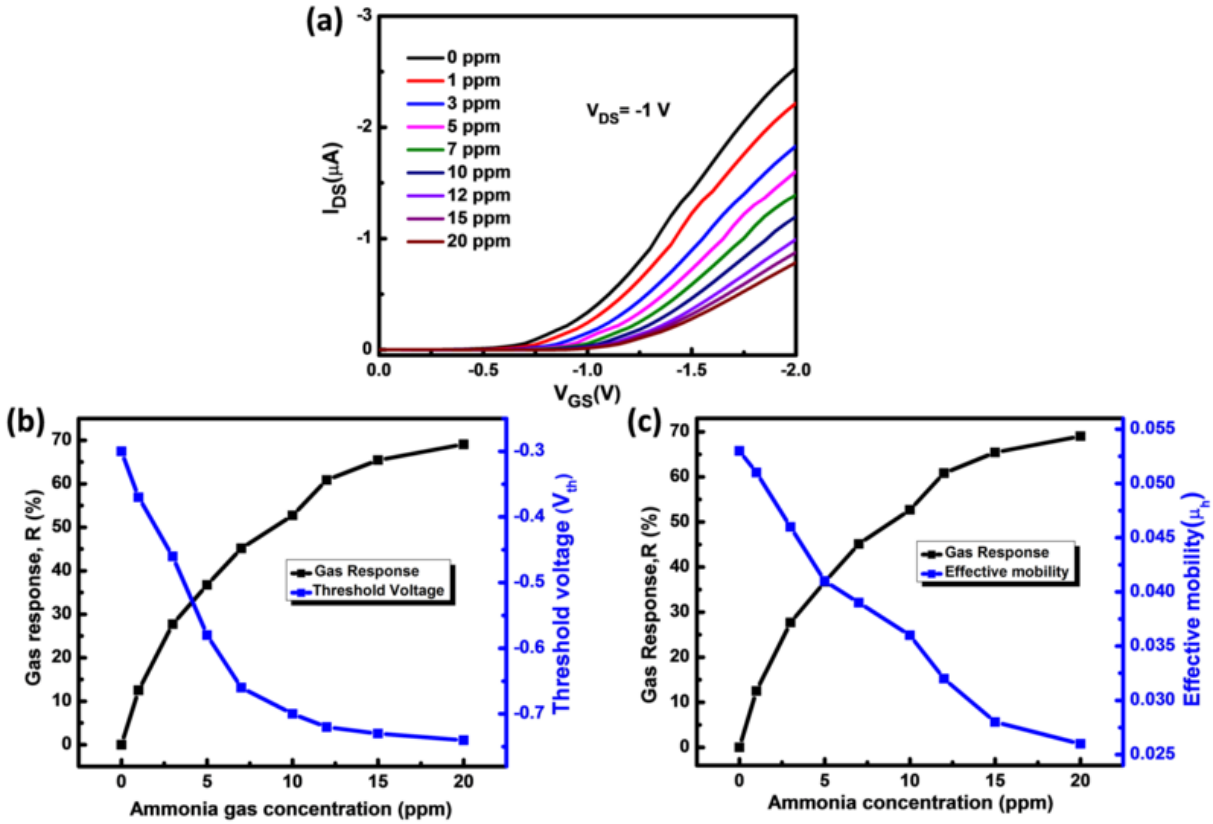

Fig. 6.3. (a) Transfer characteristics of fibrous polymer film based OTFT sensor at V_{DS} = -1V, and (b), & (c) Corresponding Shift in threshold voltage (V_{th}) and mobility (μ_h) with different concentrations of ammonia (0 ppm-20 ppm).

As a function of NH_3 concentrations Fig. 6.3(b) shows the fast sensing response of the OTFT sensor. When the artificial OTFT channels are exposed to ammonia gas, equation (3.2) can be used to determine the sensor's response (R).

Table-6.1: Variation in OTFT parameters and the sensitivity of polymeric fibrous film with different NH_3 concentrations

NH_3 (ppm)	**On current I_{on} (µA)**	**Effective Mobility μ_h ($cm^2V^{-1}sec^{-1}$)**	**Threshold voltage V_{TH} (V)**	**Gas Response R (%)**
0	-2.53	0.053	-0.48	0
1	-2.21	0.051	-0.56	12.50
3	-1.83	0.046	-0.64	27.70
5	-1.60	0.041	-0.69	36.72
7	-1.39	0.039	-0.76	45.11
10	-1.19	0.037	-0.80	52.71
12	-0.99	0.032	-0.82	60.84
15	-0.87	0.028	-0.84	65.44
20	-0.78	0.026	-0.85	69.04

The response (sensitivity) of the pure polymeric fibrous OTFT sensor at 5 ppm concentration of NH_3 is 69.04 %, which is calculated by the constant value of V_{DS}= -1 V corresponding to the Fig 6.3(a). The limit of detection of the sensor was also estimated with help of the following equation (3.3). And the calculated the LOD of the fabricated is 0.41 ppm. Which shows additionally that, even at lower ammonia concentrations, the fibrous polymer based sensor

exhibits a rather acceptable response. If I compared this study to the previous one which is discussed in chapter 5, it can be concluded that this ionic dielectric based OTFT works significantly wider range of concentration of NH_3 gas w.r.t the SiO_2 gate dielectric device whereas sensitivity of earlier device is more in lower concentration range.

6.3.4. Selectivity Analysis

As illustrated in Fig. 6.4, the OTFT sensors were used for other interfering gases as methane (CH_4), propane (C_3H_8), carbon dioxide (CO_2), carbon monoxide (CO) to identify the general applicability of the sensor to examine the response of other reductive and oxidative gases. Even at lower NH_3 concentrations than any other gases, the device responded to NH_3 gas considerably more strongly than any other gas. This finding implies that the fibrous OTFT sensor exhibits notable improvements in selectivity, and indicates its considerable potential for use in low-cost, portable chemical sensors.

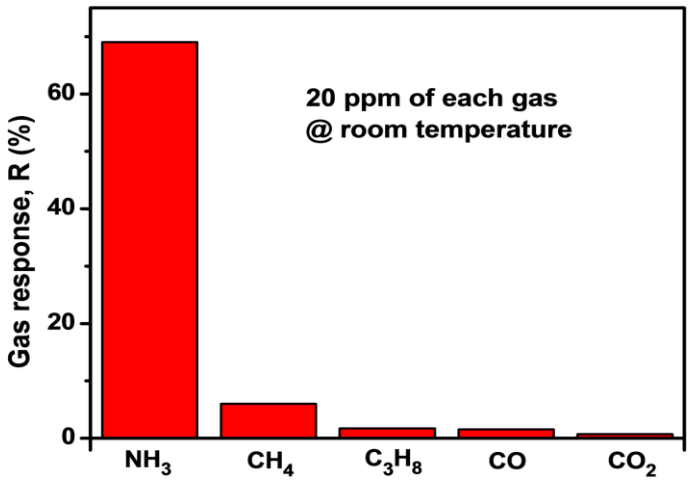

Fig. 6.4. Selectivity analysis of homo-junction based OTFT sensor.

Table-6.2: Comparative performance of the NH_3 sensor w.r.t the earlier reports.

Device design	**Sensing material**	**Film deposition technique**	**Operating voltage/ Temp.**	**Response (Gas concentration)**	**Resp. /Rec. time**	**Remark**
OTFT	P3HT-MoS_2	FTM	-60V/25°C	63% (100PPM)	-	High operating voltage [210]
MSM	PQT-12	Spin coating	-5 V/RT	8% (100 PPM)	8s/103s	Poor sensing response [24]
OTFT	PQT-12/CdSe	FTM	-40 V/RT	51% (100PPM)	50s/200s	High response time/ high operating voltage [211]
OTFT	PBTTT Nanowire	FTM	-30V/25°C	74.8% (5 PPM)	2s/12s	High operating voltage [212]
OTFT (This work)	PBTTT Nanowire	FTM	-2 V/25°C	69.04% (20 PPM)	5s/10s	Low operating voltage/ quick response-recovery time

6.3.5. Broadband photo sensing properties

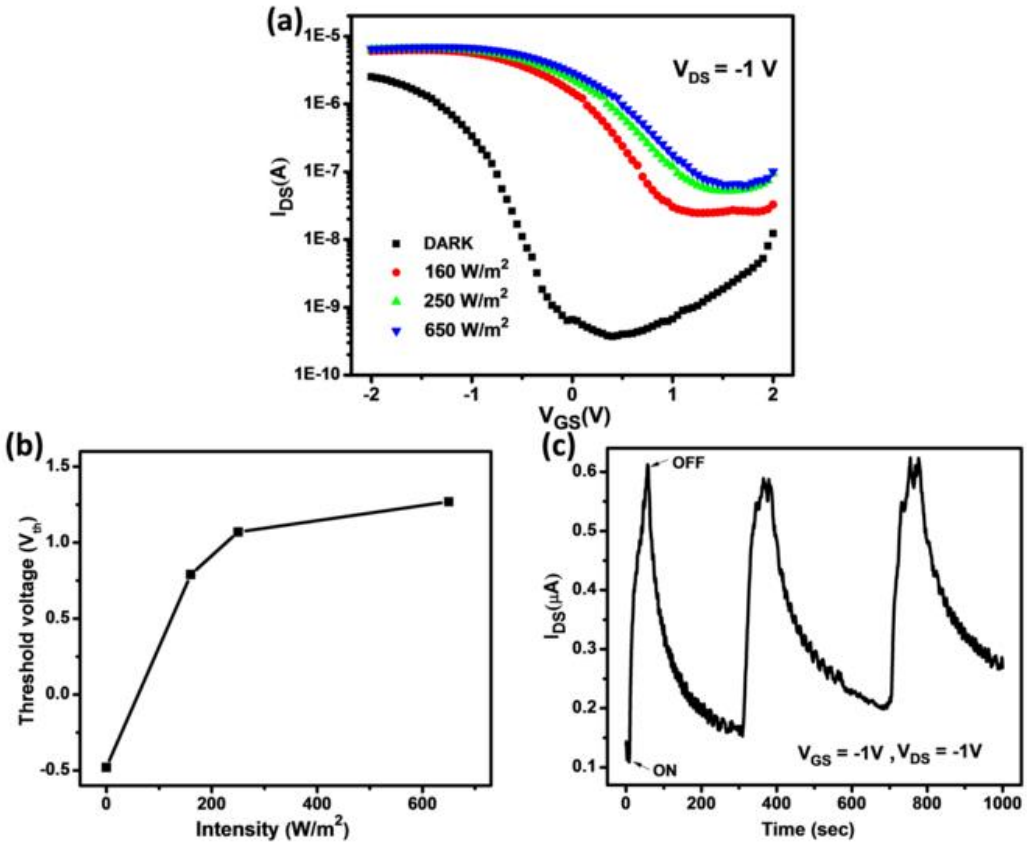

Fig. 6.5. (a) Transfer characteristics of homo-junction photosensitive OTFT (V_{DS} = - 1 V) in dark and under various intensities of white light, (b) Threshold voltage shift of the photo-detector under a range of white light intensities, (c) Transient analysis of the designed photo-detector at V_{DS} = - 1 V and V_{GS} = - 1 V.

Apart from NH_3 sensitivity, we also examined the photo-detection capabilities of the designed OTFT in ambient circumstances. The electrical properties of fabricated phototransistors under a range of white light intensities, from dark to 650 W/m^2, are demonstrated in Fig. 6.5(a). This

electrical statistics, which is the result of photocurrent production in the OTFT hybrid channel, suggests a significant improvement in both ON and OFF currents.

Based on the findings, it appears that the variation of OFF current this device is significantly higher than it's ON current variation, which can be recognized to the large number of photo-generated carriers (both electron and hole) that reduces the sheet resistance largely. The photo-generated charge carrier in this depleted region greatly enhances the channel conductivity and increases the OFF current of the device.

In addition, the shifts of threshold voltage the photo-transistor varied largely under intensities of white light as illustrated in Fig. 6.5(b). With 650 W/m^2 light intensity, the threshold voltage shift can reach up to ~2 V. Fig. 6.5(c) shows the phototransistor's transient photo-response, indicating a rapid response but a longer decay time for the device. This larger decay time of the photocurrent is because of the large channel length of OTFT and lower carrier mobility of PBTTT-C14 polymer film.

6.4. Conclusion

A highly sensitive, low operating voltage OTFT based NH_3 sensor and broadband photo-transistor has been fabricated by a simplistic, cost-effective and high yield method. Fibrous polymer thin film of PBTTT-C14 has been used as the NH_3 and photo-sensitive film of the OTFT device. A significant variation in the accumulation mode drain current of the OTFT has been observed due to the minute variation in NH_3 gas concentration, which leads to the considerable variation in OTFT parameters and acquired a response of ~ 69% at 20 ppm concentration of NH_3. In addition, this homo-junction based sensor demonstrates exceptional sensitivity, selectivity with a low concentration detection limit of NH_3 up to 0.41 ppm. Besides,

this fabricated device also shows large OFF current variation under various white light intensities demonstrating its high photo-sensitivity under white light. Briefly, this polymer homo-junction based OTFT meets the majority of the basic necessities for its realistic application as an NH_3 sensor and broadband photo-detector. It attains exceptional sensitivity with rapid response/recovery times with an extensive range of detecting abilities.

Chapter 7

Summary and Future scope of Research

In this thesis, I have successfully demonstrated the design, fabrication, and characterization of organic thin-film transistor (OTFT) based ammonia sensor utilizing polythiophene derivative PBTTT-C14 or PBTTT-C14 based nano-composite as the active semiconducting material. The fabrication of the sensing layer is done by an inexpensive and simple technique named FTM method. The integration of PBTTT-C14 a conducting polymer with notable charge transport properties and high environmental stability, with OTFT technology provides a promising platform for the detection of NH_3 in various applications, ranging from industrial safety to environmental monitoring. Additionally, photo-sensitivity of the devices is also investigated in some studies.

The outcomes verified that the ammonia-sensing capabilities of PBTTT-C14 based hetero-junction and homo-junctions OTFTs appeared promising. The current-voltage parameters of the OTFTs changed significantly in the presence of NH_3 gas, suggesting a noticeable ammonia response at lower concentrations in both accumulation and depletion modes. This performance was illustrated as a result of NH_3 molecules interacting with the polymer/nano-composite surface, which changed the concentration of charge carriers in the active channel. With a detection limit in the low parts per million (ppm) ranges, the sensor showed a significant improvement in sensitivity with rising NH_3 concentration, qualifying it for use in gas detection applications. The current-voltage parameters of the OTFTs changed significantly in the presence of NH_3 gas, suggesting a detectable ammonia response. The primary objective was to explore the sensitivity, selectivity, and stability of sensors in response to ammonia gas. In photo-sensitivity investigations of both the ON and OFF currents of the fabricated device show larger variation due to the enhancement in channel conductivity.

7. 1. Key Contributions:

7.1.1. Design and Fabrication: Along with the unique conjugated structure, PBTTT-C14 also exhibits excellent electrical conductivity and good stability, which are essential for the reliable operation of OTFTs in sensing applications. Its tunable properties through doping and processing conditions make it a promising candidate for detecting gases like ammonia.

For the fabrication of the π-conjugated polymers based organic electronic devices, FTM is an efficient process which offers a thinner layer of the active materials and improves the possibility of gas interaction at the dielectric-semiconductor interface for the aim of enhanced gas sensitivity.

7.1.2. Performance of the sensor: PBTTT-C14 based heterojunction or homo-junction OTFT sensor offers higher sensitivity as they displayed a significant change in drain current (I_D) even at low ammonia concentrations by a distinct shift in its electrical characteristics as threshold voltage, charge carrier mobility in the presence of NH_3 at varying concentrations, which indicates its potential for detecting trace amounts of NH_3. Both accumulation and depletion modes provide significant change in drain current, which is linear with the gas concentrations.

For the selectivity, these OTFT sensors demonstrated selective sensitivity towards NH_3 over other common environmental interfering gases confirming its utility in selective gas detection. Other key performance metrics such as response time, recovery time, and detection limit were evaluated, showing that OTFT sensors are competitive with other conventional sensor technologies.

7.1.3. Sensing Mechanism: The OTFT sensor operates through a change in the electronic conductivity of the active polymeric layer in response to NH_3 gas exposure. The interaction between ammonia and the sensor's surface modifies the charge distribution in the active layer, leading to a measurable change in drain current, which can be correlated with NH_3 concentration. Additionally, in our study we have examined accumulation and depletion mode operations with NH_3 concentration and found that the OFF current variation is much higher than the ON current variation. A comparative device performance of the NH_3 sensors that I developed is listed in Table 7.1.

Table - 7.1. Represents the Comparative performance of the fabricated sensors

Material	**NH_3 Concentration**	**Response**	**Detection limit**	**Off- current factor**
PBTTT-C14	0 ppm - 50 ppm	35.6%	0.82 ppm	~1.98
PBTTT-C14/MoS_2-QDs	0 ppm - 50 ppm	84.66%	0.317 ppm	~$3X10^3$
PBTTT-C14/WS_2-QDs	0 ppm - 10 ppm	50%	0.44 ppm	~10^3
Fibrillar PBTTT-C14	0 ppm - 5 ppm	74.8%	0.67 ppm	~10^2
Fibrillar PBTTT-C14 (Low operating voltage, <2 V)	0 ppm - 20ppm	69.04%	0.41 ppm	-

This thesis works demonstrated that the developed sensor exhibited a high sensitivity and selectivity towards NH_3 gas, with a wide detection range and a fast response time. The sensor's capability to operate at room temperature and its potential for real-time monitoring of ammonia concentration make it an attractive solution for applications in environmental monitoring, industrial safety, and agricultural practices. Moreover, the results showed good reproducibility and stability, which are crucial for practical deployment.

7.1.4. Real-World Application Scenarios: Ammonia (NH_3) is a toxic, pungent gas prevalent in agriculture, industry, and the environment. It poses serious health and environmental risks, contributing to pollution when released in large amounts. While vital in fertilizer production and promising as a hydrogen carrier, its hazardous nature makes effective detection crucial for safety and regulatory compliance. Ammonia detection has a wide range of potential applications across environmental, medical, industrial, and consumer sectors.

1. **Environmental NH_3 Detection in Agriculture -** In agriculture, real-time monitoring of ammonia emissions is critical, particularly in livestock farms and areas with heavy fertilizer use. Excessive ammonia not only poses health risks to farm workers and animals but also contributes to environmental issues like soil acidification and eutrophication. Integrating NH_3 sensors into farm management systems can enable precision agriculture practices, optimize fertilizer application, and improve air quality control within animal housing.
2. **Medical Diagnostics (Kidney & Liver Function Monitoring) -** In the medical field, elevated levels of ammonia in breath, sweat, or bodily fluids can serve as non-invasive biomarkers for diagnosing conditions such as liver dysfunction (e.g., hepatic

encephalopathy) and kidney disease. Wearable or portable ammonia sensors could offer real-time patient monitoring, aiding early intervention and disease management.

3. **Food Spoilage Monitoring -** Another important application of ammonia sensors is in food safety, where ammonia is a byproduct of protein decomposition. Smart packaging equipped with NH_3 sensors can indicate spoilage in meat, fish, and dairy products, improving supply chain transparency and reducing food waste.
4. **Industrial Safety and Workplace Exposure -** Industrial environments also benefit from ammonia detection, as it is commonly used in refrigeration and chemical processes. Detecting leaks quickly is vital to ensure worker safety and comply with health regulations. Finally, in urban settings, ammonia contributes to air pollution and the formation of fine particulate matter (PM2.5). Deploying NH_3 sensors across cities can help monitor air quality, inform public health policies, and support the development of cleaner, healthier environments.

In summary, the rising need for reliable ammonia detection—driven by environmental, industrial, and safety concerns calls for cost-effective, portable sensors with high sensitivity and selectivity. This study addresses that need by focusing on the detection of low airborne ammonia concentrations, essential for protecting both human health and the environment.

7.2. Future Directions:

Future work can focus on optimizing the sensor's performance further, exploring the use of additional functionalization strategies and offering a cost-effective, flexible, and scalable solution for environmental and industrial monitoring. Researchers are working to overcome the limitations of OTFT ammonia sensors by Nano-structuring the polymer to increase surface area

and improve gas adsorption, hybridizing polythiophene with inorganic nano-particles or metal oxides to enhance sensitivity and selectivity, developing more stable materials to improve the longevity of the sensors.

An alternative organic semiconductors and dielectric combinations may be used to compare the performances of a gas sensor. As the carrier transport is confined in between the OSC and dielectric, it also plays the major role during sensing measurement. The successful realization of an OTFT sensor by using appropriate surface treatment of dielectric may be used to tune the sensor response. The solution-processable low voltage working OTFT may be used to design flexible sensors. Further, the impact of mechanical deformation on the OTFTs built on the flexible substrate may also be analyzed.

Additionally, as the demand for advanced, real-time, and highly selective gas detection systems increases especially in domains like environmental monitoring, healthcare diagnostics, and industrial safety, future research is likely to focus on the integration of thin-film gas sensors with machine learning, which offers a promising path for enhancing gas detection through advanced pattern recognition and multiplexed sensing. Machine learning can improve selectivity, compensate for cross-sensitivity, and enable accurate classification of gas types and concentrations based on sensor response patterns. When organized into sensor arrays, thin-film platforms can detect multiple analyte simultaneously, forming the basis of compact, high-performance "electronic nose" systems. These platforms are ideal for applications in environmental monitoring, industrial safety, and medical diagnostics.

Overall, future efforts may explore miniaturized, low-power systems compatible with flexible or wearable electronics, as well as edge computing for real-time decision-making. The convergence

of advanced materials, scalable fabrication techniques, and adaptive AI models holds the potential to revolutionize gas sensing across numerous domains.

References

References

[1] S. R. Forrest, "The path to ubiquitous and low-cost organic electronic appliances on plastic," *nature,* vol. 428, pp. 911-918, 2004.

[2] H. Ma, H. L. Yip, F. Huang, and A. K. Y. Jen, "Interface engineering for organic electronics," *Advanced Functional Materials,* vol. 20, pp. 1371-1388, 2010.

[3] M. Fahlman, S. Fabiano, V. Gueskine, D. Simon, M. Berggren, and X. Crispin, "Interfaces in organic electronics," *Nature Reviews Materials,* vol. 4, pp. 627-650, 2019.

[4] H. Sirringhaus, T. Kawase, R. Friend, T. Shimoda, M. Inbasekaran, W. Wu, *et al.*, "High-resolution inkjet printing of all-polymer transistor circuits," *Science,* vol. 290, pp. 2123-2126, 2000.

[5] A. Nawaz, L. Merces, L. M. Ferro, P. Sonar, and C. C. Bufon, "Impact of Planar and Vertical Organic Field-Effect Transistors on Flexible Electronics," *Advanced Materials,* vol. 35, p. 2204804, 2023.

[6] J. Bauri, R. B. Choudhary, and G. Mandal, "Recent advances in efficient emissive materials-based OLED applications: a review," *Journal of Materials Science,* vol. 56, pp. 18837-18866, 2021.

[7] O. Ostroverkhova, "Organic optoelectronic materials: mechanisms and applications," *Chemical reviews,* vol. 116, pp. 13279-13412, 2016.

[8] L. Torsi, M. Magliulo, K. Manoli, and G. Palazzo, "Organic field-effect transistor sensors: a tutorial review," *Chemical Society Reviews,* vol. 42, pp. 8612-8628, 2013.

[9] N. S. Yusof, M. F. P. Mohamed, N. A. Ghazali, M. F. A. J. Khan, S. Shaari, and M. N. Mohtar, "Evolution of solution-based organic thin-film transistor for healthcare monitoring–from device to circuit integration: A review," *Alexandria Engineering Journal,* vol. 61, pp. 11405-11431, 2022.

[10] J. Liu, M. Gao, J. Kim, Z. Zhou, D. S. Chung, H. Yin, *et al.*, "Challenges and recent advances in photodiodes-based organic photodetectors," *Materials Today,* vol. 51, pp. 475-503, 2021.

[11] H. Ren, J. D. Chen, Y. Q. Li, and J. X. Tang, "Recent progress in organic photodetectors and their applications," *Advanced Science,* vol. 8, p. 2002418, 2021.

[12] R. Ruiz, D. Choudhary, B. Nickel, T. Toccoli, K.-C. Chang, A. C. Mayer, *et al.*, "Pentacene thin film growth," *Chemistry of Materials,* vol. 16, pp. 4497-4508, 2004.

References

[13] C. D. Dimitrakopoulos and D. J. Mascaro, "Organic thin-film transistors: A review of recent advances," *IBM Journal of research and development,* vol. 45, pp. 11-27, 2001.

[14] D.-Y. Khang, H. Jiang, Y. Huang, and J. A. Rogers, "A stretchable form of single-crystal silicon for high-performance electronics on rubber substrates," *Science,* vol. 311, pp. 208-212, 2006.

[15] M. J. Panzer and C. D. Frisbie, "High charge carrier densities and conductance maxima in single-crystal organic field-effect transistors with a polymer electrolyte gate dielectric," *Applied physics letters,* vol. 88, 2006.

[16] Q. Tang, H. Li, M. He, W. Hu, C. Liu, K. Chen, *et al.*, "Low threshold voltage transistors based on individual single-crystalline submicrometer-sized ribbons of copper phthalocyanine," *Advanced Materials,* vol. 18, pp. 65-68, 2006.

[17] H. Shirakawa, E. J. Louis, A. G. MacDiarmid, C. K. Chiang, and A. J. Heeger, "Synthesis of electrically conducting organic polymers: halogen derivatives of polyacetylene,(CH) x," *Journal of the Chemical Society, Chemical Communications,* pp. 578-580, 1977.

[18] H. C. Kang and K. Geckeler, "Enhanced electrical conductivity of polypyrrole prepared by chemical oxidative polymerization: effect of the preparation technique and polymer additive," *Polymer,* vol. 41, pp. 6931-6934, 2000.

[19] A. L. Aldaba, Á. González-Vila, M. Debliquy, M. Lopez-Amo, C. Caucheteur, and D. Lahem, "Polyaniline-coated tilted fiber Bragg gratings for pH sensing," *Sensors and Actuators B: Chemical,* vol. 254, pp. 1087-1093, 2018.

[20] S. Hong, F. S. Cannon, P. Hou, T. Byrne, and C. Nieto-Delgado, "Adsorptive removal of sulfate from acid mine drainage by polypyrrole modified activated carbons: effects of polypyrrole deposition protocols and activated carbon source," *Chemosphere,* vol. 184, pp. 429-437, 2017.

[21] M. R. Chandra, P. S. P. Reddy, T. S. Rao, S. Pammi, K. S. Kumar, K. V. Babu, *et al.*, "Enhanced visible-light photocatalysis and gas sensor properties of polythiophene supported tin doped titanium nanocomposite," *Journal of Physics and Chemistry of Solids,* vol. 105, pp. 99-105, 2017.

[22] T. Yamamoto, "Molecular assembly and properties of polythiophenes," *NPG Asia Materials,* vol. 2, pp. 54-60, 2010.

References

[23] Q. Meng, K. Cai, Y. Chen, and L. Chen, "Research progress on conducting polymer based supercapacitor electrode materials," *Nano Energy*, vol. 36, pp. 268-285, 2017.

[24] C. Kumar, G. Rawat, H. Kumar, Y. Kumar, R. Prakash, and S. Jit, "Flexible poly (3, 3‴-dialkylquaterthiophene) based interdigitated metal-semiconductor-metal ammonia gas sensor," *Sensors and Actuators B: Chemical*, vol. 255, pp. 203-209, 2018.

[25] N. Parveen, M. O. Ansari, T. H. Han, and M. H. Cho, "Simple and rapid synthesis of ternary polyaniline/titanium oxide/graphene by simultaneous TiO 2 generation and aniline oxidation as hybrid materials for supercapacitor applications," *Journal of Solid State Electrochemistry*, vol. 21, pp. 57-68, 2017.

[26] X. Wu and M. Lian, "Highly flexible solid-state supercapacitor based on graphene/polypyrrole hydrogel," *Journal of Power Sources*, vol. 362, pp. 184-191, 2017.

[27] S. Tiwari, A. K. Singh, L. Joshi, P. Chakrabarti, W. Takashima, K. Kaneto, *et al.*, "Poly-3-hexylthiophene based organic field-effect transistor: Detection of low concentration of ammonia," *Sensors and Actuators B: Chemical*, vol. 171, pp. 962-968, 2012.

[28] M. O. Ansari and F. Mohammad, "Thermal stability of HCl-doped-polyaniline and TiO2 nanoparticles-based nanocomposites," *Journal of Applied Polymer Science*, vol. 124, pp. 4433-4442, 2012.

[29] R. Kumar, M. O. Ansari, and M. Barakat, "DBSA doped polyaniline/multi-walled carbon nanotubes composite for high efficiency removal of Cr (VI) from aqueous solution," *Chemical engineering journal*, vol. 228, pp. 748-755, 2013.

[30] V. Singh, S. Mohan, G. Singh, P. Pandey, and R. Prakash, "Synthesis and characterization of polyaniline–carboxylated PVC composites: application in development of ammonia sensor," *Sensors and Actuators B: Chemical*, vol. 132, pp. 99-106, 2008.

[31] S. Tiwari, A. K. Singh, and R. Prakash, "Poly (3-hexylthiophene)(P3HT)/graphene nanocomposite material based organic field effect transistor with enhanced mobility," *Journal of nanoscience and nanotechnology*, vol. 14, pp. 2823-2828, 2014.

[32] F.-H. Lu, M.-G. Mohamed, T.-F. Liu, C.-G. Chao, L. Dai, and S.-W. Kuo, "A quenching method for the preparation of metal oxide–polythiophene composites having fiber structures," *RSC Advances*, vol. 4, pp. 64525-64534, 2014.

References

[33] Y. Wang, X. Qing, Q. Zhou, Y. Zhang, Q. Liu, K. Liu, *et al.*, "The woven fiber organic electrochemical transistors based on polypyrrole nanowires/reduced graphene oxide composites for glucose sensing," *Biosensors and Bioelectronics,* vol. 95, pp. 138-145, 2017.

[34] S.-X. Zhou, X.-Y. Tao, J. Ma, C.-H. Qu, Y. Zhou, L.-T. Guo, *et al.*, "Facile synthesis of self-assembled polyaniline nanorods doped with sulphuric acid for high-performance supercapacitors," *Vacuum,* vol. 143, pp. 63-70, 2017.

[35] A. Tsumura, H. Koezuka, and T. Ando, "Macromolecular electronic device: Field-effect transistor with a polythiophene thin film," *Applied Physics Letters,* vol. 49, pp. 1210-1212, 1986.

[36] S. Locci, M. Morana, E. Orgiu, A. Bonfiglio, and P. Lugli, "Modeling of short-channel effects in organic thin-film transistors," *IEEE Transactions on Electron Devices,* vol. 55, pp. 2561-2567, 2008.

[37] A. Miller and E. Abrahams, "Impurity conduction at low concentrations," *Physical Review,* vol. 120, p. 745, 1960.

[38] M. Vissenberg and M. Matters, "Theory of the field-effect mobility in amorphous organic transistors," *Physical Review B,* vol. 57, p. 12964, 1998.

[39] K. Myny, "The development of flexible integrated circuits based on thin-film transistors," *Nature electronics,* vol. 1, pp. 30-39, 2018.

[40] A. Sharma, C. Madhu, and J. Singh, "Performance evaluation of thin film transistors: history, technology development and comparison: a review," *Int. J. Comput. Appl,* vol. 89, pp. 36-40, 2014.

[41] K. Schnittker, M. Tursunniyaz, and J. B. Andrews, "Recent advances in printable carbon nanotube transistors for large-area active matrices," *Journal of Information Display,* vol. 22, pp. 193-209, 2021.

[42] K. Takimiya, H. Ebata, K. Sakamoto, T. Izawa, T. Otsubo, and Y. Kunugi, "2, 7-Diphenyl [1] benzothieno [3, 2-b] benzothiophene, a new organic semiconductor for air-stable organic field-effect transistors with mobilities up to 2.0 cm2 V-1 s-1," *Journal of the American Chemical Society,* vol. 128, pp. 12604-12605, 2006.

References

[43] F. Paulus, C. Tyznik, O. D. Jurchescu, and Y. Vaynzof, "Switched-on: progress, challenges, and opportunities in metal halide perovskite transistors," *Advanced Functional Materials,* vol. 31, p. 2101029, 2021.

[44] H. S. White, G. P. Kittlesen, and M. S. Wrighton, "Chemical derivatization of an array of three gold microelectrodes with polypyrrole: fabrication of a molecule-based transistor," *Journal of the American Chemical Society,* vol. 106, pp. 5375-5377, 1984.

[45] W. Tang, Y. Huang, L. Han, R. Liu, Y. Su, X. Guo, *et al.*, "Recent progress in printable organic field effect transistors," *Journal of Materials Chemistry C,* vol. 7, pp. 790-808, 2019.

[46] X. Guo, Y. Xu, S. Ogier, T. N. Ng, M. Caironi, A. Perinot, *et al.*, "Current status and opportunities of organic thin-film transistor technologies," *IEEE transactions on electron devices,* vol. 64, pp. 1906-1921, 2017.

[47] H. Klauk, U. Zschieschang, J. Pflaum, and M. Halik, "Ultralow-power organic complementary circuits," *nature,* vol. 445, pp. 745-748, 2007.

[48] H. Matsui, Y. Takeda, and S. Tokito, "Flexible and printed organic transistors: From materials to integrated circuits," *Organic Electronics,* vol. 75, p. 105432, 2019.

[49] B. King and B. H. Lessard, "Review of recent advances and sensing mechanisms in solid-state organic thin-film transistor (OTFT) sensors," *Journal of Materials Chemistry C,* 2024.

[50] K. E. Strawhecker, S. K. Kumar, J. F. Douglas, and A. Karim, "The critical role of solvent evaporation on the roughness of spin-cast polymer films," *Macromolecules,* vol. 34, pp. 4669-4672, 2001.

[51] N. Yamasaki, Y. Miyake, H. Yoshida, A. Fujii, and M. Ozaki, "Solution flow assisted fabrication method of oriented π-conjugated polymer films by using geometrically-asymmetric sandwich structures," *Japanese Journal of Applied Physics,* vol. 50, p. 020205, 2011.

[52] H. A. Becerril, M. E. Roberts, Z. Liu, J. Locklin, and Z. Bao, "High-performance organic thin-film transistors through solution-sheared deposition of small-molecule organic semiconductors," *Advanced Materials,* vol. 20, pp. 2588-2594, 2008.

References

[53] M. Karakawa, M. Chikamatsu, Y. Yoshida, M. Oishi, R. Azumi, and K. Yase, "High-performance poly (3-hexylthiophene) field-effect transistors fabricated by a slide-coating method," *Applied physics express*, vol. 1, p. 061802, 2008.

[54] A. Dauendorffer, S. Miyajima, S. Nagamatsu, W. Takashima, S. Hayase, and K. Kaneto, "One-step deposition of self-oriented β-phase polyfluorene thin films for polarized polymer light-emitting diodes," *Applied physics express*, vol. 5, p. 092101, 2012.

[55] A. Dauendorffer, S. Nagamatsu, W. Takashima, and K. Kaneto, "Optical and transport anisotropy in poly (9, 9'-dioctyl-fluorene-alt-bithiophene) films prepared by floating film transfer method," *Japanese Journal of Applied Physics*, vol. 51, p. 055802, 2012.

[56] M. Brinkmann, L. Hartmann, L. Biniek, K. Tremel, and N. Kayunkid, "Orienting Semi-Conducting π-Conjugated Polymers," *Macromolecular rapid communications*, vol. 35, pp. 9-26, 2014.

[57] H. Sirringhaus, R. Wilson, R. Friend, M. Inbasekaran, W. Wu, E. Woo, *et al.*, "Mobility enhancement in conjugated polymer field-effect transistors through chain alignment in a liquid-crystalline phase," *Applied Physics Letters*, vol. 77, pp. 406-408, 2000.

[58] S. Schott, E. Gann, L. Thomsen, S. H. Jung, J. K. Lee, C. R. McNeill, *et al.*, "Charge-transport anisotropy in a uniaxially aligned diketopyrrolopyrrole-based copolymer," *Advanced Materials*, vol. 27, pp. 7356-7364, 2015.

[59] L. Biniek, N. Leclerc, T. Heiser, R. Bechara, and M. Brinkmann, "Large scale alignment and charge transport anisotropy of pBTTT films oriented by high temperature rubbing," *Macromolecules*, vol. 46, pp. 4014-4023, 2013.

[60] F. Yang, S. Cheng, X. Zhang, X. Ren, R. Li, H. Dong, *et al.*, "2D organic materials for optoelectronic applications," *Advanced Materials*, vol. 30, p. 1702415, 2018.

[61] H. Lee, J. H. Kim, K. P. Dhakal, J. W. Lee, J. S. Jung, J. Joo, *et al.*, "Anisotropic optical absorption of organic rubrene single nanoplates and thin films studied by μ-mapping absorption spectroscopy," *Applied Physics Letters*, vol. 101, 2012.

[62] K. Liu, B. Ouyang, X. Guo, Y. Guo, and Y. Liu, "Advances in flexible organic field-effect transistors and their applications for flexible electronics," *npj Flexible Electronics*, vol. 6, p. 1, 2022.

References

[63] Y. Cui, L. Hong, and J. Hou, "Organic photovoltaic cells for indoor applications: opportunities and challenges," *ACS applied materials & interfaces,* vol. 12, pp. 38815-38828, 2020.

[64] S. Jakher and R. Yadav, "Organic thin film transistor review based on their structures, materials, performance parameters, operating principle, and applications," *Microelectronic Engineering,* p. 112193, 2024.

[65] W. H. Organization and W. H. Organization, "out of 10 people worldwide breathe polluted air, but more countries are taking action. 2018," *URL: http://www. who. int/news-room/detail/02-05-2018-9-out-of-10-people-worldwide-breathe-polluted-air-but-more-countries-are-taking-action*.

[66] R. Malik, V. K. Tomer, Y. K. Mishra, and L. Lin, "Functional gas sensing nanomaterials: A panoramic view," *Applied Physics Reviews,* vol. 7, 2020.

[67] S. W. Lee, W. Lee, Y. Hong, G. Lee, and D. S. Yoon, "Recent advances in carbon material-based NO2 gas sensors," *Sensors and Actuators B: Chemical,* vol. 255, pp. 1788-1804, 2018.

[68] K. Toda, R. Furue, and S. Hayami, "Recent progress in applications of graphene oxide for gas sensing: A review," *Analytica chimica acta,* vol. 878, pp. 43-53, 2015.

[69] K. Xu, C. Fu, Z. Gao, F. Wei, Y. Ying, C. Xu, *et al.*, "Nanomaterial-based gas sensors: A review," *Instrumentation Science & Technology,* vol. 46, pp. 115-145, 2018.

[70] K. M. Tripathi, T. Kim, D. Losic, and T. T. Tung, "Recent advances in engineered graphene and composites for detection of volatile organic compounds (VOCs) and non-invasive diseases diagnosis," *Carbon,* vol. 110, pp. 97-129, 2016.

[71] T. T. Tung, M. T. Tran, J.-F. Feller, M. Castro, T. Van Ngo, K. Hassan, *et al.*, "Graphene and metal organic frameworks (MOFs) hybridization for tunable chemoresistive sensors for detection of volatile organic compounds (VOCs) biomarkers," *Carbon,* vol. 159, pp. 333-344, 2020.

[72] J. E. Ellis and A. Star, "Carbon nanotube based gas sensors toward breath analysis," *ChemPlusChem,* vol. 81, pp. 1248-1265, 2016.

[73] T. Han, A. Nag, S. C. Mukhopadhyay, and Y. Xu, "Carbon nanotubes and its gas-sensing applications: A review," *Sensors and Actuators A: Physical,* vol. 291, pp. 107-143, 2019.

References

[74] S. Z. N. Demon, A. I. Kamisan, N. Abdullah, S. A. M. Noor, O. K. Khim, N. A. M. Kasim, *et al.*, "Graphene-based Materials in Gas Sensor Applications: A Review," *Sensors & Materials,* vol. 32, 2020.

[75] Y. Zhu, Z. Li, L. Zhang, B. Wang, Z. Luo, J. Long, *et al.*, "High-efficiency monolayer molybdenum ditelluride light-emitting diode and photodetector," *ACS applied materials & interfaces,* vol. 10, pp. 43291-43298, 2018.

[76] H. Zhang, H.-M. Cheng, and P. Ye, "2D nanomaterials: beyond graphene and transition metal dichalcogenides," *Chemical Society Reviews,* vol. 47, pp. 6009-6012, 2018.

[77] J. Sakamoto, J. van Heijst, O. Lukin, and A. D. Schlüter, "Two-dimensional polymers: just a dream of synthetic chemists?," *Angewandte Chemie International Edition,* vol. 48, pp. 1030-1069, 2009.

[78] A. Ramaprasad, D. Latha, and V. Rao, "Synthesis and characterization of polypyrrole grafted chitin," *Journal of physics and chemistry of solids,* vol. 104, pp. 169-174, 2017.

[79] P. Dariyal, S. Sharma, G. S. Chauhan, B. P. Singh, and S. Dhakate, "Recent trends in gas sensing via carbon nanomaterials: outlook and challenges, Nanoscale Adv. 3 (2021) 6514–6544," ed.

[80] A. Katariya and J. Rani, "Review on two-dimensional organic semiconductors for thin film transistor application," *Materials Today: Proceedings,* vol. 46, pp. 2322-2325, 2021.

[81] L. Yang, X. Huang, A. Gogoll, M. Strømme, and M. Sjödin, "Conducting redox polymer based anode materials for high power electrical energy storage," *Electrochimica Acta,* vol. 204, pp. 270-275, 2016.

[82] S. Haraguchi, Y. Tsuchiya, T. Shiraki, K. Sada, and S. Shinkai, "Control of polythiophene redox potentials based on supramolecular complexation with helical schizophyllan," *Chemical communications,* pp. 6086-6088, 2009.

[83] A. Nautiyal, M. Qiao, J. E. Cook, X. Zhang, and T.-S. Huang, "High performance polypyrrole coating for corrosion protection and biocidal applications," *Applied Surface Science,* vol. 427, pp. 922-930, 2018.

[84] X. Liu, W. Zheng, R. Kumar, M. Kumar, and J. Zhang, "Conducting polymer-based nanostructures for gas sensors," *Coordination Chemistry Reviews,* vol. 462, p. 214517, 2022.

References

[85] M. E. Roberts, A. N. Sokolov, and Z. Bao, "Material and device considerations for organic thin-film transistor sensors," *Journal of Materials Chemistry,* vol. 19, pp. 3351-3363, 2009.

[86] L. Kumar, I. Rawal, A. Kaur, and S. Annapoorni, "Flexible room temperature ammonia sensor based on polyaniline," *Sensors and Actuators B: Chemical,* vol. 240, pp. 408-416, 2017.

[87] W.-C. Chen and T.-C. Wen, "Electrochemical and capacitive properties of polyaniline-implanted porous carbon electrode for supercapacitors," *Journal of power sources,* vol. 117, pp. 273-282, 2003.

[88] S. Muthusamy, J. Charles, S. Sekar, S. Rajan, and S. K. Kannan, "Versatile Gas Sensing at Room Temperature: Facile Fabrication of a PANI-PB-ZnO Hybrid Nanocomposite for Detecting Ammonia, Acetone, and Ethanol," *Journal of Electronic Materials,* vol. 53, pp. 2168-2180, 2024.

[89] Y. Yang, S. Li, W. Yang, W. Yuan, J. Xu, and Y. Jiang, "In situ polymerization deposition of porous conducting polymer on reduced graphene oxide for gas sensor," *ACS applied materials & interfaces,* vol. 6, pp. 13807-13814, 2014.

[90] G. Kiani, A. Nourizad, and R. Nosrati, "In-situ chemical synthesis of polypyrrole/silver nanocomposite for the use as a room temperature ammonia gas sensor," *Fibers and Polymers,* vol. 19, pp. 2188-2194, 2018.

[91] N. Kemp, A. Kaiser, H. Trodahl, B. Chapman, R. Buckley, A. Partridge, *et al.*, "Effect of ammonia on the temperature-dependent conductivity and thermopower of polypyrrole," *Journal of Polymer Science Part B: Polymer Physics,* vol. 44, pp. 1331-1338, 2006.

[92] J.-H. Cho, J.-B. Yu, J.-S. Kim, S.-O. Sohn, D.-D. Lee, and J.-S. Huh, "Sensing behaviors of polypyrrole sensor under humidity condition," *Sensors and Actuators B: Chemical,* vol. 108, pp. 389-392, 2005.

[93] F. Liao, C. Chen, and V. Subramanian, "Organic TFTs as gas sensors for electronic nose applications," *Sensors and Actuators B: Chemical,* vol. 107, pp. 849-855, 2005.

[94] M. M. Ling and Z. Bao, "Thin film deposition, patterning, and printing in organic thin film transistors," *Chemistry of materials,* vol. 16, pp. 4824-4840, 2004.

References

[95] J. Locklin, M. E. Roberts, S. C. Mannsfeld, and Z. Bao, "Optimizing the Thin Film Morphology of Organic Field-Effect Transistors: The Influence of Molecular Structure and Vacuum Deposition Parameters on Device Performance," *Journal of Macromolecular Science Part C: Polymer Reviews,* vol. 46, pp. 79-101, 2006.

[96] P. Kumar, A. Sharma, S. Yadav, and S. Ghosh, "Morphology optimization for achieving air stable and high performance organic field effect transistors," *Organic Electronics,* vol. 14, pp. 1663-1672, 2013.

[97] V. Babrauskas, "The West, Texas, ammonium nitrate explosion: A failure of regulation," *Journal of fire sciences,* vol. 35, pp. 396-414, 2017.

[98] K. E. Wyer, D. B. Kelleghan, V. Blanes-Vidal, G. Schauberger, and T. P. Curran, "Ammonia emissions from agriculture and their contribution to fine particulate matter: A review of implications for human health," *Journal of Environmental Management,* vol. 323, p. 116285, 2022.

[99] K. Ramaiyan, L.-k. Tsui, E. L. Brosha, C. Kreller, J. R. Stetter, T. Russ, *et al.*, "Recent developments in sensor technologies for enabling the hydrogen economy," *ECS Sensors Plus,* vol. 2, p. 045601, 2023.

[100] H. G. Hansma, "Atomic force microscopy and spectroscopy of silk from spider draglines, capture-web spirals, and silkworms," *Biotechnology of silk,* pp. 123-136, 2014.

[101] N. Marturi, "Vision and visual servoing for nanomanipulation and nanocharacterization in scanning electron microscope," Université de Franche-Comté, 2013.

[102] A. Tricoli, M. Righettoni, and A. Teleki, "Semiconductor gas sensors: dry synthesis and application," *Angewandte Chemie International Edition,* vol. 49, pp. 7632-7659, 2010.

[103] R. Jana, S. Hajra, P. M. Rajaitha, K. Mistewicz, and H. J. Kim, "Recent advances in multifunctional materials for gas sensing applications," *Journal of Environmental Chemical Engineering,* p. 108543, 2022.

[104] A. Mirzaei, J.-H. Kim, H. W. Kim, and S. S. Kim, "Resistive-based gas sensors for detection of benzene, toluene and xylene (BTX) gases: a review," *Journal of Materials Chemistry C,* vol. 6, pp. 4342-4370, 2018.

[105] H. Ji, W. Zeng, and Y. Li, "Gas sensing mechanisms of metal oxide semiconductors: a focus review," *Nanoscale,* vol. 11, pp. 22664-22684, 2019.

References

[106] S. Y. Park, Y. Kim, T. Kim, T. H. Eom, S. Y. Kim, and H. W. Jang, "Chemoresistive materials for electronic nose: Progress, perspectives, and challenges," *InfoMat,* vol. 1, pp. 289-316, 2019.

[107] V. Solanki, A. Banerjee, and K. Nanda, "Conductometric room temperature ammonia sensor based on porous tin oxide," *Sensors and Actuators B: Chemical*, vol. 366, p. 131942, 2022.

[108] S. Kulkarni, Y. Navale, S. Navale, F. Stadler, N. Ramgir, and V. Patil, "Hybrid polyaniline-WO3 flexible sensor: a room temperature competence towards NH3 gas," *Sensors and Actuators B: Chemical,* vol. 288, pp. 279-288, 2019.

[109] R. A. Michaels, "Emergency planning and the acute toxic potency of inhaled ammonia," *Environmental health perspectives,* vol. 107, pp. 617-627, 1999.

[110] H. Tang, L. N. Sacco, S. Vollebregt, H. Ye, X. Fan, and G. Zhang, "Recent advances in 2D/nanostructured metal sulfide-based gas sensors: mechanisms, applications, and perspectives," *Journal of Materials Chemistry A*, vol. 8, pp. 24943-24976, 2020.

[111] H.-T. Jung, "The Present and Future of Gas Sensors," vol. 7, ed: ACS Publications, 2022, pp. 912-913.

[112] R. Mishra, S. Upadhyay, A. Kushwaha, T.-H. Kim, G. Murali, R. Verma, *et al.*, "SnO 2 quantum dots decorated on RGO: A superior sensitive, selective and reproducible performance for a H 2 and LPG sensor," *Nanoscale*, vol. 7, pp. 11971-11979, 2015.

[113] D. Bandgar, S. Navale, M. Naushad, R. Mane, F. Stadler, and V. Patil, "Ultra-sensitive polyaniline–iron oxide nanocomposite room temperature flexible ammonia sensor," *RSC advances,* vol. 5, pp. 68964-68971, 2015.

[114] S. Han, X. Zhuang, W. Shi, X. Yang, L. Li, and J. Yu, "Poly (3-hexylthiophene)/polystyrene (P3HT/PS) blends based organic field-effect transistor ammonia gas sensor," *Sensors and Actuators B: Chemical*, vol. 225, pp. 10-15, 2016.

[115] P. K. Kannan, D. J. Late, H. Morgan, and C. S. Rout, "Recent developments in 2D layered inorganic nanomaterials for sensing," *Nanoscale,* vol. 7, pp. 13293-13312, 2015.

[116] M. Mathew, P. V. Shinde, R. Samal, and C. S. Rout, "A review on mechanisms and recent developments in pn heterojunctions of 2D materials for gas sensing applications," *Journal of Materials Science,* vol. 56, pp. 9575-9604, 2021.

References

[117] R. Kumar, W. Zheng, X. Liu, J. Zhang, and M. Kumar, "MoS2-based nanomaterials for room-temperature gas sensors," *Advanced Materials Technologies,* vol. 5, p. 1901062, 2020.

[118] Y. Niu, R. Wang, W. Jiao, G. Ding, L. Hao, F. Yang, *et al.*, "MoS2 graphene fiber based gas sensing devices," *Carbon,* vol. 95, pp. 34-41, 2015.

[119] T. Zhou and T. Zhang, "Recent Progress of Nanostructured Sensing Materials from 0D to 3D: Overview of Structure–Property-Application Relationship for Gas Sensors," *Small Methods,* vol. 5, p. 2100515, 2021.

[120] K. Rathi and K. Pal, "Ruthenium-decorated tungsten disulfide quantum dots for a CO2 gas sensor," *Nanotechnology,* vol. 31, p. 135502, 2020.

[121] S. Watanabe, K. Ando, K. Kang, S. Mooser, Y. Vaynzof, H. Kurebayashi, *et al.*, "Polaron spin current transport in organic semiconductors," *Nature Physics,* vol. 10, pp. 308-313, 2014.

[122] L. H. Jimison, A. Salleo, M. L. Chabinyc, D. P. Bernstein, and M. F. Toney, "Correlating the microstructure of thin films of poly [5, 5-bis (3-dodecyl-2-thienyl)-2, 2-bithiophene] with charge transport: Effect of dielectric surface energy and thermal annealing," *Physical Review B,* vol. 78, p. 125319, 2008.

[123] R. K. Pandey, A. S. Tripathi, S. S. Pandey, and R. Prakash, "Optoelectrical anisotropy in graphene oxide supported polythiophene thin films fabricated by floating film transfer," *Carbon,* vol. 147, pp. 252-261, 2019.

[124] M. á Lee, D. á Gupta, N. á Zhao, M. á Heeney, and I. á McCulloch, "H. áSirringhaus," *Adv. Funct. Mater,* vol. 21, p. 932, 2011.

[125] M. Pandey, S. S. Pandey, S. Nagamatsu, S. Hayase, and W. Takashima, "Solvent driven performance in thin floating-films of PBTTT for organic field effect transistor: Role of macroscopic orientation," *Organic Electronics,* vol. 43, pp. 240-246, 2017.

[126] C. Kumar, G. Rawat, H. Kumar, Y. Kumar, R. Prakash, and S. Jit, "Electrical and ammonia gas sensing properties of poly (3, 3‴-dialkylquaterthiophene) based organic thin film transistors fabricated by floating-film transfer method," *Organic Electronics,* vol. 48, pp. 53-60, 2017.

References

[127] H. Mishra, S. Umrao, J. Singh, R. K. Srivastava, R. Ali, A. Misra, *et al.*, "pH dependent optical switching and fluorescence modulation of molybdenum sulfide quantum dots," *Advanced Optical Materials,* vol. 5, p. 1601021, 2017.

[128] P.-G. Su, F.-Y. Chen, and C.-H. Wei, "Simple one-pot polyol synthesis of Pd nanoparticles, TiO2 microrods and reduced graphene oxide ternary composite for sensing NH3 gas at room temperature," *Sensors and Actuators B: Chemical,* vol. 254, pp. 1125-1132, 2018.

[129] A. Kalita, S. Hussain, A. H. Malik, N. V. Subbarao, and P. K. Iyer, "Vapor phase sensing of ammonia at the sub-ppm level using a perylene diimide thin film device," *Journal of Materials Chemistry C,* vol. 3, pp. 10767-10774, 2015.

[130] S. Vieira, P. Beecher, I. Haneef, F. Udrea, W. I. Milne, M. A. Namboothiry, *et al.*, "Use of nanocomposites to increase electrical “gain” in chemical sensors," *Applied Physics Letters,* vol. 91, 2007.

[131] J. Yu, X. Yu, L. Zhang, and H. Zeng, "Ammonia gas sensor based on pentacene organic field-effect transistor," *Sensors and Actuators B: Chemical,* vol. 173, pp. 133-138, 2012.

[132] Y. Chen, G. Xie, T. Xie, Y. Liu, H. Du, Y. Su, *et al.*, "Thin film transistors based on poly (3-hexylthiophene)/[6, 6]-phenyl C61 butyric acid methyl ester hetero-junction for ammonia detection," *Chemical Physics Letters,* vol. 638, pp. 87-93, 2015.

[133] M. A. Iqbal, X. Fang, Y. Abbas, X. Weng, T. He, and Y.-J. Zeng, "Unlocking high-performance near-infrared photodetection: polaron-assisted organic integer charge transfer hybrids," *Light: Science & Applications,* vol. 13, pp. 1-12, 2024.

[134] S. Mukherjee, R. Maiti, A. K. Katiyar, S. Das, and S. K. Ray, "Novel colloidal MoS2 quantum dot heterojunctions on silicon platforms for multifunctional optoelectronic devices," *Scientific reports,* vol. 6, p. 29016, 2016.

[135] D. Kwak, Y. Lei, and R. Maric, "Ammonia gas sensors: A comprehensive review," *Talanta,* vol. 204, pp. 713-730, 2019.

[136] S. Ghosh, K. Das, N. Tripathy, G. Bose, D. Kim, T. Lee, *et al.*, "Ammonia Sensing Behavior of Zinc Oxide Thin Films and Nanostructures," *IUP Journal of Electrical & Electronics Engineering,* vol. 9, 2016.

References

[137] W. Yin, X. Bai, P. Chen, X. Zhang, L. Su, C. Ji, *et al.*, "Rational control of size and photoluminescence of WS2 quantum dots for white light-emitting diodes," *ACS Applied Materials & Interfaces,* vol. 10, pp. 43824-43830, 2018.

[138] V. Babar, S. Sharma, and U. Schwingenschlögl, "New paradigm for gas sensing by two-dimensional materials," *The Journal of Physical Chemistry C,* vol. 123, pp. 13104-13109, 2019.

[139] J. N. Gavgani, A. Hasani, M. Nouri, M. Mahyari, and A. Salehi, "Highly sensitive and flexible ammonia sensor based on S and N co-doped graphene quantum dots/polyaniline hybrid at room temperature," *Sensors and Actuators B: Chemical,* vol. 229, pp. 239-248, 2016.

[140] D. Zhang, Z. Kang, X. Liu, J. Guo, and Y. Yang, "Highly sensitive ammonia sensor based on PSS doped ZIF-8-derived porous carbon/polyaniline hybrid film coated on quartz crystal microbalance," *Sensors and Actuators B: Chemical,* vol. 357, p. 131419, 2022.

[141] Z. Zhao, C. Xu, L. Niu, X. Zhang, and F. Zhang, "Recent Progress on Broadband Organic Photodetectors and their Applications," *Laser & Photonics Reviews,* vol. 14, p. 2000262, 2020/11/01 2020.

[142] X. Yang, Y. Liu, H. Lei, and B. Li, "An organic–inorganic broadband photodetector based on a single polyaniline nanowire doped with quantum dots," *Nanoscale,* vol. 8, pp. 15529-15537, 2016.

[143] B. N. Pal, I. Robel, A. Mohite, R. Laocharoensuk, D. J. Werder, and V. I. Klimov, "High-Sensitivity p–n Junction Photodiodes Based on PbS Nanocrystal Quantum Dots," *Advanced Functional Materials,* vol. 22, pp. 1741-1748, 2012/04/24 2012.

[144] T. Zhu, L. Shen, D. Zhang, J. Zheng, and X. Gong, "Solution-Processed Ternary Perovskite-Organic Broadband Photodetectors with Ultrahigh Detectivity," *ACS Applied Materials & Interfaces,* vol. 14, pp. 18744-18750, 2022/04/27 2022.

[145] M. S. Wagh, G. H. Jain, D. R. Patil, S. A. Patil, and L. A. Patil, "Modified zinc oxide thick film resistors as NH3 gas sensor," *Sensors and Actuators B: Chemical,* vol. 115, pp. 128-133, 2006/05/23/ 2006.

References

[146] H. Tang, M. Yan, H. Zhang, S. Li, X. Ma, M. Wang, *et al.*, "A selective NH3 gas sensor based on Fe2O3–ZnO nanocomposites at room temperature," *Sensors and Actuators B: Chemical*, vol. 114, pp. 910-915, 2006/04/26/ 2006.

[147] N. Goel, K. Kunal, A. Kushwaha, and M. Kumar, "Metal oxide semiconductors for gas sensing," *Engineering Reports*, p. e12604, 2022.

[148] A. Dey, "Semiconductor metal oxide gas sensors: A review," *Materials Science and Engineering: B*, vol. 229, pp. 206-217, 2018.

[149] M. A. Farea, H. Y. Mohammed, S. M. Shirsat, P. W. Sayyad, N. N. Ingle, T. Al-Gahouari, *et al.*, "Hazardous gases sensors based on conducting polymer composites," *Chemical Physics Letters*, vol. 776, p. 138703, 2021.

[150] S. Iqbal and S. Ahmad, "Recent development in hybrid conducting polymers: synthesis, applications and future prospects," *Journal of industrial and engineering chemistry*, vol. 60, pp. 53-84, 2018.

[151] C. Anichini, W. Czepa, D. Pakulski, A. Aliprandi, A. Ciesielski, and P. Samorì, "Chemical sensing with 2D materials," *Chemical Society Reviews*, vol. 47, pp. 4860-4908, 2018.

[152] A. Manikandan, Y.-Z. Chen, C.-C. Shen, C.-W. Sher, H.-C. Kuo, and Y.-L. Chueh, "A critical review on two-dimensional quantum dots (2D QDs): From synthesis toward applications in energy and optoelectronics," *Progress in Quantum Electronics*, vol. 68, p. 100226, 2019/11/01/ 2019.

[153] N. Yue, J. Weicheng, W. Rongguo, D. Guomin, and H. Yifan, "Hybrid nanostructures combining graphene–MoS2 quantum dots for gas sensing," *Journal of Materials Chemistry A*, vol. 4, pp. 8198-8203, 2016.

[154] L. Najafi, B. Taheri, B. Martín-García, S. Bellani, D. Di Girolamo, A. Agresti, *et al.*, "MoS2 Quantum Dot/Graphene Hybrids for Advanced Interface Engineering of a CH3NH3PbI3 Perovskite Solar Cell with an Efficiency of over 20%," *ACS Nano*, vol. 12, pp. 10736-10754, 2018/11/27 2018.

[155] X. Huang, N. Hu, R. Gao, Y. Yu, Y. Wang, Z. Yang, *et al.*, "Reduced graphene oxide–polyaniline hybrid: preparation, characterization and its applications for ammonia gas sensing," *Journal of Materials Chemistry*, vol. 22, pp. 22488-22495, 2012.

References

[156] T. Xie, G. Xie, Y. Su, D. Hongfei, Z. Ye, and Y. Jiang, "Ammonia gas sensors based on poly (3-hexylthiophene)-molybdenum disulfide film transistors," *Nanotechnology*, vol. 27, p. 065502, 2016.

[157] S. Gupta, B. N. Pal, and R. Prakash, "Enhancement of ammonia gas sensitivity and selectivity by depleted layer of PBTTT-C14/MoS2-QDs heterojunction based thin film transistor," *Sensors and Actuators B: Chemical*, p. 134251, 2023.

[158] X. Duan, Q. Liu, and X. Su, "Fluorometric determination of the activity of alkaline phosphatase based on a system composed of WS 2 quantum dots and MnO 2 nanosheets," *Microchimica Acta*, vol. 186, pp. 1-8, 2019.

[159] L. Lin, Y. Xu, S. Zhang, I. M. Ross, A. C. Ong, and D. A. Allwood, "Fabrication of luminescent monolayered tungsten dichalcogenides quantum dots with giant spin-valley coupling," *ACS nano*, vol. 7, pp. 8214-8223, 2013.

[160] Z. Wang, L. Huang, X. Zhu, X. Zhou, and L. Chi, "An ultrasensitive organic semiconductor NO2 sensor based on crystalline TIPS-Pentacene films," *Advanced Materials*, vol. 29, p. 1703192, 2017.

[161] T. Xie, G. Xie, Y. Zhou, J. Huang, M. Wu, Y. Jiang, *et al.*, "Thin film transistors gas sensors based on reduced graphene oxide poly (3-hexylthiophene) bilayer film for nitrogen dioxide detection," *Chemical Physics Letters*, vol. 614, pp. 275-281, 2014.

[162] S. Gupta, B. N. Pal, and R. Prakash, "Enhancement of ammonia gas sensitivity and selectivity by depleted layer of PBTTT-C14/MoS2-QDs heterojunction based thin film transistor," *Sensors and Actuators B: Chemical*, vol. 393, p. 134251, 2023.

[163] H. K. Chitte, G. N. Shinde, N. V. Bhat, and V. E. Walunj, "Synthesis of polypyrrole using ferric chloride (FeCl3) as oxidant together with some dopants for use in gas sensors," *Journal of sensor technology*, vol. 1, p. 47, 2011.

[164] L. T. Zegebreal, N. A. Tegegne, and F. G. Hone, "Recent progress in hybrid conducting polymers and metal oxide nanocomposite for room-temperature gas sensor applications: A Review," *Sensors and Actuators A: Physical*, p. 114472, 2023.

[165] I. P. Liu, C.-H. Chang, and B.-Y. Ke, "Ammonia Sensing Performance of a GaN-Based Semiconductor Diode with a Solution-Processed Pt/GaOx Schottky Contact," *ACS Applied Electronic Materials*, vol. 1, pp. 1474-1481, 2019/08/27 2019.

References

[166] R. Gond, P. Shukla, B. Prakash, and B. Rawat, "Vertically Aligned MoS2/ZnO Heterostructure for Highly Selective NH3 Sensing at Room Temperature," *ACS Applied Electronic Materials,* vol. 6, pp. 2728-2738, 2024/04/23 2024.

[167] A. V. Raghu, K. K. Karuppanan, and B. Pullithadathil, "Highly Surface Active Phosphorus-Doped Onion-Like Carbon Nanostructures: Ultrasensitive, Fully Reversible, and Portable NH3 Gas Sensors," *ACS Applied Electronic Materials,* vol. 1, pp. 2208-2219, 2019/11/26 2019.

[168] C. Zhang, P. Chen, and W. Hu, "Organic field-effect transistor-based gas sensors," *Chemical Society Reviews,* vol. 44, pp. 2087-2107, 2015.

[169] B. Nketia-Yawson, A. R. Jung, Y. Noh, G.-S. Ryu, G. D. Tabi, K.-K. Lee, *et al.*, "Highly Sensitive Flexible NH3 Sensors Based on Printed Organic Transistors with Fluorinated Conjugated Polymers," *ACS Applied Materials & Interfaces,* vol. 9, pp. 7322-7330, 2017/03/01 2017.

[170] B. King and B. H. Lessard, "Review of recent advances and sensing mechanisms in solid-state organic thin-film transistor (OTFT) sensors," *Journal of Materials Chemistry C,* vol. 12, pp. 5654-5683, 2024.

[171] M. Wu, S. Hou, X. Yu, and J. Yu, "Recent progress in chemical gas sensors based on organic thin film transistors," *Journal of Materials Chemistry C,* vol. 8, pp. 13482-13500, 2020.

[172] A. Verma, S. Gupta, V. Mishra, and R. Prakash, "A Low Voltage, Self-Oriented Organic Polymer Nanocomposite-Based Flexible TFT for Ammonia Gas Sensing at Room Temperature," *IEEE Transactions on Electron Devices*, 2023.

[173] A. Verma, R. Gupta, A. S. Verma, and T. Kumar, "A review of Composite Conducting Polymer-based Sensors for detection of industrial waste gases," *Sensors and Actuators Reports,* p. 100143, 2023.

[174] H. Li, W. Shi, J. Song, H.-J. Jang, J. Dailey, J. Yu, *et al.*, "Chemical and biomolecule sensing with organic field-effect transistors," *Chemical reviews,* vol. 119, pp. 3-35, 2018.

[175] J. Lu, D. Liu, J. Zhou, Y. Chu, Y. Chen, X. Wu, *et al.*, "Porous organic field-effect transistors for enhanced chemical sensing performances," *Advanced Functional Materials,* vol. 27, p. 1700018, 2017.

[176] M. Mirza, J. Wang, D. Li, S. A. Arabi, and C. Jiang, "Novel Top-Contact Monolayer Pentacene-Based Thin-Film Transistor for Ammonia Gas Detection," *ACS Applied Materials & Interfaces*, vol. 6, pp. 5679-5684, 2014/04/23 2014.

[177] X. Tian, X. Cui, Y. Xiao, T. Chen, X. Xiao, and Y. Wang, "Pt/MoS2/Polyaniline Nanocomposite as a Highly Effective Room Temperature Flexible Gas Sensor for Ammonia Detection," *ACS Applied Materials & Interfaces*, vol. 15, pp. 9604-9617, 2023/02/22 2023.

[178] W. Serrano, A. Meléndez, I. Ramos, and N. J. Pinto, "Poly (lactic acid)/poly (3-hexylthiophene) composite nanofiber fabrication for electronic applications," *Polymer International*, vol. 65, pp. 503-507, 2016.

[179] M. P. Gordon, L. T. Lloyd, and D. S. Boucher, "Poly (3-hexylthiophene) films prepared using binary solvent mixtures," *Journal of Polymer Science Part B: Polymer Physics*, vol. 54, pp. 624-638, 2016.

[180] C. Bounioux, R. Avrahami, G. Vasilyev, N. Patil, E. Zussman, and R. Yerushalmi–Rozen, "Single-step electrospinning of multi walled carbon nanotubes–Poly (3-octylthiophene) hybrid nano-fibers," *Polymer*, vol. 86, pp. 15-21, 2016.

[181] N. Kleinhenz, N. Persson, Z. Xue, P. H. Chu, G. Wang, Z. Yuan, *et al.*, "Ordering of poly (3-hexylthiophene) in solutions and films: Effects of fiber length and grain boundaries on anisotropy and mobility," *Chemistry of Materials*, vol. 28, pp. 3905-3913, 2016.

[182] M. Brinkmann and P. Rannou, "Effect of molecular weight on the structure and morphology of oriented thin films of regioregular poly (3-hexylthiophene) grown by directional epitaxial solidification," *Advanced Functional Materials*, vol. 17, pp. 101-108, 2007.

[183] S. Sun, T. Salim, L. H. Wong, Y. L. Foo, F. Boey, and Y. M. Lam, "A new insight into controlling poly (3-hexylthiophene) nanofiber growth through a mixed-solvent approach for organic photovoltaics applications," *Journal of Materials Chemistry*, vol. 21, pp. 377-386, 2011.

[184] M. K. Singh, A. Kumar, and R. Prakash, "Self-assembly of regioregular poly [2,5-bis(3-tetradecylthiophen-2-yl)thieno[3,2-b]thiophene], pBTTT-C14 in solvent-mixture and

study of its junction behaviour," *Organic Electronics,* vol. 50, pp. 138-146, 2017/11/01/ 2017.

[185] N. Kiriy, E. Jähne, H.-J. Adler, M. Schneider, A. Kiriy, G. Gorodyska, *et al.*, "One-dimensional aggregation of regioregular polyalkylthiophenes," *Nano Letters,* vol. 3, pp. 707-712, 2003.

[186] R. Traiphol, N. Charoenthai, T. Srikhirin, T. Kerdcharoen, T. Osotchan, and T. Maturos, "Chain organization and photophysics of conjugated polymer in poor solvents: Aggregates, agglomerates and collapsed coils," *Polymer,* vol. 48, pp. 813-826, 2007.

[187] C. Scharsich, R. H. Lohwasser, M. Sommer, U. Asawapirom, U. Scherf, M. Thelakkat, *et al.*, "Control of aggregate formation in poly (3-hexylthiophene) by solvent, molecular weight, and synthetic method," *Journal of Polymer Science Part B: Polymer Physics,* vol. 50, pp. 442-453, 2012.

[188] H.-W. Zan, M.-Z. Dai, T.-Y. Hsu, H.-C. Lin, H.-F. Meng, and Y.-S. Yang, "Porous organic TFTs for the applications on real-time and sensitive gas sensors," *IEEE electron device letters,* vol. 32, pp. 1143-1145, 2011.

[189] J. He, B. Liang, W. Kong, J. Dai, F. Liu, S. Pan, *et al.*, "Self-Healing, Laminated, and Low Resistance NH3 Sensor Based on 6,6′,6″-(Nitrilotris(benzene-4,1-diyl))tris(5-phenylpyrazine-2,3-dicarbonitrile) Sensing Material Operating at Room Temperature," *ACS Sensors,* vol. 9, pp. 171-181, 2024/01/26 2024.

[190] T. He, S. Sun, B. Huang, and X. Li, "MXene/SnS2 Heterojunction for Detecting Sub-ppm NH3 at Room Temperature," *ACS Applied Materials & Interfaces,* vol. 15, pp. 4194-4207, 2023/01/25 2023.

[191] W. Shi, J. Ye, J. G. Checkelsky, C. Terakura, and Y. Iwasa, "Transport Properties of Polymer Semiconductor Controlled by Ionic Liquid as a Gate Dielectric and a Pressure Medium," *Advanced Functional Materials,* vol. 24, pp. 2005-2012, 2014/04/01 2014.

[192] F. C. Spano, "Modeling disorder in polymer aggregates: The optical spectroscopy of regioregular poly (3-hexylthiophene) thin films," *The Journal of chemical physics,* vol. 122, 2005.

References

[193] M. Sundberg, O. Inganäs, S. Stafström, G. Gustafsson, and B. Sjögren, "Optical absorption of poly (3-alkylthiophenes) at low temperatures," *Solid state communications,* vol. 71, pp. 435-439, 1989.

[194] R. Hildner, A. Köhler, P. Müller-Buschbaum, F. Panzer, and M. Thelakkat, "π-Conjugated Donor Polymers: Structure Formation and Morphology in Solution, Bulk and Photovoltaic Blends," *Advanced energy materials,* vol. 7, p. 1700314, 2017.

[195] H. Tai, Y. Jiang, G. Xie, J. Yu, and X. Chen, "Fabrication and gas sensitivity of polyaniline–titanium dioxide nanocomposite thin film," *Sensors and Actuators B: Chemical,* vol. 125, pp. 644-650, 2007/08/08/ 2007.

[196] V. V. Tran, G. Jeong, K. S. Kim, J. Kim, H.-R. Jung, B. Park, *et al.*, "Facile Strategy for Modulating the Nanoporous Structure of Ultrathin π-Conjugated Polymer Films for High-Performance Gas Sensors," *ACS Sensors*, vol. 7, pp. 175-185, 2022/01/28 2022.

[197] S. Gupta, B. N. Pal, and R. Prakash, "Improved ammonia sensitivity and broadband photodetection by using PBTTT-C14/WS2-QDs nano-heterojunction based thin film transistor," *Sensors and Actuators B: Chemical,* p. 135872, 2024.

[198] H. Sirringhaus, "Device physics of solution-processed organic field-effect transistors," *Advanced Materials,* vol. 17, pp. 2411-2425, 2005.

[199] T. W. Kelley, P. F. Baude, C. Gerlach, D. E. Ender, D. Muyres, M. A. Haase, *et al.*, "Recent progress in organic electronics: Materials, devices, and processes," *Chemistry of Materials,* vol. 16, pp. 4413-4422, 2004.

[200] H. Chen, W. Zhang, M. Li, G. He, and X. Guo, "Interface engineering in organic field-effect transistors: principles, applications, and perspectives," *Chemical reviews,* vol. 120, pp. 2879-2949, 2020.

[201] Y. M. Park, J. Daniel, M. Heeney, and A. Salleo, "Room-temperature fabrication of ultrathin oxide gate dielectrics for low-voltage operation of organic field-effect transistors," *Advanced Materials,* vol. 23, pp. 971-974, 2011.

[202] J.-D. Oh, J.-W. Kim, D.-K. Kim, and J.-H. Choi, "Low-voltage organic transistors and inverters using HfOx dielectrics," *Organic Electronics,* vol. 30, pp. 131-135, 2016.

References

[203] X. Ren, Z. Lu, X. Zhang, S. Grigorian, W. Deng, and J. Jie, "Low-voltage organic field-effect transistors: challenges, progress, and prospects," *ACS Materials Letters,* vol. 4, pp. 1531-1546, 2022.

[204] A. Nigam, D. Kabra, T. Garg, M. Premaratne, and V. R. Rao, "Insight into the charge transport and degradation mechanisms in organic transistors operating at elevated temperatures in air," *Organic Electronics,* vol. 22, pp. 202-209, 2015.

[205] R. P. Ortiz, A. Facchetti, and T. J. Marks, "High-k organic, inorganic, and hybrid dielectrics for low-voltage organic field-effect transistors," *Chemical reviews,* vol. 110, pp. 205-239, 2010.

[206] A. Facchetti, M. H. Yoon, and T. J. Marks, "Gate dielectrics for organic field-effect transistors: new opportunities for organic electronics," *Advanced Materials,* vol. 17, pp. 1705-1725, 2005.

[207] L. A. Majewski, R. Schroeder, and M. Grell, "One volt organic transistor," *Advanced Materials,* vol. 17, pp. 192-196, 2005.

[208] X.-H. Zhang, B. Domercq, X. Wang, S. Yoo, T. Kondo, Z. L. Wang, *et al.*, "High-performance pentacene field-effect transistors using Al2O3 gate dielectrics prepared by atomic layer deposition (ALD)," *Organic Electronics,* vol. 8, pp. 718-726, 2007.

[209] D. K. Hwang, C. S. Kim, J. M. Choi, K. Lee, J. H. Park, E. Kim, *et al.*, "Polymer/YOx Hybrid-Sandwich Gate Dielectrics for Semitransparent Pentacene Thin-Film Transistors Operating Under 5 V," *Advanced Materials,* vol. 18, pp. 2299-2303, 2006.

[210] O. Acton, G. Ting, H. Ma, J. W. Ka, H. L. Yip, N. M. Tucker, *et al.*, "π-σ-Phosphonic Acid Organic Monolayer/Sol–Gel Hafnium Oxide Hybrid Dielectrics for Low-Voltage Organic Transistors," *Advanced Materials,* vol. 20, pp. 3697-3701, 2008.

[211] S. Gupta and B. N. Pal, "Organic Thin Film Transistor with Aligned Nanowires/Thin Film Hybrid Channel for Low-Concentration Detection of NH3 at Room Temperature," *ACS Applied Electronic Materials,* 2024.

[212] A. Verma, P. K. Sahu, V. Chaudhary, A. K. Singh, V. Mishra, and R. Prakash, "Fabrication and Characterization of P3HT/MoS_2 Thin-Film Based Ammonia Sensor Operated at Room Temperature," *IEEE Sensors Journal,* vol. 22, pp. 10361-10369, 2022.

References

[213] C. Kumar, G. Rawat, H. Kumar, Y. Kumar, A. Kumar, R. Prakash, *et al.*, "Electrical and ammonia gas sensing properties of PQT-12/CdSe quantum dots composite-based organic thin film transistors," *IEEE Sensors Journal*, vol. 18, pp. 6085-6091, 2018.

[214] S. Gupta and B. N. Pal, "Organic Thin Film Transistor with Aligned Nanowires/Thin Film Hybrid Channel for Low-Concentration Detection of NH3 at Room Temperature," *ACS Applied Electronic Materials*, vol. 6, pp. 8059-8067, 2024.

List of Research Publications

List of Research Publications

1. **Shipra Gupta,** Bhola N. Pal, Rajiv Prakash "Improved ammonia sensitivity and broadband photo-detection by using PBTTT-C14/WS2-QDs nano-heterojunction based thin film transistor" *Sensors and Actuators: B. Chemical,* **2024,** 393, 134251;

   https://doi.org/10.1016/j.snb.2023.134251

2. **Shipra Gupta,** Bhola N. Pal, Rajiv Prakash "Enhancement of ammonia gas sensitivity and selectivity by depleted layer of PBTTT-C14/MoS2-QDs heterojunction based thin film transistor" *Sensors and Actuators: B. Chemical,* **2023,** 414, 135872;

   https://doi.org/10.1016/j.snb.2024.135872

3. **Shipra Gupta** and Bhola Nath Pal "Organic thin film transistor with aligned nanowires/thin film hybrid channel for low concentration detection of NH3 at room temperature" ACS Appl. Electron. Mater. **2024** https://doi.org/10.1021/acsaelm.4c01410

4. **Shipra Gupta,** Bhola N. Pal, Rajiv Prakash "Development of Low voltage operating organic thin film transistor for ammonia and photo sensing applications" (under writing)

5. Ankit Verma , **Shipra Gupta,** V. N. Mishra, and Rajiv Prakash "A Low-Voltage, Self-Oriented Organic Polymer Nanocomposite-Based Flexible TFT for Ammonia Gas Sensing at Room Temperature" IEEE TRANSACTIONS ON ELECTRON DEVICES., VOL. 70, NO. 5, **2023** https://doi.org/10.1109/TED.2023.3255835

6. Anupama Chanda**, Shipra Gupta,** M. Vasundhara, Shalik R. Joshi, Geeta R. Muttae and Jai Singh "Study of structural, optical and magnetic properties of cobalt doped ZnO nanorods*" RSC Adv.*, **2017**, 7, 50527) DOI: 10.1039/c7ra08458g

7. J. Singh, A. Chanda, **S. Gupta,** P. Shukla, and V. Chandra "Effect of cobalt doping on structural and optical properties of ZnO Nano-particles" *AIP Conference* 1731, 050091, **2016** http://dx.doi.org/10.1063/1.4947745

List of Conferences/Workshop/Webinar

1. **International conference - Shipra Gupta,** Bhola N. Pal, Rajiv Prakash "Enhancement of Ammonia gas sensitivity at room temperature by Polythiophene/QDs hybrid film based OFET fabricated via Floating film transfer method"

   (**Poster presentation** in **ICSPT-2024** - Separation & Purification Techniques: Environmental Applications)

2. **International Conference - Shipra Gupta,** Bhola N. Pal, Rajiv Prakash Enhancement of Ammonia gas sensitivity and selectivity at room temperature by PBTTT/MoS_2-QDs hybrid film based OFET fabricated via Floating film transfer method

   (**Poster presentation** in Asian polymer association **(APA)-2023** – Polymers for Advanced Technology)

3. **International Conference - Shipra Gupta,** Jai Singh, Anupama Chanda "Dilute Magnetic Semiconducting Oxides: Cobalt doped ZnO nanoparticles" (**Poster presentation** in **IPCBS-2017**- Interface of Physical, Chemical and Biological Sciences)

4. Workshop on "Materials characterization techniques"(Online) (2020).

5. Attended One day workshop on LATEX, IIT (BHU) (2019).

6. 45th seminar on crystallography (NSC 45) (2018).

7. One day workshop on Nuclear magnetic Resonance Spectroscopy and its applications in Physics, Chemistry and Biology (2015).

List of Conferences/Workshop/Webinar

1. **Best Poster Award (International Conference) - <u>Shipra Gupta,</u>** Bhola N. Pal, Rajiv Prakash Enhancement of Ammonia gas sensitivity and selectivity at room temperature by PBTTT/MoS_2-QDs hybrid film based OFET fabricated via Floating film transfer method

   (**Poster presentation** in Asian polymer association **(APA)-2023** – Polymers for Advanced Technology)

2. **Best Poster Award (International Conference) - <u>Shipra Gupta</u>,** Jai Singh, Anupama Chanda "Dilute Magnetic Semiconducting Oxides: Cobalt doped ZnO nanoparticles" (**Poster presentation** in **IPCBS-2017**- Interface of Physical, Chemical and Biological Sciences)